Astron. Astrophys. Rev. (2006) 13(3): 159–228
DOI 10.1007/s00159-006-0028-0

PAPER

Ingrid Mann · Melanie Köhler · Hiroshi Kimura · Andrzej Cechowski · Tetsunori Minato

Dust in the solar system and in extra-solar planetary systems

Received: 7 January 2006 / Published online: 27 April 2006

Abstract Among the observed circumstellar dust envelopes a certain population, planetary debris disks, is ascribed to systems with optically thin dust disks and low gas content. These systems contain planetesimals and possibly planets and are believed to be systems that are most similar to our solar system in an early evolutionary stage. Planetary debris disks have been identified in large numbers by a brightness excess in the near-infrared, mid-infrared and/or submillimetre range of their stellar spectral energy distributions. In some cases, spatially resolved observations are possible and reveal complex spatial structures. Acting forces and physical processes are similar to those in the solar system dust cloud, but the observational approach is obviously quite different: overall spatial distributions for systems of different ages for the planetary debris disks, as opposed to detailed local information in the case of the solar system. Comparison with the processes of dust formation and evolution observed in the solar system therefore helps understand the planetary debris disks. In this paper, we review our present knowledge of observations, acting forces, and major physical interactions of the dust in the solar system and in similar extra-solar planetary systems.

Keywords Solar system: general · Solar system: formation · (Stars:) planetary systems · Interplanetary medium · Meteors · Meteoroids

I. Mann (✉) · M. Köhler · T. Minato
Institut für Planetologie, Westfälische Wilhelms-Universität, Wilhelm-Klemm-Str. 10, 48149 Münster, Germany

H. Kimura
Institute of Low Temperature Science, Hokkaido University, Sapporo, Japan

A. Cechowski
Space Research Center, Polish Academy of Sciences, Warsaw, Poland

1 Introduction

Discoveries and studies of second-generation dust disks around main-sequence stars started two decades ago, when measurements of the spectral energy distribution of Vega revealed a faint excess compared to the spectrum of the stellar photosphere in the infrared brightness (Aumann et al. 1984). This excess was found for a number of stars and was attributed to circumstellar dust with lifetimes significantly shorter than the age of the star. These systems do not necessarily contain planets, but the existence of planetesimals is certain. Like in the solar system, the planetesimals are the major source of the dust. In contrast to dust around young stars, these dust particles are produced from destruction or erosion of the parent bodies. These systems are called circumstellar debris systems, second-generation dust clouds or Vega-type objects or planetary debris disks. We will use the term planetary debris disk because it accounts for the fact that the dust is produced from planetesimals and is influenced in its dynamics by planetesimals. These systems do not necessarily contain planets, but systems which contain planets (i.e. 'real' extra-solar planetary systems) are expected to form and develop in similar ways. From our later discussion, it will become clear that the direct influence of possibly existing planets on the overall dust cloud is small compared to the influence of planetesimals. In contrast to young circumstellar systems, the dust in planetary debris disks is produced by larger parent bodies; the gas component in the planetary debris disks is tenuous and does not influence the dynamics of dust; and the planetesimals induce dust relative velocities that cause catastrophic dust collisions. It is assumed, that among the objects currently accessible to astronomical observations, these planetary debris disks resemble our solar system most closely. At least some of them contain planets. This makes them interesting targets for research.

While the formation of stars can be studied from astronomical observations, studies of the conditions of the formation and evolution of planets were for a long time limited to the case of our solar system and to classical planetology, meaning studies of meteorites and lunar samples, studies of craters on planetary surfaces, observations of planets, and recent space exploration of planets and minor solar system objects. Planet formation around other stars was hidden in dense protoplanetary clouds and planet evolution was not observable due to the large distance and faint brightness of these systems. The discoveries of extra-solar planets and following revision of the models of planet formation showed how the perception of the solar system (from earth) limits our view of the solar system and even more so of planetary systems in general.

A topic of special interest within the topics of astronomical and planetary research is that of the formation of terrestrial planets and among those the evolution of habitable planets like earth. The role of debris disks in this context is manifold: Planetary debris provide a local flux of material onto a planet, i.e. delivering solids and volatiles onto the surface or into the atmosphere. For the planetary debris disks that are currently observed around other stars, impacts in most cases would be catastrophic for terrestrial planets, significantly altering their surface and atmosphere. Therefore, the evolution of habitable planets is closely connected to the evolution of the planetary debris disks that they are embedded in. As far as observations are concerned, the spatial distribution of the planetary debris allows to infer the distribution of planetesimals as their parent bodies and as their perturbers.

The spatial distribution of debris may also reveal the presence of earth-mass planets; these cannot be observed directly but their gravity shapes the structure of the observed dust cloud.

We note that even for future improved dedicated observation facilities the existence of planetary debris disks hampers the astronomical observation of extrasolar earth-like planets.

The similarity of the planetary debris disks to the solar system dust cloud has been pointed out before. The latter is less dense than the currently observed circumstellar debris disks, but the acting forces and major physical processes are identical. In contrast to circumstellar systems, studying the solar system dust cloud is easier, since we can derive many of the influencing quantities directly from observations, from laboratory studies of returned samples, and from space measurements. On the other hand, we will see that our view is limited to measurements near earth orbit. A comparative review of the solar system dust cloud and the planetary debris disks should therefore provide the current knowledge of the physical processes of the solar system dust in order to allow its extrapolation to the other systems.

A further important topic of planetary and astrophysical research is the evolution of dust material within the interstellar medium and the connection between dust in the interstellar medium and dust in a planetary system. Observations range here from the dust properties in the interstellar medium (ISM), properties of circumstellar dust in systems of different evolutionary stages, to properties of cometary dust. They permit a comparative study of the optical and thermal properties of dust in these different systems. Dust material evolution in the planetary debris disks is similar to the evolution of dust and small bodies in the outer solar system. Dust measurements from spacecraft and laboratory analysis of collected samples support the observational studies of cometary dust as primitive solar system dust with further complementary information.

In this paper, we review present knowledge of the dust in the solar system and in extra-solar planetary debris disks. We first present observation methods and results about dust in the solar system (Sect. 2) and planetary debris disks (Sect. 3). In Sect. 4, we describe the main acting forces and effects. The spatial distributions of dust are discussed in Sect. 5, and this is partly related to the collisional evolution and the observation of gas components (Sect. 6). We then introduce the concept of ‘astrospheres’ (Sect. 7) being the regions of influence of the stellar wind around stars. They are of interest for estimating stellar wind fluxes and for conditions of interstellar dust entering the planetary debris disks. The optical properties and thermal properties of dust (Sect. 8) are important for interpreting observational data and for understanding the material evolution in planetary systems. We summarize the review in Sect. 9.

2 Dust in the solar system

2.1 Observations

Detection methods of dust and meteorites in interplanetary space are limited to certain size ranges and biased by particle characteristics (orbital parameters, albedo, composition, etc.) (see Fig. 1). Most methods are limited to the near-earth

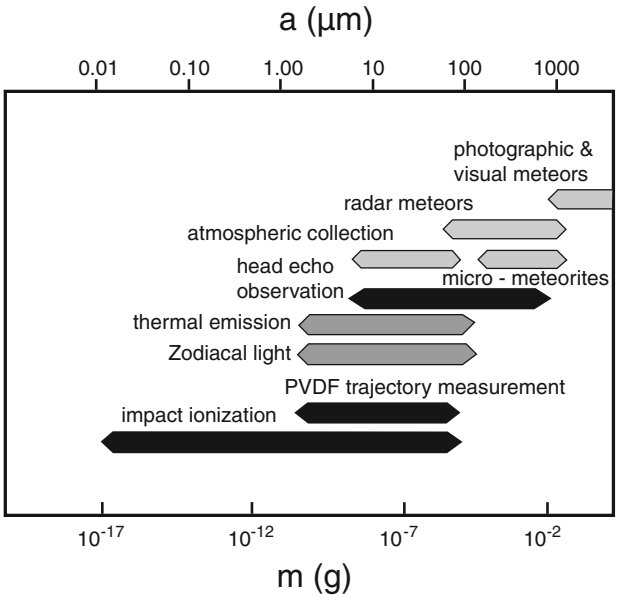

Fig. 1 Detection methods: Shown are different detection methods of dust near earth and the approximate size (i.e. radii) or mass range over which these methods detect particles. The *dark bars* denote detection methods that provide orbital information, the *grey bars* denote methods that provide brightness information integrated along the line of sight, the *light grey bars* denote detection of single particles or events where the orbital information is not clear. Conversion between sizes shown on the upper scale and masses shown on the lower scale are made assuming spherical particles with bulk density 2.5 g cm^{-3} (Mann et al. 2004a)

environment. Thermal emission and scattered light brightness of the zodiacal light describe the size range of particles from 1 to 100 μm. They provide information averaged over large spatial regions mainly between 0.3 and 1.7 AU distance from the Sun and close to the ecliptic plane. Only few studies exist about dust in the outer solar system and near the Sun. In-situ measurements best describe particles that yield a large flux rate, i.e. particles with sizes below 1 μm. Aside from the measurements near comet Halley and recent measurement with the Cassini mission, in-situ measurements gave no direct information about dust composition. The observation of meteors provides total fluxes as well as some information about the composition of the in-falling bodies. Atmospheric collection of interplanetary dust particles (IDPs) and collection of micrometeorites allow a direct analysis in the laboratory.

2.1.1 Zodiacal light measurements

Brightness observations The observed brightness is produced by solar radiation scattered at dust and thermal radiation emitted from dust particles along the line of sight (LOS). The brightness observed for a given longitude ($\lambda - \lambda_\odot$) and a given latitude ($\beta_{\rm los}$) in geocentric coordinates of the LOS is the signal integrated over the entity of dust particles in a given volume element in space. Brightness observations yield a good data set of the visible zodiacal light brightness from

about 15° latitude and longitude from the Sun out to the Gegenschein as well as infrared observations, usually at elongation larger than 60°, where the elongation denotes the angle of the LOS from the Sun-ward direction (Leinert et al. 1998). The visible brightness decreases smoothly with increasing elongation of the LOS from the Sun and increases again by a factor of 2 at elongations larger than 170° (the Gegenschein). As opposed to the solar radiation, the zodiacal light is polarised as a result of the scattering properties of dust particles. Detailed descriptions of the brightness analysis and the LOS integrals have been given before (Dumont 1973; Röser and Staude 1978; Giese et al. 1986). The coordinates describing the dust distribution are given in heliocentric coordinates, solar distance r and helioecliptic latitude $\beta_\odot$. The number density of dust in a given volume in space is

$$n(r, \beta_\odot) = \int_{s_1}^{s_2} \frac{\mathrm{d}n}{\mathrm{d}s} \mathrm{d}s, \tag{1}$$

where $\mathrm{d}n/\mathrm{d}s$ is the differential size distribution of dust and s_1 and s_2 denote the minimum and maximum sizes of the dust.

Due to the decreasing number density and low solar illumination, the outer regions of the dust cloud have only a small contribution to the brightness seen from earth. Based on different models to describe the zodiacal light, it is possible to estimate from which region dust particles contribute to the observed brightness (Giese et al. 1986). At 45° as well as at 90° latitude of the LOS the contribution from distances >2.6 AU is less than 1%, with the contribution to the brightness at 90° elongation dropping more steeply than at 45°.

First thermal emission observations of the solar system dust over a wide range of elongations have been made from ballistic rocket Murdock and Price (1985). Satellite observations cover smaller ranges of elongations than these rocket observations or than visible observations (Levasseur-Regourd et al. 2001). Initial analysis of infrared measurements in terms of absolute brightness was difficult and did not agree with the analysis of visual zodiacal light data (Kneissel and Mann 1991). Major progress of the infrared satellite measurements, as will be discussed later in the paper, was to reveal spatial structures and spectral features in the emission brightness.

Some optical observations were carried out from spacecraft away from 1 AU: after the Helios spacecraft measured the zodiacal light brightness for fixed elongations as function of the distance of observation from the Sun, the data were used to derive the radial slope of the zodiacal light brightness to be close to $B(r) \propto r^{-2.3}$, as well as to invert the average scattering function of particles (Leinert et al. 1982a). The zodiacal light at medium elongations is not very sensitive to the exact slope of the scattering function and its variation predominantly reflects the spatial variation of dust number density which was shown to be r^{-n} with $n = 1.0$–1.3 (Leinert and Grün 1990).

The Pioneer 10 and 11 spacecraft also carried a photopolarimeter to map the zodiacal light and background starlight in two broad bandpasses centred at 0.44 and 0.64 μm (Pellicori et al. 1973). The change in brightness of the zodiacal light with Sun–spacecraft distance, r, allowed to derive the radial gradient of the spatial density distribution of the zodiacal particles. The best fit radial gradient, r^{-n}, was found to be $n = 1.0$–1.5, with a cut-off at 3.3 AU. No further decrease in brightness with distance was detected beyond the asteroid belt ($r > 3.3$ AU). The

Fig. 2 The zodiacal light: The zodiacal light is produced by scattering of Sunlight at interplanetary dust particles distributed in the solar system along the ecliptic plane and under good conditions is visible to the bare eye. This image is taken from Mauna Kea, Hawaii with an analogue (35-mm film) camera with fish-eye lens (focal length = 8 mm). The brightness of the zodiacal light forms a faint, almost horizontal band. The left-hand side of the band shows a bright spot of the Sun-ward direction and the right-hand side shows a slight enhancement of the Gegenschein. The brightness of the Milky Way ranges from the *lower left* to *the upper right* of the image showing how the ecliptic is tilted relative to the galactic plane. Four meteors relevant to Leonid shower are seen in the *lower part* of the image. The faint brightness at the *lower right part* and *upper left part* of the image is due to OH-airglow emission (courtesy of Masateru Ishiguro, JAXA, Japan)

lack of a radial gradient between 3.3 and 5.0 AU and comparison of the measured background with predicted integrated starlight indicate that the residual scattering from outer solar-system dust is smaller than $10^{-7}\,\mathrm{Wm}^{-2}\,\mu\mathrm{m}^{-1}\,\mathrm{sr}^{-1}$ at $0.4\,\mu$m (Hanner et al. 1981). This puts a limit to the dust density as discussed in the context of in-situ measurements given later in the paper.

Polarisation observations As opposed to the intensity, the polarisation of the zodiacal light describes the local polarisation of interplanetary dust and is only weakly dependent on the spatial distribution. The linear polarisation of the zodiacal light is a smooth function of elongation with a maximum of approximately 20% around elongation $\epsilon = 60^\circ$ and a negative branch at backscatter direction with a minimum of a few percent along the ecliptic plane (Leinert 1975; Leinert et al. 1998; Levasseur-Regourd 1996). This dependence of polarisation has been established with ground-based, balloon-borne, aircraft-borne, rocket-borne and space-borne telescopes (Behr and Siedentopf 1953; Blackwell 1956; Blackwell and Ingham 1961a,b,c; Dumont and Sanchez 1975a,b, 1976; Frey et al.

1974; Leinert et al. 1974). The linear polarisation at the anti-solar point is found to be zero (Frey et al. 1974; Dumont 1965; Dumont and Sanchez 1975a). The polarisation of the zodiacal light in the ecliptic is nearly constant within the error bars in the wavelength range $\lambda = 260$–900 nm but tends to increase toward the red and the ultraviolet (Peterson 1961; Pitz et al. 1979; Van de Noord 1970; Weinberg and Hahn 1980).

In the early 1970s, Wolstencroft and Bandermann (1973, 1974) claimed the detection of significant angular structure and day-to-day variations in the polarisation of the zodiacal light near the anti-solar point and stirred up further discussions (Sparrow and Weinberg 1975; Bandermann and Wolstencroft 1977). Such variations in the polarisation were not detected at smaller elongation by the Helios 1 and 2 measurements discussed later. Detections of significant circular polarisation in the zodiacal light were reported by Wolstencroft and Rose (1967) and Wolstencroft and Kemp (1972), while Staude and Schmidt (1972) showed from their observations that circular polarisation is zero within the accuracy of 0.1%.

Helios 1 and 2 measured the polarisation of the zodiacal light in U, B and V spectral bands between 0.3 and 1.0 AU from the Sun. The polarisation measured by Helios along the ecliptic latitudes of 16° and 31° is a smooth function of elongation with a maximum around $\epsilon = 52°$ and reaches zero around $\epsilon = 161°$ Leinert et al. 1981, 1982a. The polarisation shows the highest value in the B band and the lowest value in the *U* band, irrespective of heliocentric distance (Leinert et al. 1981). The polarisation is stable with time between 1974 and 1981 and is found to increase with heliocentric distance approximately proportional to $r = 0.3$, where r denotes the heliocentric distance (Leinert et al. 1982a,b).

Cosmic Background Explorer (COBE) observed the polarisation at wavelengths of 1.2, 2.2 and 3.5 μm (Berriman et al. 1994): The polarisation at $\epsilon = 90°$ along the ecliptic plane showed blue colour, namely, and it decreases with wavelength.

F-corona and Sungrazing comets observations The zodiacal light brightness smoothly continues to small elongations of the LOS into the solar corona (Mann 1998b; Levasseur-Regourd et al. 2001). Scattering of solar radiation at electrons, ions and dust particles produces the coronal brightness. Analysis of the *F*-corona produced from dust is especially hampered by the signal of the *K*-corona produced by scattering at electrons near the Sun. Moreover, the observations are hampered by the presence of coronal and atmospheric stray light and therefore *F*-corona observations are preferably made in the near-infrared and during solar eclipses or with coronagraphs from space.

The brightness from dust particles (*F*-corona) is the predominant component of the corona brightness beyond 4 $R_\odot$ distance from the centre of the Sun, which corresponds to an elongation of about 1° of the LOS from the centre of the solar disk. The ambiguities of the LOS inversion also limit the results that can be derived about near-solar dust from the remote observations. The diffraction part in the forward scattering at a small scattering angle is very effective, the light scattered (with small scattering angles) by obstacles near the observer is very intense and yields a strong contribution to the brightness (depending on the size distribution of dust), as pointed out already by van de Hulst (1947). The polarisation of the zodiacal light decreases smoothly at small elongations toward the solar *F*-corona (Blackwell and Petford 1966). The average polarisation and albedo, as well as

the spectral variation of the albedo, change with distance from the Sun and with latitude possibly indicating a change of particles properties as well as of the dust-cloud composition (Kneissel and Mann 1991; Mann 1998a).

Early observations with space coronagraphs (Michels et al. 1982) reported the appearance of Sungrazing comets in the corona. During the Solar and Heliospheric Observatory (SOHO) mission, Sungrazing comets are frequently observed with the SOHO/Large Angle and Spectrometric Coronagraph Experiment (LASCO) (Biesecker et al. 2002). The number of comets observed with a limit of ninth magnitude is about 60 comets per year and the extrapolated total is 180 comets per year. Most of these comets have sizes of the 10–100 m range and are associated to the Kreutz group Sungrazing comets that originate from the same parent body that fragmented when it encountered the Sun (Marsden 1967; Biesecker et al. 2002). The H_2O outgassing of Sungrazers was observed with the Ultraviolet Coronagraph Spectrometer (UVCS) aboard SOHO: the cometary hydrogen Ly-α signal was interpreted in terms of interactions of coronal protons with atoms created by the photodissociation of water (Bemporad et al. 2005). Additional Ly-α emission has been ascribed to the sublimation of dust particles, whose end products neutralize coronal protons via charge exchange processes (Bemporad et al. 2005).

2.1.2 Cometary dust observations

Cometary dust is observed from its light scattering and thermal emission directly in the coma. Regardless of the difference in the properties of comets, the dust particles have common characteristics in their optical properties that are distinctly different from interplanetary dust: they have a lower albedo and often show stronger emission features than those observed in the zodiacal light. Cometary dust is usually assumed to be more pristine than other dust components in the solar system and it is often used for comparison to dust observations around other stars. The cometary dust properties will be further discussed in Sect. 8.

2.1.3 Meteor observations

The flux of small solid bodies into the earth atmosphere is known for a long time from the existence of meteors, so-called shooting stars. A meteoroid that enters the earth atmosphere and atoms ablated from the meteoroid collide with atmospheric constituents. Meteoroid and atmospheric atoms and molecules undergo dissociation and ionisation and form an expanding column of partially ionised plasma along the trajectory of the meteoroid. This plasma cloud that is generated in the atmosphere produces the brightness that is commonly ascribed as meteor. The physics of the meteor phenomenon was recently reviewed by Ceplecha et al. (1998). Some meteors occur in streams, indicating that they are fragments of the same parent body, but the majority of meteors belong to the class of sporadic meteors. It should be noted that the orbital distribution of the sporadic meteors derived from observations is different from the orbital distribution of dust derived from zodiacal light inversion (Kneissel and Mann 1990). The difference in orbital distributions is plausible, since zodiacal light observations are biased to dust with high albedo (Mann et al. 2006).

2.1.4 Laboratory measurements of collected samples

Direct laboratory analysis of cosmic dust particles has been, up to now, only feasible for collected samples. Depending on a variety of different parameters connected to the entry velocity and to the conditions of re-radiation of the entry heat, these collected particles have survived the entry un-melted or only partly melted. Cosmic dust particles collected in the stratosphere by high-flying aircraft cover the size range from 5 to 50 μm, these particles are often denoted as interplanetary dust particles ('IDPs') (Brownlee 1978; Jessberger et al. 2001; Rietmeijer 1998). Cosmic dust particles that are collected from Antarctic Ice and Greenland ice samples as well as from the ocean floor have typically sizes of 20 μm to 1 mm (Maurette et al. 1991; Kurat et al. 1994) (often denoted as 'micrometeorites').

The presence of solar wind noble gases confirms the extraterrestrial nature of the IDPs (Hudson et al. 1981). Also nuclear tracks, in majority generated by solar energetic particles ('solar flare tracks'), have been identified in collected stratospheric cosmic dust and indicate their exposure age to be approximately 10,000 years (Bradley et al. 1984).

Simulating the heating of dust particles with typical entry velocities showed that the entry processes depend on the orbits of the dust particles: The atmospheric-entry conditions inferred for the major fraction of the collected stratospheric cosmic dust is consistent with parent bodies in the main asteroid belt (Flynn 1989).

While for the single particle it is not possible to use the heating history as indicator of the parent bodies, for the case of two specific particles, the density of solar flare tracks clearly exceeded the values that are typical for dust from comets or asteroids, suggesting that they originate from the Kuiper belt (Flynn 1996). There is evidence that some of the materials in the collected samples are very pristine. The so-called anhydrous chondritic IDPs are thought to be among the most primitive samples, among them cluster IDPs are thought to be cometary dust, since their enhanced D/H ratio suggests a pristine nature (Messenger 2000). These interplanetary dust particles contain GEMS (glass with embedded metal and sulphides) with high abundances. It is suggested that GEMS are either interstellar silicate grains or they would be the oldest known solar nebula solids.

Although the number of dust particles collected and analysed is limited, we can infer from the analysis of dust samples the presence of silicates, carbon compounds, sulphides and metals. We can moreover assume that although fluffy, the majority of dust particles in the solar system show only moderate porosity. There is no evidence for largely elongated particles. Particles of irregular structure re composed of submicrometre constituents.

2.1.5 Direct measurements from spacecraft

Instruments on spacecraft measure dust, predominantly of sizes below 100 μm limited by statistics of the low flux rates. Most in-situ experiments from spacecraft make use of the large speed of impacting particles: They detect the material of the dust particle and of the target, evaporated and ionised upon impact (impact ionisation detectors). The interplanetary dust has been measured near ecliptic by the Helios spacecraft from 1 AU to a distance as close as 0.3 AU from the Sun. A

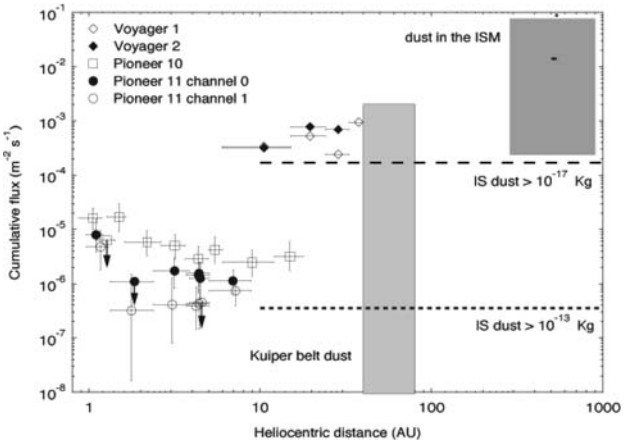

Fig. 3 Dust measurements in the outer solar system: Shown are data from Voyager measurements for masses $m > 1.2 \times 10^{-14}$ kg and for Pioneer measurements for masses $m > 10^{-13}$ kg (note that the channels have different mass thresholds). The *dashed horizontal lines* denote a constant flux of interstellar dust that a spacecraft moving in interstellar upwind direction would detect if moving approximately 10 AU per year. Note that these fluxes are for large interstellar particles that are not influenced by the solar and interstellar magnetic fields. The *shaded areas* depict the range of possible fluxes due to the dust component in the Kuiper belt and due to the dust in the interstellar medium beyond the heliopause (Mann et al. 2004a)

number of spacecraft (Pioneer 8/9, HEOS 2, Hiten, etc.) measured the dust near 1 AU, covering a broad mass range down to 2×10^{-19} kg (HEOS 2). The surfaces of atmosphere-less bodies in the solar system provide a natural area for the indirect detection of dust: Analysis of micro-craters on samples of the lunar surface that were brought back to earth with the Apollo flights enabled detailed studies of the dust flux near 1 AU (Fechtig et al. 2001).

Measurements outside of 1 AU are shown in Fig. 3. Ulysses at distance 1.7–5 AU measured an average flux of $1.5 \times 10^{-4}\,\mathrm{m^{-2}\,s^{-1}}$ (Grün et al. 1994), where about half of the particles had impact speeds corresponding to dust in hyperbolic orbits (β-meteoroids). The flux of β-meteoroids was studied in detail for three selected suitable parts of the Ulysses orbit: The study showed that the β-meteoroids cover a broad range of dust masses and a wide range of orbital perihelia, which agrees with β-meteoroids being produced by collisional fragmentation (Wehry and Mann 1999). First data of the interstellar dust flux were derived from Ulysses measurements (Grün et al. 1994).

In-situ dust measurements at heliocentric distances >5 AU were made aboard Pioneer 10 and 11, detecting dust up to 18 AU (Humes 1980). The resulting flux, $4 \times 10^{-6}\,\mathrm{m^{-2}\,s^{-1}}$ for particles with masses of 8×10^{-13} kg, was nearly constant between 3 and 18 AU. These measurements are possibly hampered by saturation of the detectors and the derived dust fluxes are too high to be in agreement with optical measurements (see Sect. 2.1.1) onboard the same spacecraft (Mann and Hanner 1998). Aside from Pioneer measurements, the plasma wave detectors aboard Voyager 1 and 2 detected plasma clouds produced by dust impacts onto the spacecraft, showing dust impacts from 6 to 51 AU (Voyager 1) and

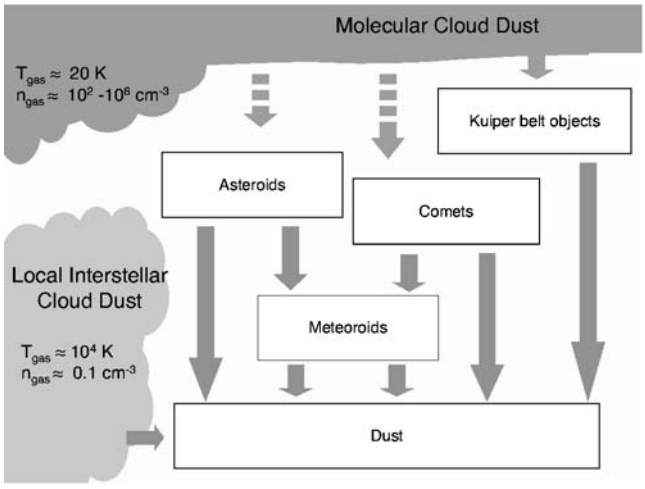

Fig. 4 The sources of dust in our planetary system: The main sources of dust in the solar system are comets, asteroids, Kuiper belt objects and interstellar medium dust. The solar system objects are produced from cold molecular cloud dust that is processed in the protoplanetary nebula. In contrast to the cold and dense molecular cloud environment, the local interstellar cloud dust that streams directly into the solar system is embedded in a warm tenuous gas (Mann et al. 2006)

33 AU (Voyager 2). The detected average flux amounts to $5 \times 10^{-4}\,\mathrm{m}^{-2}\,\mathrm{s}^{-1}$ with the mass threshold of $\sim 10^{-14}$ kg (Gurnett et al. 1997). Note that the Voyager measurements are from instruments designed for measuring plasma parameters and therefore data interpretation is difficult. The fluctuations of measured Voyager fluxes, like those of Pioneers, exceed statistical limits, but do not show a clear trend in the variation with heliocentric distance. It should be noted that the Pioneer and Voyager dust measurements may include both interstellar dust as well as dust produced in the Kuiper belt (Mann and Kimura 2000).

2.2 Sources of solar system dust

The main sources of dust in the solar system are comets, asteroids and Kuiper belt objects. The dust particles are released with the activity of cometary nuclei, produced by collisional fragmentation either of the parent bodies or by collision of larger meteoroids that originate from these parent bodies. A further source of dust are particles entering the solar system from the interstellar medium and impact ejecta generated by impact of interstellar dust onto the Kuiper belt objects. The relative contributions of these different sources are uncertain and vary with size of the particles and with location within the solar system dust cloud.

2.2.1 Asteroids

The number of asteroids as well as their relative velocities show that catastrophic collisions must take place in the asteroid belt. This is supported by observation of asteroids with similar orbital parameters: they are the fragments of the same parent

body (Hirayama 1918). Collisional models of asteroids and their debris (Dohnanyi 1969) show the mass distribution of fragments produced by catastrophic collisions, this is in accordance with the mass distribution derived from observations. These collisions produce meteoritic fragments over a broad mass range. Estimates of the absolute dust production rate from asteroids range from 10^9 to 10^{11} kg per year (Mann et al. 1996). These values are either comparable with, or less than, the dust supply by comets.

A clear indication for the dust production from asteroids is observed with dust bands. Dust bands were firstly noticed in the data of the Infrared Astronomical Satellite (IRAS) as pairs of slight, symmetrically placed enhancements superimposed to the background of the zodiacal emission brightness measured at 12 and 25 μm. The dust bands are explained with particles that move in orbits with similar orbital elements and that are fragments produced upon collision of asteroidal bodies. In some cases, the derived orbital parameters indicate the connection of the dust band to an asteroid family (Sykes 1990).

2.2.2 Comets

The production of dust by comets is obvious from the observation of dust tails. The estimates of the dust production rate in comets are listed in Tables 1 and 2. Most of the estimates of the dust production rate are, as a result of the wavelength of observation, limited to a certain size range of particles as well as they are valid for a narrow range of the orbit of the parent body. Variation of cometary activity and uncertainties in determining the size distribution of ejected particles make it difficult to estimate the total mass production from a single comet. The maximum value of mass loss rate for short-period comets is 144000 kg/s for comet Halley and for a long-period comet the maximum value is 1800000 kg s^{-1} for comet Hale–Bopp. The mass loss rates derived from observations are listed in Tables 1 and 2. For the cases of Hyakutake and Hale–Bopp it is nicely seen that the derived mass loss rate increases with the wavelength of observations. This indicates that the observed larger particles determine the total mass loss rate.

A significant amount of the small dust particles that generates the brightness of the tail are in hyperbolic orbits after release from the comet and therefore do not significantly contribute to the solar system dust cloud. Larger dust particles and meteoroids stay in bound heliocentric orbits and are subsequently fragmented by mutual catastrophic collisions. Meteoroid streams that cross the earth orbit cause meteor showers, some of which directly can be traced back to their parent comets. Moreover, the observation of cometary "dust trails" with IRAS revealed the existence of larger cometary fragments (Sykes et al. 1986): These spatially concentrated trails of dust particles with sizes larger than the typical zodiacal dust are associated with short-period comets. The age of a typical trail is of the order of 100 years. More recent dust trails were also detected in optical observations, and the data indicate the albedo of dust in the trails is low (Ishiguro et al. 1999).

2.2.3 Interstellar medium

The motion of the Sun relative to the local interstellar medium causes a flux of interstellar matter in the form of neutral gas and dust into the solar system. The

Table 1 Estimates of dust mass loss rate from observations of short-period comets

Comet	Q_{dust} (kg s^{-1})	r_{h} (AU)	Data	References
1P/Halley	11.4–1,44,000	0.90–2.84	VIS	(1), (2), (3), (4), (5)
1P/Halley	<52,000	0.89	VIS[a]	(6)
1P/Halley	100–15,000	0.89–2.81	IR	(7), (8), (9)
1P/Halley	1500	0.89	radio	(10)
1P/Halley	5000–10,000	0.89	direct	(11), (12)
2P/Encke	0.76–2000	0.33–1.89	VIS	(13), (2), (14), (15)
2P/Encke	22–230	0.35–1.17	IR	(16), (17), (9)
4P/Faye	125	1.59–1.60	VIS	(18)
6P/d'Arrest	1.3–382	1.16–2.19	VIS	(19), (15)
8P/Tuttle	3.67–29.22	0.78–1.89	VIS	(2)
9P/Tempel 1	<390	1.49	IR	(9)
10P/Tempel 2	2.72–64.63	1.39–1.74	VIS	(2)
10P/Tempel 2	50–500	1.3–2.9	IR	(20)
16P/Brooks 2	7.69–9.25	1.86	VIS	(2)
19P/Borrelly	140–341	1.34–1.52	VIS	(2), (4), (21), (22)
21P/Giacobini-Zinner	16.7–1253	1.03–1.73	VIS	(2), (23), (4), (24), (5)
21P/Giacobini-Zinner	80–380	1.03–1.57	IR	(17), (25)
22P/Kopff	453.6	1.68	VIS	(2)
22P/Kopff	130	1.59	VIS	(26)
22P/Kopff	1000	1,91	IR	(9)
23P/Brorsen-Metcalf	100–300	0.72–0.97	VIS	(24)
23P/Brorsen-Metcalf	300	0.51	IR	(27)
26P/Grigg-Skjellerup	4.43–4.54	1.04	VIS	(2)
26P/Grigg-Skjellerup	200	1	VIS	(28)
26P/Grigg-Skjellerup	20	1.02	IR	(17)
27P/Crommelin	130	1.01	IR	(29)
27P/Crommelin	1200	1.02	IR	(17)
29P/Schwassmann-Wachmann 1	600 ± 300	5.77	VIS	(30)
38P/Stephan-Oterma	22.63–226.1	1.73–3.04	VIS	(2)
38P/Stephan-Oterma	0–250	1.57–2.17	VIS	(24)
45P/Honda-Mrkos-Pajdusakova	1	0.96–0.98	VIS	(31)
46P/Wirtanen	4–20	1.06–2.45	VIS	(32), (33)
46P/Wirtanen	1.5 ± 0.5–2 ± 1	2.0–2.5	IR	(34)
55P/Tempel-Tuttle	210	1.15	IR	(9)
59P/Kearns-Kwee	18.52–40.46	2.22–2.27	VIS	(2)
64P/Swift-Gehrels	12.76–15.19	1.36–1.53	VIS	(2)
65P/Gunn	100–300	2.6–2.9	IR	(34)
67P/Churyumov-Gerasimenko	20–170	1.35–1.88	IR	(17)
73P/Schwassmann-Wachmann 3	1.67	1.440	VIS	(15)
73P/Schwassmann-Wachmann 3	$\sim$120	0.97	IR	(35), (9)
78P/Gehrels 2	20.79	2.36	VIS	(2)
81P/Wild 2	19.8–545	1.49–2.62	VIS	(15)
81P/Wild 2	570–2000	1.58–1.88	IR	(9), (36)
86P/Wild 3	24.49–24.96	2.41	VIS	(2)
103P/Hartley 2	100	1.03	VIS	(14)

Table 1 Continued

Comet	Q_{dust} (kg s^{-1})	r_{h} (AU)	Data	References
109P/Swift-Tuttle	5000 ± 3000	1–2.5	VIS	(37)
109P/Swift-Tuttle	300–1500	0.98–1.13	IR	(38)
126P/IRAS	300	3.3	IR	(9)
D/1993 F2 Shoemaker-Levy 9	6–22	5.39–5.41	VIS	(39)

Note. (1), Suto et al. (1987); (2) Newburn Jr. and Spinrad (1989); (3) Rozenbush et al. (1989); (4) Singh et al. (1992); (5) Singh et al. (1997); (6) Thomas and Keller (1991); (7) Tokunaga et al. (1986); (8) Hanner et al. (1987b); (9) Lisse (2002); (10) Edenhofer et al. (1987); (11) Mazets et al. (1986); (12) Mazets et al. (1987); (13) Sekanina and Schuster (1978b); (14) Epifani et al. (2001); (15) Sanzovo et al. (2001); (16) Ney (1982); (17) Krishna Swamy (1991); (18) Lamy et al. (1996); (19) Sekanina and Schuster (1978a); (20) Fulle (1996); (21) Lamy et al. (1998b); (22) Weaver et al. (2003); (23) Landaberry et al. (1991); (24) Sanzovo et al. (1996); (25) Hanner et al. (1992); (26) Lamy et al. (2002); (27) Lynch et al. (1992); (28) Fulle et al. (1993b); (29) Eaton and Zarnecki (1985); (30) Fulle (1992); (31) Lamy et al. (1999); (32) Lamy et al. (1998a); (33) Fulle (2000); (34) Colangeli et al. (1998); (35) Lisse et al. (1998); (36) Hanner and Hayward (2003); (37) Fulle et al. (1994); (38) Fomenkova et al. (1995); (39) Hahn and Rettig (2000).

[a]At Giotto encounter.

majority of interstellar dust particles of sizes below 0.1 μm are deflected from entering the solar system and move around the heliopause (Czechowski and Mann 2003a), which is an asymmetric structure formed by interaction of the solar wind and interstellar medium ionised gases. The conditions for particles to enter the solar system depend on the dust charging (Kimura and Mann 1998a) and plasma conditions (Linde and Gombosi 2000; Czechowski and Mann 2003b). The dust fluxes in the inner heliosphere depend on the influence of radiation pressure, solar gravity and Lorentz forces on the interstellar dust (Mann and Kimura 2000). All the listed effects are correlated to the dust properties. The first observational evidence of interstellar dust came from an earth-orbiting satellite measuring a variation in the dust flux along the earth's orbit. This variation was explained by gravitational focussing of interstellar dust by the Sun (Bertaux and Blamont 1976). Measurements aboard the Ulysses spacecraft have detected both interstellar dust particles (Grün et al. 1994) and neutral interstellar helium (Witte et al. 1993). The in-situ experiments have detected particles with masses beyond 10^{-20} kg. Inside, 3 AU interstellar particles have been detected up to masses of 10^{-12} kg and beyond 3 AU up to masses slightly above 10^{-14} kg. The mass density is determined by the upper end of the distribution and amounts to 2.8×10^{-23} kg m^{-3} (Mann and Kimura 2000). The initial direction of the flux is almost parallel to the ecliptic plane at $72° \pm 2.4°$ ecliptic longitude and $-2.5 \circ \pm 2.7°$ ecliptic latitude (Grün et al. 1994).

2.2.4 Kuiper belt objects

Shortly after the discovery of the first Kuiper belt objects, it was suggested that Kuiper belt objects may serve as a source of dust in the solar system. Collisions of predominantly those Kuiper belt objects that are below the present limit of detection should create a dust disk in the trans-Neptunian's region (Jewitt and Luu 1995). Estimates for the total dust production rate range from 9×10^5 to 3×10^8 kg s^{-1} (Stern 1995, 1996). It was further proposed that impacts of

Table 2 Estimates of dust mass loss rate derived from observations of long-period comets

Comet	$Q_{\rm dust}$ (kg s^{-1})	$r_{\rm h}$ (AU)	Data	References
C/1956 R1 Arend-Roland	75,000	0.32	VIS	(1)
C/1969 Y1 Bennett	1400–13,000	0.64–1.1	IR	(2), (3)
C/1973 E1 Kohoutek	12–48,000	0.85–1.33	VIS	(4)
C/1973 E1 Kohoutek	161.6	0.96	VIS	(5)
C/1973 E1 Kohoutek	490–25,000	0.15–0.96	IR	(2)
C/1974 C1 Bradfield	46–1900	0.51–0.83	IR	(3)
C/1975 N1 Kobayashi-Berger-Milon	78–2600	0.43–1.02	IR	(2), (3)
C/1975 V1 West	690–1,20,000	0.20–1.12	IR	(2), (3)
C/1979 Y1 Bradfield	1.63–441	0.57–1.75	VIS	(5), (6)
C/1980 E1 Bowell	500–3244	3.39–5.55	VIS	(6)
C/1980 V1 Meier	57.18	2.19	VIS	(5)
C/1980 Y1 Bradfield	1500–8300	0.28–0.79	IR	(3)
P/1980 Y2 Panther	577.8	1.86	VIS	(5)
C/1983 H1 IRAS-Araki-Alcock	200–22,000	1.01	IR	(3), (7)
C/1983 J1 Sugano-Saigusa-Fujiwara	0	1.06–1.08	VIS	(5)
C/1983 J1 Sugano-Saigusa-Fujiwara	<2	1.04–1.08	IR	(8), (3)
C/1984 V1 Levy-Rudenko	0.9–16.9	1.40–2.17	VIS	(9)
C/1985 R1 Hartley-Good	0.044–0.0874	1.25–1.28	VIS	(10)
C/1985 R1 Hartley-Good	4.47–14.5	0.98–1.27	VIS	(11), (12)
C/1985 T1 Thiele	58.2–96.2	1.48	VIS	(11)
C/1986 P1 Wilson	8.4–500	1.36–3.74	IR	(14), (3)
C/1986 P1 Wilson	683–1080	1.28–1.36	VIS	(11)
C/1987 P1 Bradfield	2120–2870	0.94–1.01	VIS	(11)
C/1987 P1 Bradfield	400–2000	0.87–1.45	IR	(13)
C/1988 A1 Liller	5000	0.9	VIS	(15)
C/1988 A1 Liller	529–2160	1.08–1.54	VIS	(11)
C/1989 Q1 Okazaki-Levy-Rudenko	450	0.95	IR	(16), (7)
C/1989 X1 Austin	30,000	0.36	VIS	(17)
C/1989 X1 Austin	300	0.78	IR	(18)
C/1989 X1 Austin	510^{+510}_{-205}	0.94	IR	(19)
C/1989 X1 Austin	2400	0.94	IR	(16), (7)
C/1990 K1 Levy	500–11,000	1.05–3.01	VIS	(6)
C/1990 K1 Levy	8700–9300	1.52–1.57	IR	(20)
C/1990 K1 Levy	6100	1.14	IR	(16), (7)
C/1995 O1 Hale–Bopp	500–58,800	2.4–13	VIS	(21), (22)
C/1995 O1 Hale–Bopp	30,000–1,50,000	2.54–4.58	IR	(23), (24), (7)
C/1995 O1 Hale–Bopp	1,00,000–18,00,000	0.91–3.17	submm	(25)
C/1995 O1 Hale–Bopp	15,00,000	0.91–1.01	mm	(26)
C/1996 B2 Hyakutake	1000–8000	0.5–1.5	VIS	(27)
C/1996 B2 Hyakutake	1860–3445	1.14–1.18	IR	(28)
C/1996 B2 Hyakutake	13,000	1.03	IR	(7)
C/1996 B2 Hyakutake	28,000	1.06–1.08	submm	(29)

Table 2 Continued

Comet	$Q_{\rm dust}$ (kg s^{-1})	$r_{\rm h}$ (AU)	Data	References
C/1999 S4 LINEAR	6300	1.07	IR	(7)
C/1999 S4 LINEAR	90	0.77	radio	(30)
C/1999 T1 McNaught-Hartley	100–300	1.20–1.27	VIS	(31)
C/2001 A2 LINEAR	∼900	1.30	IR	(7)

Note. (1) Finson and Probstein (1968); (2) Ney (1982); (3) Krishna Swamy (1991); (4) Fulle (1988); (5) Newburn Jr. and Spinrad (1989); (6) Sanzovo et al. (1996); (7) Lisse (2002); (8) Hanner et al. (1987a); (9) Sanzovo et al. (2001); (10) Landaberry et al. (1991); (11) Singh et al. (1992); (12) Singh et al. (1997); (13) Hanner et al. (1990); (14) Hanner and Newburn (1989); (15) Fulle et al. (1992); (16) Lisse et al. (1998); (17) Fulle et al. (1993a); (18) Hanner et al. (1993) ; (19) Lisse et al. (1994); (20) Lynch et al. (1992); (21) Fulle et al. (1998); (22) Rauer et al. (1997); (23) Lellouch et al. (1998); (24) Grün et al. (2001); (25) Jewitt and Matthews (1999); (26) de Pater et al. (1998); (27) Fulle et al. (1997); (28) Sarmecanic et al. (1997); (29) Jewitt and Matthews (1997); (30) Altenhoff et al. (2002); (31) Moreno et al. (2003).

interstellar dust particles onto Kuiper belt objects are an efficient source of ejecta particles with radii smaller than 10 μm. For this, the dust production rate ranges from 4×10^2 to 3×10^4 kg s^{-1} (Yamamoto and Mukai 1998). The latter dust production by impacts depends critically on the assumed surface properties of the icy Kuiper belt objects.

3 Circumstellar planetary debris dust

Discoveries and studies of planetary debris disks started two decades ago, when measurements of the spectral energy distribution of Vega revealed a faint excess in the infrared brightness. The excess is attributed to circumstellar dust and the dust lifetime is below the age of the central stars. The debris shells are observed around main-sequence or "old" pre-main-sequence stars younger than the Sun. The circumstellar structure cannot clearly be determined from the infrared excess alone. Measurements at far-infrared and submillimetre range, as well as observations of emission features allow to estimate the size distribution of the dust and to distinguish the dust from interstellar dust. Some relatively nearby systems can be studied with spatially resolved observations.

3.1 Detection of planetary debris disks from spectral energy distributions

3.1.1 Mid-infrared excess

Vega observations with IRAS showed the first infrared excess of circumstellar dust around a main-sequence star (Aumann et al. 1984). IRAS firstly measured the infrared excess also around other stars. Observations were made in spectral intervals centred around wavelengths of 12, 25, 60 and 100 μm; for further discussion of IRAS observations see Backman and Paresce (1993).

3.1.2 Search for near-infrared emission from near-star components

The majority of observations of circumstellar dust describe "cold" dust components that cause a far-infrared excess brightness. Some data of stars with "warm" dust components have been derived from ISO observations (Fajardo-Acosta et al. 1998): For eight systems, a 12 μm excess emission produced by dust that is located between 1 and 10 AU (angular radius 0.0028–0.074 arcsec, distances 70–250 pc) was observed. The dust temperatures range from 200 to 500 K and are below the average temperature for the solar system zodiacal cloud. The observed flux densities (0.085–0.155 Jy at 12 μm) exceed the flux estimate for a solar system type zodiacal dust cloud seen from 10 pc (0.0001 Jy at 10 μm). These 'warm' dust components are of special interest, since they are in regions where the habitable zones of these planetary systems are expected. In future, VLTI observations may allow searching for such near-star dust components.

3.1.3 VLTI observations

Interferometric measurements in the near-infrared are of special interest, since they can possibly resolve the most inner 10 AU of a planetary debris disk and therefore the regions of possible habitable planets as well as, even further inward the regions of dust sublimation. High-resolution observations of the stellar photosphere also allow confining stellar evolution models and determining the ages of the host stars of the planetary debris disks: Di Folco and collaborators have used the VLTI during commissioning period to study five nearby Vega-type stars in the K- and H bands (Di Folco et al. 2004). By direct size measurements of the stellar photospheres, they could improve estimates of the age of the stars, which will help understanding the time evolution of the planetary debris disks. They further obtained information about two of the dust disks.

3.1.4 Millimetre and submillimetre observations

Stars that harbour very cold disks may not reveal an observable excess of mid-infrared brightness, and moreover the detection of emission at large wavelength precludes the contribution of small dust particles, which could be interstellar dust. This shows that submillimetre observations are beneficial for analyzing spectral energy distributions not only by extending the observed spectral range. The advantage of the positional accuracy in comparison to the infrared data is mentioned later. Several searches have been carried out with the Submillimeter Common-User Bolometer Array (SCUBA) at James Clerk Maxwell Telescope (JCMT). They concentrated on different samples of stars with known infrared excess (Sylvester et al. 1996, 1994; Wyatt et al. 2003; Sheret et al. 2004). Sheret et al. (2004) carried out new observations and compiled the submillimetre observations, which were photometric and in some cases mapping observations: The photometric fluxes range from 0.066 to 1.925 Jy at 450 μm and between 0.0024 and 0.384 Jy at wavelength 850 μm. In roughly half of the 21 objects, only upper limits of the flux could be derived. The total amount of mass contained in the dust in these systems is estimated with between about 1/1000 and several earth masses. While these observations are of A-, F-, G- and K-type stars, recently some M-type

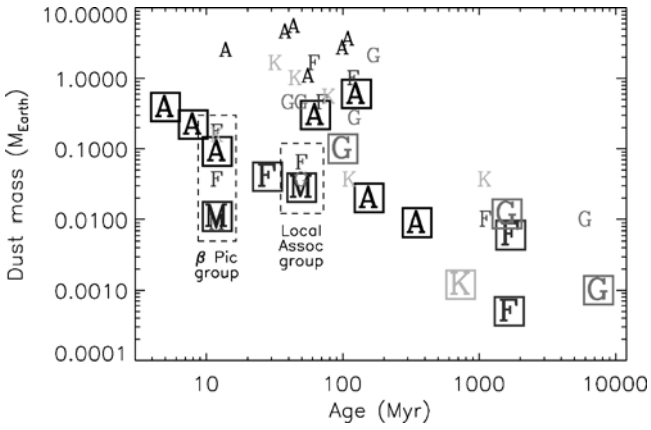

Fig. 5 The dust mass versus age of the star derived from submillimetre searches for planetary debris disks. Detected debris disks are shown as large letters in boxes; the letters denote the spectral type of the star. The small letters denote the non-detections and the given dust masses are upper limits, assuming 30 K dust temperature in interpreting the 850 μm non-detections. Observational data are from Wyatt (2003); Sheret et al. (2004); Liu et al. (2004) and this figure is from the latter reference

stars were observed (Liu et al. 2004). The observed dependence of debris mass and age of the stars is shown in Fig. 5.

3.1.5 Correlation of infrared excess and planet detection

For a long time, the direct observation of both a planet and a dust disk around a star was limited to one case only and it seems that only few stars host both inner giant planets and detectable planetary debris disks. Beichman et al. (2005) have searched for infrared excesses toward 26 field stars of type F-, G-, and K known to have one or more planets and have detected 70 μm excesses (but no excess at 24 μm) around six stars. The excesses are consistent with the presence of Kuiper belt analogues with 100 times more emitting surface area than in the solar system. A search for debris disks in the submillimetre regime around nearby stars that host giant planets resulted in no positive detection, implying that typical dust masses in these systems are less than 0.02 earth masses (Greaves et al. 2004a).

3.1.6 Need for spatially resolved observations

Measurements of the spectral energy distribution are a good tool to find evidence for circumstellar dust and planetary debris disks in surveys. It is interesting to note that the irregular structure of the dust disks may even be detected by photometry of the stars: Variations of the β Pictoris brightness from 1999 to 2002 were found to have a weak long-term variation of -0.8×10^{-3} mag per year (Lecavelier Des Etangs et al. 2005). The authors note that similar variations of the star have been observed before and suggest that they are caused by either dust inhomogeneities transiting the star or by variations of the dust structure. Nevertheless, observations of the infrared excess alone may not provide enough information to clearly identify a planetary debris disk and/or to study its properties.

Kalas et al. (2001) point out that in some cases of Vega-like stars, the dust responsible for excess thermal emission may originate from the interstellar medium rather than from a planetary debris system. They carried out coronagraphic optical observations of six Vega-like stars with reflection nebulosities. For five of them they found the emissivity is similar to that of the Pleiades, and concluded that they are caused by interstellar dust. Also, the confusion with background brightness components is possible. Sheret et al. (2004) have observed stars with known infrared excess in the submillimetre regime with SCUBA in order to confirm their origin from a circumstellar dust and to constrain the spectral energy distributions. Compared to the IRAS measurements, the SCUBA observations have a smaller positional uncertainty and therefore can be used to confirm whether the observed infrared brightness is really associated to the star and not to a background source. For the case of HD 123160, the existence of a dust disk could be rejected because the thermal emission brightness was detected with an offset of 10 arcsec from the star Sheret et al. (2004).

3.2 Spatially resolved observations of planetary debris disks

By far the best explored Vega-type object is β Pictoris, for which detailed images both in the visual and infrared have been obtained (Table 3). Resolved in visual–near-infrared (i.e. in scattered light) is also the disk around HR 4796A, which has a M companion star. Resolved in infrared and submillimetre (i.e. thermal emission) are more stars such as Vega (α Lyrae), ϵ Eridani and Fomalhaut (α Piscis Austrini) and 55 Cancri, which is known to host both a disk, resolved in the near-infrared, and a planet (Trilling and Brown 1998; Dominik et al. 1998; Trilling et al. 2000). Detailed information for some systems is given in the following sections and further discussion of the spatial distribution will follow in Sect. 5.

3.2.1 β Pictoris

Probably the most massive debris disk is observed around β Pictoris (HD 39060), a young main sequence star of spectral type A5 IV (Weinberger et al. 2003). Early studies assumed its distance from the Sun as 16.4 pc (Lanz 1986) and early studies of the dust disk refer to this value. According to measurements of the Hipparcos satellite, the distance is 19.28 ± 0.19 pc (Crifo et al. 1997). Also, various numbers for the stellar photospheric temperature exist such as $T_{\rm eff} = 8250$ K (Wahhaj et al. 2003) and $T_{\rm eff} = 8500$ K (Heinrichsen et al. 1999). The age of the star is assumed by Crifo et al. (1997) as 8×10^6 years, while other authors assume 2×10^8 years (Wahhaj et al. 2003) and $1\text{–}3 \times 10^8$ years (Kalas and Jewitt 1995), respectively. The stellar radius is $1.46\,R_\odot$ (Heinrichsen et al. 1999), the luminosity is 8.7 times the solar luminosity $L_\odot$ (Crifo et al. 1997) and its mass $1.7\text{–}1.8\,M_\odot$. Its proximity to the Sun and the high number density of the dust debris disk allowed for detailed imaging observations over a wide spectral range (see Table 3). They revealed the heterogeneity of the spatial distribution and allowed to infer the sizes of dust particles. Also some gas component are observed (see Sect. 6.1).

Table 3 Observations of the dust disk around β Pictoris and the distance of the observed dust from the star

Reference	Wavelength	Range (AU)
(1)	0.67 μm (R filter)	100–400
(2)	B, R, V, I filter	100–800
(3)	R linear polarised	300–600
(4)	B, V, R filter	40–300
(5)	0.67 μm (R filter)	40–100, 100–300
(6)	10 μm	<90
(7)	0.67 μm (R filter)	50–100, 100–800
(8)	B, V, R, I linear polarised	150–350
(9)	1.2 μm (J filter)	20–80
(10)	2.2 μm (K filter)	24–100
(11)	2.4–45.2 μm	<100
(12)	25 and 60 μm	
(13)	6–13 μm	<70
(14)	10–200	
(15)	790 μm	ca. 500–800
(16)	0.67 μm (R filter)	120–1834
(17)	11.7 μm, 17.9 μm	Up to 77
(18)	17.9 μm	Up to 100
(19)	1.2 mm	Up to 1050
(20)	12 μm	<90
(21)	12 μm	<90
(22)	12 μm	<200
(23)	K linear polarised	50–150

Note. The listed distances are those given by the authors. (1) Smith and Terrile (1984); (2) Paresce and Burrows (1987); (3) Gledhill et al. (1991); (4) Lecalvelier Des Etangs et al. (1993); (5) Golimowsky et al. (1993); (6) Lagage and Pantin (1994); (7) Kalas and Jewitt (1995) ; (8) Wolstencroft et al. (1995) ; (9) Mouillet et al. (1997b); (10) Mouillet et al. (1997a); (11) Pantin et al. (1997); (12) Heinrichsen et al. (1999); (13) Lagage et al. (1999); (14) Heap et al. (2000) ; (15) Kalas et al. (2000); (16) Larwood and Kalas (2001); (17) Weinberger et al. (2003); (18) Wahhaj et al. (2003); (19) Liseau et al. (2003); (20) Liseau et al. (2003); (21) Okamoto et al. (2004); (22) Telesco et al. (2005); (23) Tamura et al. (2006).

3.2.2 Fomalhaut

Fomalhaut (HD 216956) is a A3V main-sequence star at a distance of 7.69 pc (Holland et al. 1998) from the solar system. Its photospheric temperature is about $T_{\rm eff} = 9000$ K (Backman and Paresce 1993) and its luminosity as $13 L_\odot$ (Dent et al. 2000) to $16 L_\odot$ (Holland et al. 1998). The stellar radius and mass are assumed to be $1.7\,R_\odot$ and $2.3\,M_\odot$, respectively, the age is of the order of 100 Myr. Early observations at 0.87 and 1.3 mm show brightness excess but do not allow for reliably estimating the extension of the disk (Chini et al. 1990). Further submillimetre observations revealed a disk-like structure (Holland et al. 1998). Mapping at 450 and 850 μm with SCUBA showed a close to edge on narrow ring of dust around 150 AU from the star, with possibly azimuthal density variations along the ring: Observations at 450 μm, where the telescope beam size is equivalent to a resolution of 50 AU, reveal the existence of a clump or a ring arc (Holland et al. 2003). No gas disk was observed around Fomalhaut (Liseau 1999).

3.2.3 Vega

Vega (HD 172167) is a bright A0 V main sequence star at distance 7.76 pc from the Sun with an age of approximately 350 Myr (Aumann et al. 1984), luminosity of $60L_{\odot}$, mass of $2.5M_{\odot}$ and effective photospheric temperature of the order of $T_{\rm eff} = 9500$ K (Ciardi et al. 2001) (see also for detailed discussion). Photometry with ISOPHOT shows excess brightness of a factor of 1.7 at 25 μm, a maximum excess factor of 21 at 120 and 150 μm, and excess factor of 15 at 200 μm (Heinrichsen et al. 1998). Spatially resolved ISOPHOT data were obtained at 60 and 90 μm. Observations at 2.2 μm wavelength (K-band) show small, hotter dust particles located close to the star: With model calculations, the observed flux contribution of 3–6% can be reproduced by dust within 4 AU from the star (Ciardi et al. 2001). Observations at 0.87 and 1.3 mm show brightness excess beyond the stellar photospheric flux fitted with a blackbody curve by a factor of 3.7 and 1.7, respectively (Chini et al. 1990). These initial observations at 0.87 and 1.3 mm showed that the excess brightness is offset from the star and indicated that the dust cloud lies between 40 and 74 AU distance (Chini et al. 1990). Further submillimetre observations of emission peaks offset from the star indicated a possible disk-like structure (Holland et al. 1998; Dent et al. 2000). Mapping observations at 1.3 mm provided an image of several emission enhancements located along a circumstellar ring of 95 AU radius (Koerner et al. 2001). Observations with higher resolution and sensitivity showed that a large fraction of the observed emission is due to two dust emission peaks northeast and southwest from the star (Wilner et al. 2002). A search for planets showed that planetary companions in the debris disk can be excluded to a level of 6–8 Jupiter masses (Macintosh et al. 2003).

3.2.4 ε Eridani

ε Eridani (HD 22049) is a nearby 0.5–1 Gyr (730 Myr (Macintosh et al. 2003), 800 Myr (Henry et al. 1996)) old K2V star with a stellar mass of $0.8\,M_{\odot}$ (Quillen and Thorndike 2002). The star has a distance of 3.22 pc from the Sun (Greaves et al. 1998), and a stellar luminosity of $0.33\,L_{\odot}$ (Dent et al. 2000), an effective temperature of 5050 K (Saar and Osten 1997). Images of ε Eridani at 850 μm shows a signal out to about 115 AU radius (35 arcsec offset) with an emission peak at 60 AU and a reduced emission at 30 AU, which possibly indicates the inner edge of a ring-like dust distribution (Greaves et al. 1998). The dust ring is seen almost face-on. These results are confirmed with more recent observations, which also achieved the first imaging at 450 μm (Greaves et al. 2005). Asymmetries and bright peaks are also observable in the image. From observations of the excess emission at 100 μm Chini et al. (1990), in contrast, derive an inner and outer radius as 4 and 25 AU for dust particles of sizes between 162 and 486 μm, a total dust mass of $4.2 \times 10^{-9}\,M_{\odot}$, and temperatures at the inner and outer edge as 135 and 45 K, respectively. From ISO observations (60 and 90 μm mapping and low-resolution spectroscopy between 5.8 and 11.6 μm), Walker and Heinrichsen (2000) give a total mass of the dust disk of $1.1 \times 10^{-9}\,M_{\odot}$. A search for planets showed that planetary companions in the debris disk can be excluded to a level of 5 Jupiter masses (Macintosh et al. 2003). The gas component in the dust ring around ε Eridani ($m_{\rm gas}/M_{\rm dust} < 10^{-3}$) seems negligible (Liseau 1999).

3.2.5 AU Microscopii

With AU Microscopii (HD 197481), the first imaging of planetary debris around an M-type star was achieved. From SCUBA observations of the 850 μm excess emission Liu, Kalas and Mathews inferred the presence of a debris disk and confirmed this with spatially resolved observations using an optical stellar coronagraph (Liu et al. 2004; Kalas et al. 2004). Initial imaging revealed a dust signal between 50 and 210 AU where the dust lifetime exceeds the age of the star. The SCUBA data further suggest that the system is gas-poor, and that the inner disk void extends to approximately 17 AU, if the spectral energy distribution is explained with blackbody temperature of dust. The system appears in age similar to the β Pictoris disk (Kalas et al. 2004). Further imaging observations of scattered light show that the inner disk is asymmetric with various substructures; a change in the radial slope of the surface brightness profile is seen in the data at 35 and 33 AU, respectively (Liu 2004; Metchev et al. 2005). H-band imaging observations exclude the existence of planets larger than Jupiter-mass at distances larger than 20 AU from the star (Metchev et al. 2005).

3.2.6 HD 32297

A system that possibly reveals an asymmetric structure as consequence of interactions with the interstellar medium is the planetary debris disk around the A0 star HD 32297 (see also Sect. 7). IRAS observations indicated the existence of a dust disk and a nearly edge-on disk was imaged with HST in scattered light at 1.1 μm that extends to at least 400 AU (3.3 arcsec) along its major axis (Schneider et al. 2005). Optical stellar coronagraph observations from Mauna Kea show the dust structure from 560 to 1680 AU distance from the star is extremely asymmetric towards the southern wing which is in the vicinity of a relatively dense interstellar gas cloud and comparison to the HST data indicates the dust is probably blue (Kalas 2006).

3.2.7 τ Ceti

With 850 μm observations of τ Ceti (HD 10700), the first dust disk around a Sun-like (G8V) star of late main-sequence age was recently confirmed by imaging (Greaves et al. 2004b). The debris disk extends out to a radius of about 55 AU comparable to the Kuiper belt, but the dust mass is at least an order of magnitude greater than in the Kuiper belt.

3.2.8 η Corvi

For η Corvi (HD 109085) first spatially resolved observations of dust around a main-sequence F star were achieved in the submillimetre and mid-infrared with SCUBA (Wyatt et al. 2005) as two peaks in the emission brightness offset from the central star at projected distance of 100 AU. The observations at 450 and 850 μm are explained with a disk of radius 150 ± 20 AU seen at $45° \pm 25°$ inclination. The inner zone of the disk within 100 AU appears to be cleared of dust emitting in the submillimetre regime. When fitting the spectral energy distribution taking into

account mid-infrared data this is, in contrast, best explained with an additional hot dust component corresponding to a distance of only 1–2 AU (Wyatt et al. 2005).

3.2.9 HD 141569

An example for a relatively young system (<5 Myrs) for which the dust dynamics is still influenced by remnant gas is HD 141569. Spatially resolved observations of scattered light of its circumstellar dust disk were obtained with the Hubble Space Telescope at 1.1 and 1.6 μm wavelength (Augereau et al. 1999a,b; Weinberger et al. 1999). Refined observations with higher signal-to-noise ratio and spatial resolution reveal the heterogeneity of the disk with two ring-like structures at distances of about 200 and 325 AU from the star as well as an arc-like structure and a change of the tilt of the symmetry plane (Mouillet et al. 2001). Additional ground-based near-infrared (2.2 μm) observations allowed to constrain minimum grain size and size distribution in the disk (Boccaletti et al. 2003). Mid-infrared imaging at $\lambda = 12.5$, 17.9 and 20.8 μm fit to a flat radially symmetric inner dust disk indicating that near- and mid-infrared brightness picture the inner and outer parts of a common disk structure (Marsh et al. 2002). Both, the influence of a planet and the influence of stellar companions are discussed as possible perturbations to cause the observed structures (Wyatt 2005; Augereau and Papaloizou 2004).

3.3 Polarization measurements of planetary debris disks

Gledhill et al. (1991) measured the linear polarization in the R-band of the disk around β Pictoris in the range 15–30 arcsec from the star (i.e., roughly 300–600 AU). The degree of linear polarization along the mid-plane was $17 \pm 3\%$ with a dip around 24 arcsec in the northeast direction and a dip around 20 arcsec in the southwest direction. Linear polarization outward from about 150 AU in the B-, V-, R- and I-band confirmed the overall trend of the previous R-band data (Wolstencroft et al. 1995). Krivova et al. (2000) modelled the polarization of the disk using Mie theory and concluded that grains smaller than micrometre sizes are depleted in comparison to a power-law size distribution; in particular, in the southwest side of the disk. Tamura et al. (2006) measured the linear polarization of the inner K-band brightness and explain the polarization data with a model of ice-filled fluffy aggregate particles (see Fig. 6).

3.4 Dust sources in planetary debris disks

For the spatially resolved observations of the disks, their wide extension indicates that planetesimal-size objects are present and act as perturbers (Backman and Paresce 1993). These are also expected to feed the dust disks by collisional fragmentation. Moreover, there is some evidence for phenomena similar to cometary activity: Doppler shifted circumstellar components (Lagrange et al. 1989) observed in stellar photospheric UV absorption lines of the β Pictoris are explained with comets falling onto the star (Beust et al., 1989, and references therein). It is

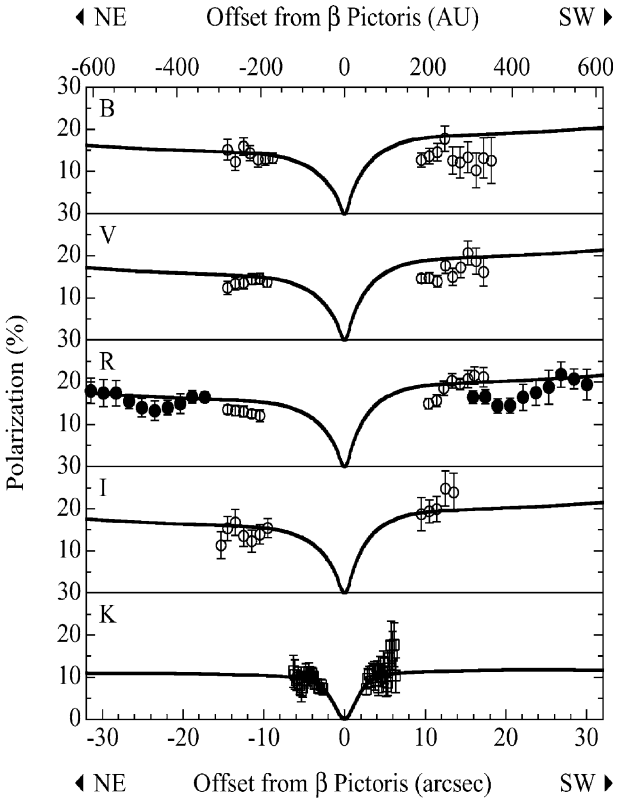

Fig. 6 The observed linear polarization as function of offset from β Pictoris: *filled circles* denote R-band data (Gledhill et al. 1991), *open circles* denote B-, V-, R-, and I-band data (Wolstencroft et al. 1995), and *squares* denote K-band data (Tamura et al. 2006). The *solid line* gives the model calculation (Tamura et al. 2006). This figure is adapted from Tamura et al. (2006)

suggested that the comets may have been brought to star-grazing orbits by perturbations of (yet unknown) planets (Beust and Morbidelli 1996; Levison et al. 1994).

4 Forces and effects

The major forces on the dust particles are the gravitational force and radiation pressure force of the central star. In some cases, stellar wind forces can be equally important as radiation pressure force, but the parameters of the stellar winds are uncertain. Surface charges of dust in planetary debris disks are expected to be slightly higher than that in the solar system. This is a result of enhanced photoionization. Lorentz force is important for small particles only and therefore has no significant influence on the observed dust components. Dust destruction by sublimation occurs far inward from 1 AU for refractory particles in the considered systems. Ices sublimate at several astronomical units distance and also UV

radiation can cause chemical alteration and erosion of the particles. The main destruction mechanism for dust in these systems is collisional fragmentation.

4.1 Gravitational forces

The gravity of the central star is the dominant force for most objects in circumstellar systems and their motion is roughly approximated as Keplerian orbits. For small dust particles, forces due to the stellar light and wind and Lorentz force can significantly affect their motions. This is because the gravity is proportional to the volume of dust particles, the forces caused by impact of photons and stellar wind particles are roughly proportional to the cross-section, and Lorentz force is proportional to the radius of the dust particles, provided that the particles are charged to the same potential.

The gravitational force, F_{g}, acting on a body with mass, m, is expressed as

$$F_{\mathrm{g}} = -G\frac{M_* m}{r^2} \tag{2}$$

where G is the gravitational constant, M_* is the mass of the star, and r is heliocentric distance of the body from the star.

Dust is further influenced by the gravitational force of the planets. Distant, non-resonant interactions cause small periodic oscillations of the orbital elements of the dust particles on long timescales. These are the most common planetary perturbations and they cause the rotational symmetry of the dust cloud, as well as of those meteoroids that are associated to the sporadic meteors. More severe perturbations occur for close encounters with the planets. Resonant perturbations occur when the orbital periods of planets and dust particles are such that the planet imposes a periodic perturbation, which will be discussed in Sect. 5.

4.2 Radiation pressure forces

The absorption and scattering of stellar light by dust particles lead to the radiation pressure on the dust, which is usually the most important non-gravitational force that determines the orbital evolution of dust. The resulting radiation pressure force, F_{PR}, is expressed as the product of momentum flux of the incident light and the cross-section:

$$F_{\mathrm{PR}} = \frac{L_*}{4\pi r^2 c} A\langle Q_{\mathrm{PR}}\rangle \tag{3}$$

where L_* is the stellar luminosity, c the speed of light, A the geometrical cross-section of dust and $\langle Q_{\mathrm{PR}}\rangle$ the radiation pressure coefficient averaged over the stellar spectrum $F_*(\lambda)$ defined as

$$\langle Q_{\mathrm{PR}}\rangle = \frac{\int_0^\infty F_*(\lambda)\, Q_{\mathrm{PR}}(m^*, \lambda)\, \mathrm{d}\lambda}{\int_0^\infty F_*(\lambda)\, \mathrm{d}\lambda}. \tag{4}$$

The cross-section $A\langle Q_{\mathrm{PR}}\rangle$ is similar to the geometrical cross-section A when the size of dust is much larger than the wavelength of typical incident light (geometrical optics). For small particles, $\langle Q_{\mathrm{PR}}\rangle$ strongly depends on the wavelength of light,

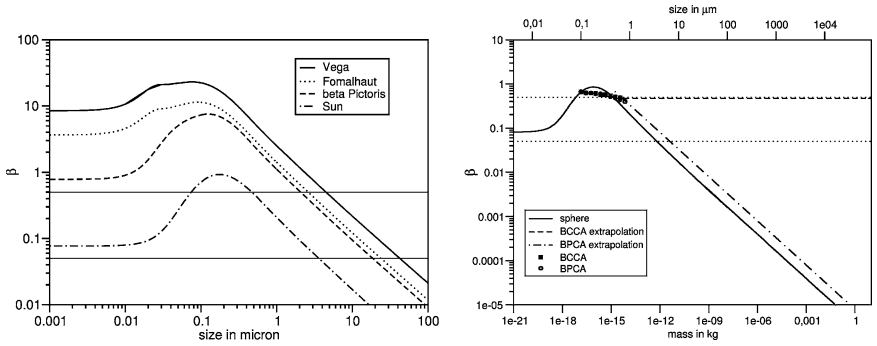

Fig. 7 Calculated β values for astronomical silicate. *Left*, for spherical grains in different systems; *right*, for BCCA and BPCA aggregates (*symbols*) in the solar system, compared to spherical grains (*solid line*) (Köhler 2005). The *dashed line* and the *dashed-dotted line* give the estimated extrapolations curves for the β values for larger aggregates. The *horizontal lines* in both figures indicate the limit of particles in bound and unbound orbits. The *upper line* for particles released by parent bodies on circular orbits and the *lower line* for particles released by parent bodies on high eccentric orbits ($e = 0.9$). Note that results are similar for small BPCA and BCCA particles. The particle model and light scattering calculations will be explained in Sect. 8

shape of dust and material composition of the particle through its optical constant m^*. For dust much smaller than the incident wavelength of light, the cross-section is proportional to the volume of dust (Rayleigh limit); $A\langle Q_{\rm PR}\rangle \propto V$.

The importance of the radiation pressure is commonly measured by the ratio of radiation pressure to gravity of the star as

$$\beta_{\rm PR} = \frac{F_{\rm PR}}{F_{\rm G}} = \frac{L_* A\langle Q_{\rm PR}\rangle}{4\pi G M_* mc}. \tag{5}$$

Note that the ratio $\beta_{\rm PR}$ is independent of heliocentric distance r. As seen in Eq. (5), $\beta_{\rm PR}$ is inversely proportional to the radius of the large dust where geometrical optics is applicable. For small dust, i.e. in the Rayleigh limit, $\beta_{\rm PR}$ is constant with size. Figure 7 shows that for some systems, $\beta_{\rm PR} > 1$ applies for all small particles, while for other systems, β can be below 1 again for particles in the Rayleigh limit. If the radiation pressure overcomes the stellar gravity, the dust is not in bound orbit around the star. Large bound-orbiting dust particles can suffer mutual collisions and produce small fragments, which are then blown out. These particles in hyperbolic orbits are called β-meteoroids. Radiation-induced ejection is one of the major fates of dust. Calculation of $\beta_{\rm PR}$ have been done for spherically shaped dust and various compositions using Mie theory. According to calculated $\beta_{\rm PR}$, dust in our solar system and β Pictoris is not in bound orbits if their size is smaller than $\sim$0.1 and 1–10 μm, respectively (Burns et al. 1979; Artymowicz 1988). For dust around AU Mic, which is a M-type star of low luminosity, the radiation force is not sufficient to blow out the dust of any size (Plavchan et al. 2005).

Unless the radiation pressure is strong enough to eject dust, the force due to star light decelerates the dust and gradually decreases the heliocentric distance of the dust. This effect is known as Poynting–Robertson effect and comes from a

finite aberration angle between direction of light and moving dust. A small, non-radial component of the radiation pressure force is exerted on the orbiting dust. The more correct expression of the radiation force on dust having velocity $\mathbf{v}$ can to order v/c be written as (Burns et al. 1979)

$$\mathbf{F}_{\mathrm{PR}} = F_{\mathrm{PR}} \left[\left(1 - \frac{\mathbf{v} \cdot \mathbf{r}}{c} \right) \frac{\mathbf{r}}{r} - \frac{\mathbf{v}}{c} \right]. \tag{6}$$

The non-radial term in Eq. (6) is opposed to the velocity vector of the dust, and thus dissipates the energy and angular momentum of dust. The falling time of dust with circular orbit from heliocentric distance r to the star is given as

$$\tau_{\mathrm{PR}} = \frac{r^2 \, c}{2 \, G \, M_* \, \beta}. \tag{7}$$

The falling timescale of $\sim \mu$m sized dust from 1 AU to the Sun is several thousand years. In our zodiacal cloud, the observed radial distribution of dust $\propto r^{-1}$ can be roughly explained by the result of the inward migration due to the Poynting–Robertson effect.

Due to the higher stellar fluxes, radiation pressure force in most of the circumstellar systems exceeds those in the solar system (see Fig. 7). Recently, the progress in optical theories and computational facilities makes it possible to calculate optical properties of more realistic irregularly shaped dust that are comparable to collected IDPs. The β values calculated for irregular dust models are shown on the right-hand side of Fig. 7, they can significantly differ from those of compact particles. It should be noted that in certain cases it may not be sufficient to approximate the stellar brightness in Eq. (4) with the Planck function $B_*(T)$, but rather to consider the observed spectrum $F_*(\lambda)$ of the star (Lamy 1976; Artymowicz 1988).

Circumstellar disks around other stars observed until today have a much higher dust density than the zodiacal cloud and timescales of mutual collisions are expected to be much shorter than τ_{PR}. Inward migration of dust by Poynting–Robertson drag is inefficient in such dense disks (e.g. Wyatt 2005).

4.3 Stellar wind forces

Like stellar light gives rise to the radiation pressure forces, the impacts of solar wind particles, mainly of protons and α particles, exert both a radial force and a non-radial drag force. The effects of the force, $\mathbf{F}_{\mathrm{SW}}$, on the dynamics of dust are similar to that of the electromagnetic radiation force, $\mathbf{F}_{\mathrm{PR}}$, given by Eq. (6). The expression of $\mathbf{F}_{\mathrm{SW}}$ is given as

$$\mathbf{F}_{\mathrm{SW}} = F_{\mathrm{SW}} \left[\left(1 - \frac{\mathbf{v} \cdot \mathbf{r}}{v_{\mathrm{SW}}} \right) \frac{\mathbf{r}}{r} - \frac{\mathbf{v}}{v_{\mathrm{SW}}} \right]. \tag{8}$$

where F_{SW} is the force on the dust for $\mathbf{v} = 0$ and v_{SW} the bulk velocity of the wind. The non-radial term in Eq. (8) is referred to as plasma or pseudo-Poynting–Robertson drag force. The force F_{SW} is expressed as

$$F_{\mathrm{SW}} = \frac{\dot{M}_* v_{\mathrm{SW}}}{4\pi r^2} A \langle Q_{\mathrm{SW}} \rangle \tag{9}$$

where $\dot{M}_*$ is the mass loss rate of the central star and $A\langle Q_{\rm SW}\rangle$ the momentum transfer cross-section averaged over the wind species. For the stellar wind force, we can define $\beta_{\rm SW}$ as

$$\beta_{\rm SW} = \frac{F_{\rm SW}}{F_{\rm G}} = \frac{\dot{M}_* v_{\rm SW} A\langle Q_{\rm PR}\rangle}{4\pi G M_* m}. \tag{10}$$

The ration $\beta_{\rm SW}$ is independent of the heliocentric distance except near the star ($v_{\rm SW} \neq const$) and outside the astrosphere.

In our solar system, the wind's radial force is negligible compared to the radiation pressure; $F_{\rm SW}/F_{\rm PR} \sim 10^{-3}$. Although the momentum flux of the solar wind is 3 orders of magnitude smaller than that of the electromagnetic radiation, the plasma Poynting–Robertson drag is not negligible. From Eqs. (6) and (8), the ratio of plasma Poynting–Robertson drags force to (photon) Poynting–Robertson drag force can be written as

$$\frac{F_{\rm SW}}{F_{\rm PR}}\frac{c}{v_{\rm SW}} \simeq 0.3\left(\frac{\dot{M}_*}{\dot{M}_\odot}\right)\left(\frac{L_*}{L_\odot}\right)^{-1}\left(\frac{\langle Q_{\rm SW}\rangle}{\langle Q_{\rm PR}\rangle}\right) \tag{11}$$

where $L_\odot$ and $\dot{M}_\odot$ are solar luminosity and mass loss rate, respectively. The factor $c/v_{\rm SW}$ comes from the difference in the aberration angles.

In the case of dust disks around other main-sequence stars, the lack of clear knowledge about the stellar wind has made it difficult to discuss the wind's forces on dust. From recent HST observations, Wood et al. (2002) and Wood et al. (2005a,b) infer that the mass loss rate $\dot{M}_*$ of Sun-like stars decreases as the age of the stars increase and that in their young stages the star is up to ∼100 times more massive than the current solar value. If one combines this high mass loss rate and Eq. (11), the plasma Poynting–Robertson drag becomes much stronger than (photon) Poynting–Robertson drag and thus the timescale of inward migration can be by far shorter than previously thought (Plavchan et al. 2005). The wind's radial force can overcome the stellar gravity for small dust (smaller than ∼0.01–0.1 μm) around the high mass loss rate ($\dot{M}_\star = 100$–$1000\,\dot{M}_\odot$) stars even if one simply assumes $\langle Q_{\rm SW}\rangle \sim 1$.

Beyond the earlier simple estimations, more detailed studies of the force have been done especially for the solar system. Distant encounters between the solar wind particles and the dust particles cause dynamical friction described as the indirect or Coulomb solar wind drag (Morfill and Grün 1979). The dynamic effects of the Coulomb drag are the same as those of the direct drag, but its strength is about 3 orders of magnitude less. Mukai and Yamamoto (1982) showed that the effect of sputtering on the dust increases the drag force by a factor of <0.5. Minato et al. (2004) studied the effect of the passage of the impinging ions through small dust grain and showed that the dependence of the cross-section $A\langle Q_{\rm SW}\rangle$ on dust size is analogous to that for the electromagnetic radiation force. For dust smaller than the range of impinging ions (0.01–0.1 μm), the cross-section is proportional to the volume of dust $A\langle Q_{\rm SW}\rangle \propto V$, and for the larger dust, the cross-section is nearly its geometrical cross-section.

For small dust particles the neutral-gas drag force on dust particles in the outer solar system was shown to cause significant changes in the semimajor axes and eccentricities, leading to lifetimes of only $\sim 5 \times 10^5$ years for 1 μm dust particles (Scherer 1999).

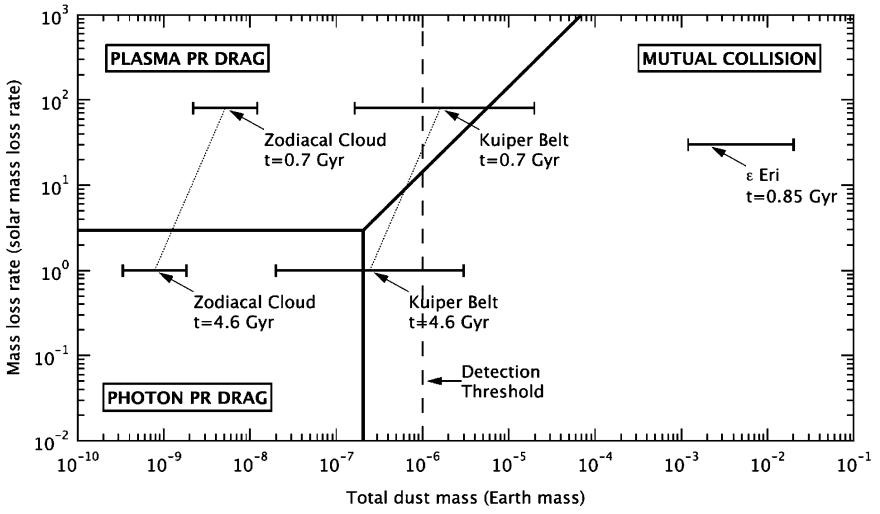

Fig. 8 The scales for photon Poynting–Robertson lifetime, plasma Poynting–Robertson lifetime and collision lifetime for dust in the solar system at present and at 0.7 Gyrs. The variation of the solar photon flux over this time is almost constant compared to variation of stellar wind flux. As a result, the plasma Poynting–Robertson effect is more important in the early solar system (Minato et al. 2006)

4.4 Lorentz force

The Lorentz force reads

$$\mathbf{F}_{\mathrm{L}} = q\mathbf{V} \times \mathbf{B}, \tag{12}$$

where q is the electric surface charge, $\mathbf{V} = \mathbf{v} - \mathbf{v}_{\mathrm{SW}}$ is the velocity of the dust relative to the solar wind, and $\mathbf{B}$ the magnetic field vector carried with the solar wind. As the dust particles move through the sectored magnetic field of the Sun with alternative polarities, the Lorentz force changes its direction. For particles in bound orbit, this causes changes in a, e and i (Morfill and Grün 1979; Consolmagno 1979, 1980; Barge et al. 1982a,b; Wallis and Hassan 1985).

Submicrometre particles, in particular when they reach the strong magnetic field near the Sun, can be ejected from the system by the Lorentz force (Hamilton et al. 1996; Mann et al. 2004b). Nanometer-sized particles are even ejected near earth orbit and by interaction with the solar wind are accelerated to solar-wind velocity (Mann et al. 2006).

4.5 Dust erosion and surface alteration

4.5.1 Dust surface charging

Photoelectron emission, sticking and recombination of plasma particles, secondary electron emission, thermionic emission and field emission electrically charge dust particles in space. The dust particle charge depends on the size, shape

Table 4 The zone of sublimation calculated for different materials

	Sphere	Fluffy	References
Graphite	$\leq 5\,R_\odot$	$\leq 2\,R_\odot$	(2), (3), (6), (8), (9)
Glassy carbon	$4\,R_\odot$	$3–4\,R_\odot$	(10), (11)
Magnetite	$10–40\,R_\odot$	–	(7)
Iron	$11–24.3\,R_\odot$	–	(4), (5)
Water ice	1–2.8 AU	–	(2), (5), (7)
FeO-poor obsidian	$1.9–7\,R_\odot$	$2.5–3\,R_\odot$	(4),(6),(7),(8), (9), (10), (11)
FeO-rich obsidian	$2.9–6\,R_\odot$	—	(6), (9)
Andesite	$9–10.5\,R_\odot$	–	(3), (4), (5)
Basalt	$6\,R_\odot$	–	(9)
Quartz	$1.5–4\,R_\odot$	–	(1), (2), (5)
Astronomical silicate	$14\,R_\odot$	–	(9)
Crystalline Mg-rich olivine	$10\,R_\odot$	$9.5–11\,R_\odot$	(12)
Amorphous Mg-rich olivine	$13.5–15.5\,R_\odot$	$12–15\,R_\odot$	(12)
Crystalline Mg-rich pyroxene	$5\,R_\odot$	$5\,R_\odot$	(12)
Amorphous Mg-rich pyroixene	$5.5–6.5\,R_\odot$	$5–6.5\,R_\odot$	(12)

Note. (1) Over (1958); (2) Mukai and Mukai (1973); (3) Mukai et al. (1974); (4) Lamy (1974a); (5) Lamy (1974b); (6) Mukai and Yamamoto (1979); (7) Mukai and Schwehm (1981); (8) Mann et al. (1994); (9) Shestakova and Tambovtseva (1995); (10) Kimura et al. (1997); (11) Krivov et al. (1998); (12) Kimura et al. (2002).

and structure of the particles, UV flux, their velocity relative to the plasma and the plasma temperature, which defines the velocity distribution of in-falling plasma particles. (To our knowledge, no detailed studies on the influence of the dust shape and structure on the charging have been carried out so far.) Since photoelectron emission, secondary electron emission and thermionic emission vary with the material, the dust surface charge also depends on the dust composition. As a result of the dominating photoelectron emission caused by the solar radiation, dust particles in the interplanetary medium, as opposed to dust in denser plasmas such as in planetary magnetospheres, are usually positively charged. The calculated charge of dust in the interplanetary medium corresponds to surface potentials relative to infinity of between 5 and 10 V (Mukai 1981). The equilibrium surface charge of dust particles of $\sim\mu$m size in the solar system is attained in timescales of around 10^4 seconds or less, i.e. in less than a day. Temporal variations of the solar wind parameters yield fluctuations of the surface charge of 20% and less (Kimura and Mann 1998b). For particle sizes of the order of 10 nm and below, charge fluctuation are important compared to the dynamical timescales (Mann et al. 2006).

The charging of dust grains in extra-solar circumstellar systems can be estimated by considering the photoelectron emission. So far, the information about stellar winds are very rare. The energy of the photons can be estimated from stellar spectrum. In the case of β Pictoris, Vega and Fomalhaut the maximum of the stellar spectrum lies at about 0.33 μm (compared to solar system $\sim$0.5 μm). As a result, the surface charges are possibly higher than those derived for dust in the solar system.

4.5.2 Sputtering

Bombardment of energetic particles onto dust particles results in sputtering of atoms and molecules from the surface of the dust particles. The mass loss rate

per surface area due to sputtering is found to be size independent and bombardment of solar wind particles causes stronger sputtering than that of cosmic rays of higher energies but lower fluences (Mukai and Schwehm 1981). The erosion by sputtering is mostly independent of the temperature of dust particles, though for ice particles its sudden increase close to the sublimation temperature is measured (Lanzerotti et al. 1982). For magnetite particles of 1 and 10 μm size at 0.5 AU, Mukai and Schwehm (1981) calculate lifetimes of 1×10^{11} s and 1×10^{12} s (3000–30,000 years) respectively. By comparison to the Poynting–Robertson lifetime, they conclude that most interplanetary dust particles for average solar wind conditions drift toward the Sun under moderate erosion by sputtering.

4.5.3 UV alteration

The stellar UV radiation deposits energy in the grains, which can, aside from heating, cause chemical alteration of the volatile and semi-volatile dust material. In particular, the desorption and chemical alteration of ices and organics are interrelated, and together with the release of light elements, the refractory organics can also form, as the structure of dust particles is changed (Mukai et al. 2001). For the photosputtering of water ice in β Pictoris, Artymowicz (1997) shows that the resulting lifetime of water ice is of the order of Kepler orbital period and below other relevant lifetimes.

4.5.4 Collisional fragmentation

Relative velocities of dust in the solar system and in extra-solar planetary systems are of the order of fractions of the orbital velocities and typically in the range of kilometre per second. Mutual collisions are therefore catastrophic and lead to the destruction of particles. Fragmentation occurs at speeds exceeding about 1 km s^{-1} and fragments are distributed according to a power-law size distribution $n(s) = s^{-p}$ with $p = 3.5$ derived from laboratory measurements (Fujiwara et al. 1977). Values of p slightly greater than 3 are derived from an analytical theory based on estimates of the propagation of shock waves in solids (Jones et al. 1996). The exact critical velocities for fragmentation and vaporization of materials depend on the impact speed, on the size of target and projectile and on the material. The amount of vaporized material is typically small but notable in the interplanetary medium (Mann and Czechowski 2005).

4.5.5 Sublimation

The sublimation of dust particles depends on the temperature and the physical and chemical properties of the dust. It was estimated for typical dust analogue materials, such as silicates, metal oxides and different forms of carbon. Dust particles composed of pure water ice are estimated to sublimate at a few astronomical units from the Sun (Mukai and Mukai 1973; Lamy 1974a; Mukai and Schwehm 1981). Contaminated water-ice dust particles attain higher temperatures and thus sublimate at larger heliocentric distances (Mukai et al. 1985). Refractory dust particles consisting of silicates, carbons and metals sublimate closer to

Table 5 Plane of symmetry of the zodiacal cloud derived from visual (VIS) and infrared (IR) observations

i (°)	Ω (°)	Data	Reference
<2	–	VIS	Robley (1975)
3.7 ± 0.6	66 ± 11	VIS	Leinert et al. (1976)
1.5 ± 0.4	96 ± 15	VIS	Dumont and Levasseur-Regourd (1978)
3.0 ± 0.3	87 ± 4	VIS	Leinert et al. (1980)
1.0 ± 0.3	20 ± 6	VIS	Winkler et al. (1985)
2.03 ∓ 0.5	57^{+7}_{-3}	VIS	Mukai et al. (2003)
1.6–3.0	77–110	IR	Murdock and Price (1985)
2.3 ± 0.1	70 ± 5	IR	Deul and Wolstencroft (1988)
1.71 ± 0.01	77.1 ± 0.4	IR	Reach (1988)
1.1 ± 0.1	79 ± 1	IR	Rowan-Robinson et al. (1990)
1.45 ± 0.1	53 ± 1	IR	Reach (1991)
1.54 ± 0.01	40.9 ± 0.4	IR	Vrtilek and Hauser (1995)
2.03 ± 0.017	77.7 ± 0.6	IR	Kelsall et al. (1999)

the Sun (Mukai and Mukai 1973; Lamy 1974a,b; Mukai et al. 1974; Mukai and Yamamoto 1979; Mukai and Schwehm 1981). The location of sublimation zones depends not only on the size and composition of the dust particles, but also on their porosities (Mann et al. 1994; Kimura et al. 1997). If dust particles are aggregates of small constituent monomers, sublimation becomes less dependent on their overall sizes but rather on the size of the constituent dust particles (Kimura et al. 2002). Table 5 gives a compilation of sublimation zones estimated for a variety of dust particles with different assumptions for composition and structure (Mann et al. 2004b).

In a different approach, Mann and Murad (2005) consider the sublimation sequence of typical meteoritic and cometary silicates and show that metal oxides (here MgO) survive up to very close distances from the Sun, while silicon oxides sublimate at lower temperatures already and pure silicon is unlikely to form. The study is based on the material parameters of enstatite but a typical and common meteoritic material. Knowledge about organic refractory components, as they are expected to be present in the cometary dust, is poor. Since the chemical appearance is not yet understood, sublimation temperatures or zones near the Sun cannot be calculated. There is also no direct evidence for the fractional sublimation of some of the dust constituents. Observations of pick-up ions in the solar wind indicate the presence of an inner source, which peaks near the Sun (0.1 to about 0.3 AU) and contains the elements present in the solar wind up to Mg as well as some molecular ions (Gloeckler et al. 2000). The inner source was recently explained with ion species that are produced by the vaporization of dust material upon mutual collisions (Mann and Czechowski 2005). The presence of the carbon source at small distances from the Sun possibly indicates that some of the organic refractories are heat resistant and sublimate inward from 0.1 AU.

5 Spatial distributions

The presence of planets shapes the dust distribution in the solar system, but this effect is comparatively small. More pronounced structures in the solar system dust

cloud are observed due to the uneven distribution of the parent meteoroid population. Consequently, the dust cloud is structured in the regions where it is locally replenished. The smooth appearance of the dust cloud near 1 AU may indicate there are less local sources than in the asteroid belt or in the inner solar system. Similarly, for the planetary debris disks, one might conclude that orbital resonances of the dust particles are smeared out, since the forces acting on the dust particles depend on the dust size. The resonances, if they are the cause of the spatial structures, may act more efficiently on the meteoroid sized parent bodies.

5.1 Spatial distributions of solar system dust

5.1.1 The spatial distribution of dust in the inner solar system

The different zodiacal models, such as those of Leinert et al. (1977), Murdock and Price (1985), Giese et al. (1986) and Good et al. (1986) converge near 1 AU in their relative slopes of the density distribution (Giese et al. 1986), but the values derived for absolute dust number densities vary. The radial slope agrees with the picture that particles are in orbits with low eccentricity and drift to the Sun under Poynting–Robertson effect. The smooth structure and the rotational symmetry of the overall dust cloud near 1 AU relative to an axis through the Sun is confirmed by zodiacal light observations. In terms of orbital evolution, it can be explained by the randomisation of the orbital elements argument of perihelion ω and of the ascending node Ω. The rotationally symmetric number density distribution n is given as a function of solar distance r and helio-ecliptic latitude (or the latitude from the plane of symmetry, respectively) $\beta_{\odot}$, radial and latitudinal dependence are often assumed to be separated: $n(r, \beta_{\odot}) = n_0 f(r) g(\beta_{\odot})$. The zodiacal light continues smoothly into the solar F-corona, but since the coronal brightness is strongly influenced by forward scattering at dust near 1 AU this does not proof a smooth continuation of the dust distribution. Findings about dust in the inner solar system will be further discussed in the next section discussing the collisional evolution.

5.1.2 Spatial distributions of dust in the outer solar system

The small number of measurements, together with the low density of the dust cloud in the outer solar system make it difficult to assess the present data. The recent studies of the interstellar dust show that the order of magnitude of detected dust fluxes in the outer solar system can well be explained with the flux of interstellar dust that is confirmed from measurements inward from 5 AU (Mann and Kimura 2000). Nevertheless, there is some experimental evidence for other dust components in the outer solar system. The variation of the Voyager flux rates is above statistical limits and hence is better explained with Kuiper belt object dust particles rather than with interstellar dust (Mann and Kimura 2000). Although the Pioneer in-situ measurements are not in agreement with the optical observations aboard the same spacecraft, they showed that the existence of dust particles beyond 5 AU is not limited to the direction of the interstellar dust flux. While Humes (1980) initially explained the Pioneer data with dust in orbits with high eccentricity and high inclination, Grün et al. (1994) suggested the flux to originate from

large interstellar particles that are focused in the solar gravity field. This was later studied in detail by Landgraf et al. (2002). Still the disagreement with the optical observations aboard Pioneer remains (see Sect. 2.1.5). Therefore, these limited experimental results should be treated with some caution.

The thermal emission brightness of the Kuiper belt object dust population is near or below observational limits set by the foreground zodiacal emission (Backman et al. 1995; Stern 1996). The optical depth of the Kuiper belt object dust is predicted between 2×10^{-7} and 2×10^{-5} (Yamamoto and Mukai 1998; Stern 1996). If Kuiper belt object dust particles are predominantly composed of icy material, they effectively sublimate between 3 and 8 AU (Mukai 1986). The ejection of Kuiper belt object dust (Liou et al. 1996) will be further discussed later in the context of resonances.

5.1.3 Plane of symmetry

The zodiacal dust is concentrated in a plane that shows a slight tilt relative to the ecliptic. Since the symmetry plane is expected to reflect the dominant perturbing forces, such as the perturbation of the planets, it should be close to the invariable plane of the solar system with inclination $i = 1.6°$ and ecliptic longitude of the ascending node $\Omega = 107°$, but different values are derived from the observations (see Table 5).

From ground-based visible light observations, Dumont and Levasseur-Regourd (1978) find the inclination of the cloud symmetry plane $i = 1.5° \pm 0.4°$ and the ecliptic longitude of the ascending node $\Omega = 96° \pm 15°$. Visible light observations at small elongations from the Helios spacecraft between 0.3 and 1 AU give $i = 3.0° \pm 0.3°$, $\Omega = 87° \pm 4°$ (Leinert et al. 1980). Infrared observations give values of $i = 1.7° \pm 0.2°$, $\Omega = 79° \pm 3°$ and $i = 3.0° \pm 0.1°$, $\Omega = 55° \pm 4°$ as listed in (Leinert et al. 1998). It should be noted that the symmetry plane is not always derived directly from the data, but may also depend on the brightness model used to fit the data. Moreover, even if we consider observations only from 1 AU, the brightness at different wavelengths and elongations originates from different locations along the LOS, and hence does not always describe the same part of the cloud.

Closer to the Sun, the Lorentz force acting on the small dust particles, may lead to the alignment of the cloud with the solar equator: $i = 7.3°$, $\Omega = 75.7°$. This can be especially the case for micrometre-size and smaller dust particles (Mann et al. 2000). Whether these small dust particles have a noticeable contribution to the LOS brightness is not clear. A change in the cloud symmetry plane closer to the Sun can also be attributed to the gravitational perturbations from Venus, the orbital plane of which has $i = 3.4°$, $\Omega = 76°$ (Gustafson 1985; Gustafson and Misconi 1986).

5.2 Local density variations

5.2.1 Dust bands and dust trails

IRAS observations in 1983 revealed the existence of several solar system dust bands, brightness enhancements caused by dust particles with similar orbital

parameters (see Sykes 1990). In some cases, the orbital parameters are similar to those of the asteroid families, but many asteroid families have no associated dust bands. Nesvorný et al. (2003) suggest this is due to the advanced age of these asteroid families and that the dust bands are primarily by-products of recent asteroid break-up events.

Narrow trails of dust coincident with the orbits of periodic comets have been found in the IRAS data (Sykes et al. 1986). The particles are in orbits close to that of the parent comet and seen both ahead and behind the comet. The trails were studied in detail for eight comets and more than 100 faint dust trails are suggested by the IRAS data (Sykes and Walker 1992). Based on this survey, the authors conclude that the trail phenomenon is common to short-period comets.

Recently, Ishiguro et al. (2002) have found the visible dust trail existed along the orbit of comet 22P/Kopff. The trail consists of large (a few centimetre) and dark (albedo of 0.01) dust grains ejected from parent comet. Ongoing observational programs show that dust trails are a common feature of comets. Similar spatial variations can be expected for planetary debris disks, but most authors concentrate on the discussion of orbital resonances to explain the spatial structures in planetary debris disks.

5.2.2 Resonances

Resonances occur when a periodic perturbation is imposed to a system that is able to oscillate, such as an object orbiting a central star. In that case, orbital resonances occur for objects in orbit whose orbital period is in (small) integer ratios to the period of a planet. Since even small perturbations tend to grow, objects may be ejected from these resonances; on the other hand, they can be trapped in the orbital resonance at least for a certain time. The most obvious case of orbital resonances in the solar system is that of the asteroids: within the asteroid belt, asteroids avoid the zones where orbital periods are in ratios 1:3, 2:5, 3:7, or 1:2 with the orbital period of Jupiter (Kirkwood gaps), while an accumulation of asteroids is seen in the range of the 1:1 resonances, for instance, (Trojans). Long-term trapping is expected for the outer mean motion resonances and for instance, for a particle approaching earth, passing the resonance gradually increases the eccentricity of the orbit until the particle reaches a planet-crossing orbit from which it is expelled by close encounter with the planet. A set of particles in librating orbits with the orbital eccentricity enhanced by this resonance would form a density enhancement that rotates with the planet (Kuchner et al. 2000). Thus, the mean motion resonances can form density wave patterns, some of which may show in circumstellar disks observable orbital periods (Ozernoy et al. 2000). The resonances can also cause a depletion of the dust inward from the orbit of the planet. The mechanism for clearing up the inner region is a temporary trapping of grains by the planet in outer resonances, which act as barriers, stopping the inward motion of dust toward the star.

Dermott et al. (1994) suggest this structure formed for interplanetary dust reaching earth orbit. As a result, faint signals due to such a local dust enhancement leading and trailing the earth were found in the COBE infrared observations of the zodiacal light (Reach et al. 1995). It is suggested that in a similar way the presence of planets would form clearance zones in planetary debris disks.

Liou et al. (1996) calculated the orbits of dust grains of diameters 1–9 μm and find that due to resonances with the outer giant planets only 20% of the grains evolve to the inner solar system. Since the zodiacal dust covers a broad size interval, where in particular the small grains might be influenced by other forces besides gravity, the features that result from resonances are possibly smeared out. A search in infrared observations for a wake of dust trailing Mars and for dust in the Trojan region near Jupiter was not successful (Kuchner et al. 2000).

Nevertheless, the resonance structures in circumstellar dust disks are possibly stronger that those observed in the solar system. The resonant structure that build up in a dust cloud depends among other on the lifetime of the particles (Ozernoy et al. 2000). Modelling a distribution of test particles shows that presence of a planet influences a dust disk via resonances and gravitational scattering and also that for a rather massive planet the arising structure may have a high contrast relative to the background dust cloud, if the lifetime of the particles is limited by collisions (Ozernoy et al. 2000). Kuchner and Holman (2003) discuss the resonant structures caused in a dust cloud by single planets in orbit with eccentricity $e < 0.6$. They find that four different types of typical resonance geometries can arise. They suggest that three of them are similar to the structures observed in the solar system dust cloud or around Vega, ε Eridani and Fomalhaut, but the enhancements are not quantified. It is also quite possible that the observed structures in the planetary debris disks are a combination of the dust band phenomenon and the resonance effect. In a model to describe the observed structure of the β Pictoris disk, Augereau et al. (1999b) suggest those do not form due to the resonances arising for the dust: rather planetesimals are perturbed by a giant planet and provide a source of the collisionally produced dust.

5.3 Spatial distributions of dust in planetary debris disks

5.3.1 Inner depletion zones

An important feature of the spatial distribution is the radial dependence of the dust spatial density. Many observed Vega-type stars have disks with the density first increasing and then increasing slower or even decreasing with decreasing distance from the star (Backman and Paresce 1993). For instance, β Pictoris was initially assumed to show an inner depletion zone at about 40 AU, and outside this distance the number density of the cross-section-dominating grains slopes as $r^{-2.7}$ to $r^{-3.4}$. For two other resolved systems – HD 141569 and HR 4796A – the brightness also increases outward from the star, reaches a maximum and then decreases (Augereau et al. 1999a,b; Schneider et al. 1999; Weinberger et al. 1999). The existence of planets and the collisional destruction of dust can both cause the inner depletion zones.

5.3.2 The β Pictoris disk observations

Aside from the existence of an inner zone of reduced dust density, spatially resolved observations show a number of spatial structures in the β Pictoris disk (see Table 6). Kalas and Jewitt (1995) used observations in the 0.67 μm (R filter) wavelength with 0.41 arcsec per pixel spatial resolution to describe five asymmetries in

Table 6 Parameters derived for the density enhancements detected around β Pictoris (Kalas et al. 2000; Wahhaj et al. 2003)

Kalas et al. (2000)				Wahhaj et al. (2003)			
Ring	Radius (AU)	Surface brightness (mag arcsec^2)	Enhancement (%)	Ring	Radius (AU)	i (°)	Optical depth
A	785	23.5	>20	A	14 ± 1	-32 ± 2	5.9×10^{-3}
B	710	23.7	10	B	28 ± 3	$+25 \pm 2$	2×10^{-3}
C	647	24.1	5	C	52 ± 2	-2 ± 2	7.7×10^{-3}
D	608	24.0	5	D	82 ± 2	$+2 \pm 2$	2.3×10^{-2}
E	575	24.0	5				
F	543	24.0	5				
G	506	24.0	5				

the β Pictoris disk. The radial extension of the disk is 790 AU in northeast direction, while it is only 650 AU in southwest direction. Later observations allowed to detect the disk further out to 1062 AU in southwest direction and 1835 AU in northeast direction (Larwood and Kalas 2001). The disk in northeast direction outside of a radius of 330 AU is brighter than that at the same distances from the star in southwest direction. The width of the disk outward from 150 AU from the star is larger in the southwest direction compared to the northeast direction. The northeast wing is more extended to the north from the symmetry axis, while the southwest wing is more extended to south from the symmetry axis ('butterfly asymmetry'). The position angle of the northeast wing differs from that of the southwest wing by 1.3°. Further imaging observations of β Pictoris were made by Kalas et al. (2000) and Wahhaj et al. (2003). Both groups observe features that indicate the existence of rings: Kalas et al. (2000) in the outer disk at 785–506 AU, while Wahhaj et al. (2003) detect features inward of 85 AU.

5.3.3 β Pictoris disk models

Kalas and Jewitt (1995) attempted to explain the asymmetries with the presence of a massive body in the disk. The required parameters were a mass of 0.3 stellar masses moving in orbit with inclination 30° to the disk at minimum distance 700 AU from the star. The resulting ring structure would be pronounced in one side of the disk, as is observed (Kalas et al. 2000). Also the influence of steller encounters was considered. This encounter would also change the orbital inclination within the disk which could account for the "butterfly asymmetry" (Kalas and Jewitt 1995).

Refined calculations (Larwood and Kalas 2001) give a value of 0.5 $M_\odot$, prograde orbit and small inclination toward the disk axis for the perturber. The small velocity would suggest it be in bound orbits around the star, while the simulations show that the perturber would destroy the formed structure during subsequent orbital periods. If the structure were formed by a single encounter then it happened 10^5 years ago (Larwood and Kalas 2001).

The same group checked for stars that have encountered the β Pictoris system during the past 10^6 years and found that 22 stars could have possibly influenced the system. While most of the encounters would generate a cloud of planetesimals

to fall into the inner parts of the system, only six encounters within 0.1 pc possibly had a direct influence on the structure of the dust disk (Kalas et al. 2001).

Wahhaj et al. (2003) discovered features in the 17.9 μm spectral regime at distances inward from 85 AU, which seen in both wings of the disk so that they might are be explained with dust rings. Table 6 lists the observed density enhancements as well as the optical depth that is associated to these rings. The outer ring, denoted as D, is generated by dust in high-eccentricity orbits, while others have circular orbits. Some of the gaps between the rings are different for the southwest and the northeast direction (Wahhaj et al. 2003).

Models to explain these rings suggest gravity perturbations due to the presence of a planet, dust ring formation due to radiation pressure, collisions or interactions with the gas component, or again the perturbations caused by the encounter of a star or massive body. Models that assume the presence of a single planet can explain the observed inner ring structure (see discussion by Wahhaj et al. (2003)), but they cannot explain the complex structure of the entire observed system (Wahhaj et al. 2003), which rather is explained with a system of planets. In this case, the rings would be located in the resonance zones of the planets. The observation of the inner system also shows inclination relative to the symmetry plane which is opposite to that of the outer dust disk.

Lecavelier Des Etangs et al. (1996) show how an asymmetric structure in the β Pictoris disk can form due to the presence of a planet and can be maintained in spite of collisional destruction. Earlier calculations had shown a horseshoe structure of dust enhancement in the resonance zones (Roques et al. 1994). The horseshoe structure varies with the size of particles and therefore is not seen in the more recent simulation, which assumed a size distribution of particles (Lecavelier Des Etangs et al. 1996). From recent studies, it appears more likely that it is the heterogeneity in the distribution of larger objects that cause the density variations in the dust cloud. Telesco et al. (2005) note from imaging observations an asymmetry in the brightness at 12 μm wavelength inward from 200 AU around β Pictoris. They suggest local dust production by catastrophic collisions of resonantly trapped planetesimals leads locally to a different size distribution of dust and therefore local brightness variations.

5.3.4 AU Microscopii disk models

Even for systems where both, the measurements of the spectral energy distribution and spatially resolved observations exist, the dust number density and size distributions cannot be unambiguously derived. This can be seen from a detailed model to describe the smooth brightness component in the dust disk of AU Microscopii (Metchev et al. 2005): Metchev et al. calculated the scattered light assuming spherical grains in an optically thin disk. They adapt a power-law size distribution and a dust material mixture that are typically assumed for interstellar medium dust. They constrain the absolute mass in the disk from submillimetre data and subsequently use colour and absolute flux of the scattered light to constrain the minimum and maximum size of the particles. The scattered light data indicate a possible lack of small particles inward from 50 AU and the authors suggest this is either due to grain growth or due to destruction by the Poynting–Robertson effect. The change in the radial slope of surface brightness

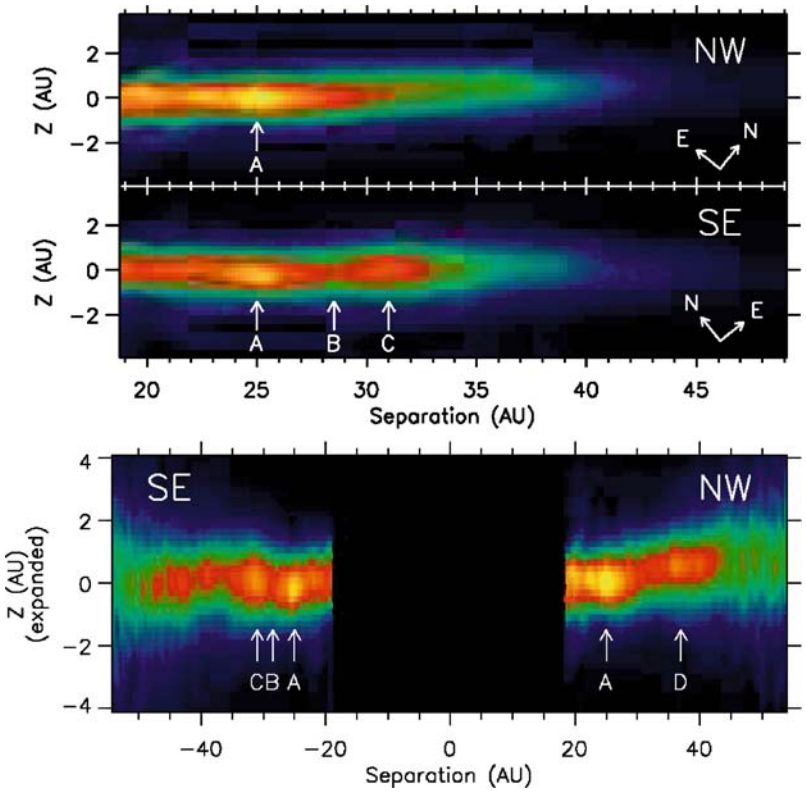

Fig. 9 Keck adaptive optics imaging of the radial substructure in the AU Microscopii disk: the *upper part* shows the brightness in the northwest wing and the mirrored image in the southeast wing, the pixel brightness has been weighted in order to highlight the structure. The *lower part* shows the entire image with the vertical axis expended by a factor of 5 showing the height difference in the northwest and the southeast wing as well as the disappearance of one of the features (Liu 2004)

that is observed near 33 AU indicates the existence of an inner void. The authors suggest the void is generated in similar ways in the AU Microscopii disk and the β Pictoris disk and results in both systems from the collisional evolution or the influence of the Poynting–Robertson effect.

5.3.5 HD 141569 disk models

The influence of companions on the structure of a dust disk has been recently studied for HD 141569 A. The star has two low mass stellar companions HD 141569 B and HD 141569 C. In order to explain the brightness observed around HD 141569, Augereau and Papaloizou (2004) study the evolution of a collisionless circumstellar dust disk under gravitational perturbation by a companion on bound eccentric orbit. Imposing the perturbations onto an initially axisymmetric disk generates a spiral structure, a wide gap in the disk and a broad faint outer extension. The simulations match the observations and the star age if the perturber

is on an elliptic orbit with a periastron distance of 930 AU and an eccentricity between 0.7 and 0.9.

5.3.6 Models of the spectral energy distribution

Models of the spectral energy distribution are of special interest for analyses of thermal emission spectra that new and future observation facilities will provide, but the information that can be derived from the spectral energy distributions is limited.

For many of the data of excess infrared emission, it is not possible to determine the dust distribution unambiguously, since there is no additional information about the spatial distribution of dust (Köhler 2005). For systems where spatially resolved data are available in addition to submillimetre data, Sheret et al. (2004) modelled the spectral energy distribution with dust emission. They showed that the dust models to describe the emission differ and possibly are correlated to the age of the stars. The authors note a tendency possibly indicating that the dust around older stars is less porous than the dust in the disks around younger stars. From the diversity in their models for the spatially resolved disks they conclude it is not possible to determine the size of an unresolved disk solely based on measurements of the spectral energy distribution.

In some cases, the spatial distribution was assumed from spatially resolved observations to estimate the dust composition from the spectral slope of the thermal emission. Li and Lunine introduced two alternative models to describe the circumstellar dust as porous aggregates. In one case, they describe the dust as aggregates of unprocessed interstellar grains; in the other case, they assume it consists of grains that are recondensed in the protostellar nebula. Both models provided a good fit the dust emission around HD 141569A. From the data they further derived the presence of a dust component with minimum size of 0.35 nm consisting of PAH molecules and confine the mass fraction of crystalline silicates to less than 10% (Li and Lunine 2003a). The same model was successful to describe the dust around HR 4796A (Li and Lunine 2003b) and around the more evolved star ε Eridani, assuming dust porosities as high as 90% (Li et al. 2003).

6 Size distribution and disk evolution models

The size distribution of particles in a dust disk is closely connected to the sources, sinks and dynamics of the particles. Mutual collisions of dust in the systems considered here occur with relative velocities of kilometre per second and more and are catastrophic. Particles are both destroyed through collisions and generated as collision fragments. The currently observed planetary debris disks have higher number densities than the solar system dust cloud and collisions are therefore more important. In most cases of planetary debris disk, collisions determine the lifetime of the dust. Also the existence of central clearance zones can partly result from collisional destruction.

Some of the observed gas emissions, especially in the case of the β Pictoris disk are not yet understood. For one, time-variable red-shifted components in the stellar spectra indicate the existence of fast evaporating bodies falling into the star.

These are explained as comet-like objects. Aside from that a component of gas in Keplerian motion is observed and its density and origin not yet understood. What comes clear from other investigations is that the gas content does not influence the dust dynamics.

6.1 Size distribution and collision evolution of solar system dust

For the asteroid belt Dohnanyi (1969) derived a power-law size distribution of $n(m) \propto m^{-\frac{11}{6}}$ or accordingly $n(s) \propto s^{-3.5}$. These distributions result when assuming equilibrium between the mass gain and mass loss of the particles over the considered size interval. When regarding the mass distribution of the flux of interplanetary meteoroids near 1 AU, this slope can be seen in the data for large particles while there is a change in the slope at masses of approximately 10^{-6}g where the Poynting–Robertson drag effectively removes particles by decelerating them toward the Sun. Later studies applied a similar approach to the interplanetary dust cloud (Dohnanyi 1978; Leinert et al. 1983).

A more detailed study to investigate the evolution from 5 AU inward to the vicinity of the Sun, included estimates of the dust production from cometary and asteroidal sources, and considered the Poynting–Robertson transport of dust particles as well as their collisional evolution (Ishimoto 1999; Ishimoto 2000). The latter calculations indicate that mutual collisions of dust inward from 1 AU shift the size distribution towards smaller particles (Ishimoto and Mann 1998; Ishimoto 2000). Collisional evolution causes a narrowing of the mass spectrum, i.e. the number of particles with masses $m < 10^{-9}$ kg is reduced. Small fragments are removed by radiation pressure and dust production inside 1 AU is needed in order to explain the interplanetary dust cloud. The most plausible sources of dust inside 1 AU are meteoroids originating from comets, while the dust supply of the frequently observed sungrazing comets is small compared to the total mass that is contained in inner solar system dust cloud (Mann et al. 2004b). It is quite possible that these sources are not homogeneously distributed and that the inner solar system dust cloud shows some temporal and/or spatial variations. Observations of the infrared F-corona brightness in 1966–1967 revealed an enhancement of the coronal brightness near $4R_{\odot}$ (MacQueen 1968; Peterson 1967, 1969), which pointed to the possible existence of a dust ring near the Sun. The formation of a feature in the near-infrared brightness does not necessarily require the presence of a dust ring but a peak feature can be explained as a geometric effect that occurs from the sharp decrease of the thermal emission brightness at the point where the LOS crosses the beginning of the dust-free zone (Peterson 1963; Mann 1992). The hump features in the brightness have not always been observed subsequently, but the correlation between the appearance or disappearance of a peak feature and the solar activity cycle is unlikely (Kimura and Mann 1998a; Ohgaito et al. 2002). It is suggested that variations of the F-corona brightness rather than indicating the presence or absence of a dust ring are due to variations of the dust cloud composition. This is in accord with the assumption that the dust cloud is locally replenished in the inner solar system (Mann et al. 2004b).

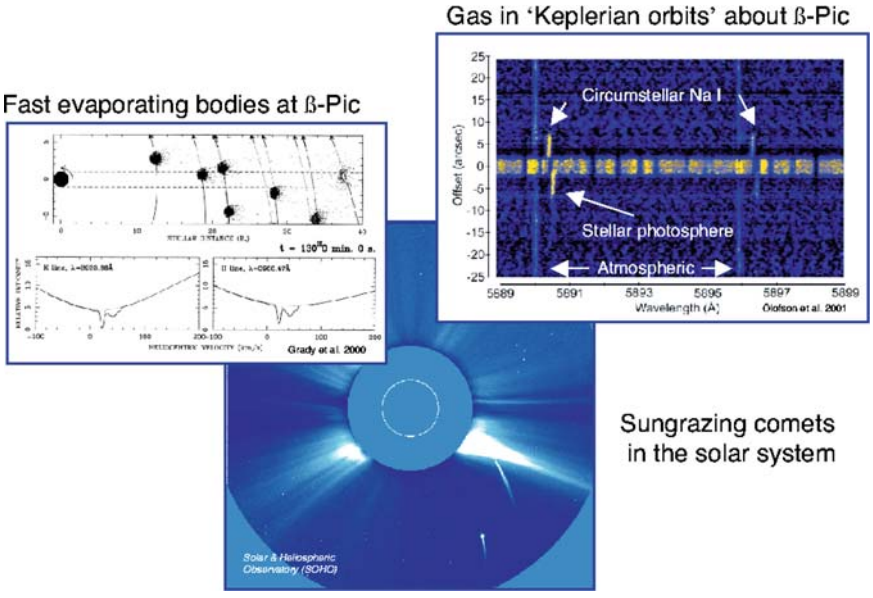

Fig. 10 Sungrazers and gas components: The *left-hand side* of the figure shows the Doppler shift of absorption lines in the spectrum of β Pictoris in the lower part and above a sketched model of fast evaporating bodies causing this Doppler-shifted component (from Grady et al. (2000)). The *right-hand side* of the figure shows observations of NaI indicating the presence of a cool gas component in orbital motion about the star (from Olofsson et al. (2001)): as opposed to the fast evaporating bodies component which is only seen moving toward the star as a red-shifted component, this gas component is seen in emission with an offset from the star both red-shifted and blue-shifted relative to the stellar spectrum. This data also show the stellar absorption line and a weak feature of (terrestrial) atmospheric gas. Finally, the *middle lower part* of figure consists of a LASCO C3 image showing two comets approaching the Sun, they do not reappear on the other side (Courtesy of SOHO/LASCO consortium. SOHO is a project of international cooperation between ESA and NASA.) The Sungrazers that are observed as often as once every second day with SOHO are in majority generated from one parent comet that was fragmented during a previous passage near the Sun. Further Sungrazers occur, but since they can only be detected with space coronagraphs their frequency is not known

6.2 Size distribution and collision evolution in planetary debris disks

The size distributions of circumstellar debris disks have been studied especially in the context of the β Pictoris system, but results are applicable to other systems with low gas contents and similar optical depths as well (Krivov et al. 2000; Artymowicz and Clampin 1997). As distinct from the solar system case β-meteoroids, for systems with higher stellar flux extend to larger sizes, and due to higher dust number densities collisions are more frequent. As a result the collision models separately consider the dust in bound orbits (α-meteoroids) and the dust in hyperbolic orbits (β-meteoroids) and the collisions between these two different populations increase the collisional fragmentation. Moreover, due to higher radiation pressure, also particles in bound orbit may have high eccentricities, which increases the relative velocities in the disks and therefore the collision rates (Artymowicz and Clampin 1997). The fragmentation of α-meteoroids by impacts of β-meteoroids

flattens the distribution of α-meteoroids in the size regime adjacent to the blow-out limit and changes the derived size distribution (Krivov et al. 2000). The latter distribution has three different slopes: steeper ones for both small β-meteoroids and large alpha-meteoroids and a gentler one in between for α-meteoroids with sizes just above the blow-out limit. The size distribution also changes within the disk.

Yet, an approximation for the size distribution $n(s) \sim s^{-q}$ is justified for simple approximations. While initially $q = 3.5$ was applied to β Pictoris (Backman and Paresce 1993), Heinrichsen et al. (1999) assume $q = 4.1$ to explain infrared observations.

However, the collision products can explain the amount of small grains that are required to explain observational data. Since β-meteoroids are continuously replenished by collisions, at any time the disc contains a substantial population of small particles. Spatially resolved observations indicate the variation of the size distribution within the disk: Weinberger et al. (2003) observed the southwest wing at wavelength 8–13 μm and detected emission features which they attribute to amorphous and crystalline silicate outward to 1 arcsec (20 AU). The features disappear at larger offset angles and the authors suggest that be explained by a high abundance of small silicate grains in the inner disk compared to the outer regions.

The collisional evolution can also explain a depletion of dust in the inner regions of planetary debris disks. Estimates of the inner depletion zone for the β Pictoris disk were derived from the spectral variation of the infrared brightness. Backman and Paresce (1993), assume 38 AU, other estimates are 50 AU (Roques et al. 1994), 20 AU (Kalas 1998) and 1 AU by Li and Greenberg (1998).

Gas observations The observation of neutral and singly ionised gas is possibly correlated to the dust collisional evolution: Liseau et al. (2003) observed in the β Pictoris disk emission the neutral sodium resonance line at distances from 30 AU to at least 140 AU from the central star. This atomic gas is coexistent with the dust particles and the Doppler shift suggests the gas is in Keplerian rotation. Recent results of spatially resolved spectroscopic observations of the disk around β Pictoris in the spectral range from 0.3 to 1 μm revealed a large number of detected lines extending over the entire field of view (i.e. distances of 8 or 12 arcsec from the star) in a disk that is significantly higher than the extension of the dust disk (Brandeker et al. 2004). The sources and mechanisms to generate these gas components are still not fully understood. Studies of the dust distribution indicate that the gas does not influence the dynamics of dust (Thébault and Augereau 2005).

6.3 Disk evolution models

Planetary debris disks evolve in the later stage of the planetary system formation: after initial growth of planetesimals in a circumstellar disk of dust and gas the relative velocities of dust and planetesimals increase so that catastrophic collisions occur. The increase of relative velocities is caused by a lack of gas and together with the presence of perturbing planetesimals, which also causes an extension of the disks in height. This stage is expected to be reached after 10 Myrs (see for instance Kenyon and Bromley 2001) and the presence of planets will cause further

perturbations. Further time evolution of the planetary debris disks is influenced by the Poynting–Roberson drag, by the possible presence of planets and by catastrophic collisions. A decrease in mass as t^{-1} is obtained for systems dominated by Poynting–Robertson drag and a decrease as t^{-2} for a system dominated by collisions (Dominik and Decin 2003).

The recently found similarities of planetary debris disk around AU Microscopii and β Pictoris motivated discussions of their disk evolution. Both systems are observed in scattered light over a large spatial extension and have similar spatial structures. In addition to this similarity AU Microscopii belongs to the group of young stars of similar age that are moving together with β Pictoris (Zuckerman et al. 2001) and therefore it is discussed whether these systems have a similar evolutionary stage (Liu 2004; Metchev et al. 2005). By comparing the timescales for mutual collisions of dust and Poynting–Robertson drag between the two systems, Metchev et al. argue that the breaks in the radial slopes of both systems are linked to one or both of these processes. Older systems, in contrast seem to have ring-like structures. Those structures are often detected in the submillimetre regime though and therefore more biased towards large dust particles. From considering the perturbing forces it is plausible that the smaller dust tends to form homogenous distributions faster, which would explain the smoother structures observed in scattered light. Estimating the time evolution from the limited spatially resolved data seems difficult and only observations of excess brightness provide a large sample of stars.

The age dependency of infrared excesses should therefore provide us with some information of the time evolution in planetary debris disks. From analysis of submillimetre observations Liu and co-workers derive the total dust mass drops by about a factor of 1000 within 10 Myrs and then decreases with $t^{-\gamma}$, with $\gamma = 0.5 - 1$ (Liu et al. 2004) (see Fig. 5). Several analyses based on the mid-infrared observations of stars with infrared excess have been made in terms of the fractional luminosity, i.e. the amount of the excess brightness given as fractional luminosity $L_{\rm IR} / L_{\odot}$. They suggested there is a global power law describing the amount of dust seen in debris disks as a function of age of the stars (see for instance Holland et al. 1998). Decin and co-workers reconsidered the observational data and come to a different conclusion not supporting this power law (Decin et al. 2003). They re-evaluated fractional luminosity and stellar age data and conclude they are widely spread for stars of most ages. The excess is more common in young stars than in old stars but there are a few very young stars with intermediate or small excesses and there seems to be a common upper limit of the infrared excess. This upper limit is possibly due to dust collisional avalanches that quickly reduce high density dust clouds (Artymowicz and Clampin 1997; Krivov et al. 2000; Dominik and Decin 2003). Several scenarios have also been suggested to explain the lack of young stars with low fractional luminosity and need to be checked with future improved observational data (Dominik and Decin 2003).

7 Interstellar dust entry and astrospheres

The entry of interstellar dust provides a further dust constituent to the planetary debris disks. It can also increase collision rates and enhance dust production in these disks. While large interstellar grains are mainly influenced by stellar gravity

and radiations pressure force when they enter the systems, the small (typical) interstellar dust particles are also influenced by the interstellar and circumstellar plasma and magnetic field configuration.

In analogy to the heliosphere around the Sun, the region around a star filled with the stellar wind plasma is called the astrosphere. The parameters of stellar winds of the systems considered here are not accessible to direct observations. In some cases, the presence and size of the astrosphere can be inferred from the enhanced density of neutral hydrogen ('hydrogen wall') that builds up in front of the astrosphere. From observations of hydrogen walls it is possible to estimate the stellar mass loss. Values derived for observed cases, lie between 0.15 and 100 of the solar mass loss.

7.1 Interstellar dust entry and astrospheres

The stellar wind outflowing from stars creates the astrospheres (the heliosphere for the case of the solar system): the regions in space from which the interstellar plasma and the interstellar magnetic field is kept out (Lallement 2001). Instead, the astrospheres contain the stellar wind plasma and the magnetic field of stellar origin. Since the stars move with respect to the interstellar medium (ISM), the astrospheres have an asymmetric structure. In the direction of the star motion relative to the ISM the outer boundary of the astrosphere (the astropause) is pushed close to the star by the pressure of the ISM. The interstellar plasma flow (but not the neutral component of the ISM) cannot cross this boundary and must re-direct itself to go around the obstacle. In result, in front of the astrosphere there is a region where the flow velocities of the neutral and ionised components of the ISM become different. This leads to an increase in the charge exchange rate between these components and results in a "hydrogen wall": the region of enhanced density and temperature of neutral hydrogen in front of the astrosphere, first predicted for the case of the heliosphere by Baranov and Malama (1993). A number of "hydrogen walls" were discovered for nearby stars (including the Sun) by observing the Doppler shift caused by the Ly-α radiation passage through the "wall" (Linsky and Wood 1996; Wood and Linsky 1998; Wood et al. 2002; Wood 2004; Wood et al. 2005a,b). As the astrospheres are tenuous extended structures, "hydrogen wall" observations are at this time the only means of discovering them. By now this has been achieved for 13 stars which are listed in Table 7. The method of observation requires that the ISM hydrogen column density is not too large along the line of sight (Wood 2004). In consequence, all but three of the detected astrospheres are within 10 pc from the Sun. Wood et al. (2005b) give results of analyses of the Ly-α data from Hubble Space Telescope Archive for 62 stars.

In the direction opposite to the star's velocity the astrosphere develops an extended 'tail'. In the case of the Sun, numerical simulations show that the 'tail' does not dissolve in the interstellar medium at least for several thousand astronomical units.

The size of the astrosphere depends first of all on the strength of the stellar wind. The observation of "hydrogen walls" is in fact the main method by which the mass loss (and therefore the stellar wind outflow) can be estimated for solar-like stars. This is done by fitting the amount of absorption by the "hydrogen wall" using the available information about the ISM, the star velocity

Table 7 List of stars for which astrospheres have been detected (based on Wood (2004); Wood et al. (2005b)

Star	Spectral type	Distance (pc)	Mass Loss ($\dot{M}_\odot$)	R_H (AU)
α Cen	G + K	1.35	2	220–400
ϵ Eri	K	3.22	30	800–1750
61 Cyg A	K	3.48	0.5	20–30
ϵ Ind	K	3.63	0.5	30–40
36 Oph	K + K	5.99	15	300–600
λ And	G + M	25.8	5	150–200
EV Lac	M	5.05	1	60–100
70 Oph	K + K	5.09	100	1000–1700
ξ Boo	G + K	6.7	5	300–500
61 Vir	G	8.53	0.3	300–450
δ Eri	K	9.04	4	200–300
HD 128987	G	23.6	–	–
DK UMa	G	32.4	0.15	200–400

Note. R_H denotes the estimated distance range to hydrogen wall in the ISM apex direction.

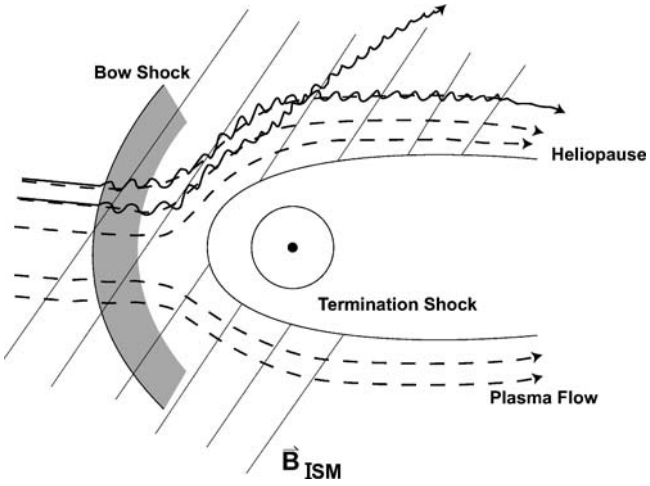

Fig. 11 The components of the heliosphere shown for the Sun moving from the right to the left relative to the surrounding interstellar medium plasma. *Thin lines* indicate the direction of the interstellar magnetic field (B_{ism}), the *dashed lines* the interstellar plasma flow. The *shaded region* behind the bow shock indicates the accumulation of neutral hydrogen ('hydrogen wall') in front of the heliosphere. The motion of two small interstellar dust particles is indicated with *solid lines*: they gyrate and slide along the magnetic field lines carried by the plasma flow

and a gas-dynamical model of the astrosphere (Wood 2004; Wood et al. 2005a). The distances to the inner and outer boundaries of the "hydrogen wall" are listed in Table 7 (R_H). Of the stars in the list, two have the estimated mass loss much higher than the Sun: ϵ Eridani (30 · solar value) and 70 Ophiuchi (100 · solar value). The sizes of their astrospheres are supposed to be about order of magnitude larger than the heliosphere.

The other factor determining the size of the astrosphere is the ISM. In dense clouds, the size of the astrosphere would contract drastically. The effect of passages through dense clouds on the heliosphere and the solar system is discussed in Yeghikyan and Fahr (2003, 2004).

The astrospheres have a possible, although minor, role in processing of the interstellar dust. The probability of a dust grain encountering an astrosphere is low. The astrosphere of the star moving at 20 km/s relative to ISM through a interstellar cloud of 10 pc size would sweep up about 10^{-8} of the cloud volume (assuming the astrosphere cross-section $\pi \cdot (300\,\mathrm{AU})^2$) within the crossing time of 5×10^5 years. With 10^3 stars in the cloud, about 10^{-5} of the dust grains will be affected within this time, 2×10^{-4} within 10^7 years and some few percent during the total grain lifetime of 10^9 years.

7.2 Interstellar dust entry

The behaviour of the dust grain encountering the astrosphere depends on two parameters. One is the radiation pressure force to gravity ratio (β). The other is the strength of the grain coupling to the magnetic field, which depends on the grain charge-to-mass ratio. For the stars hotter and more luminous than the Sun, including A and B type stars, in particular β Pictoris, the radiation pressure is the dominant force, with $\beta > 1$ for a wide range of the grain sizes. According to Artymowicz and Clampin (1997), the radiation pressure keeps the grains of 0.1 μm size from approaching closer than 765 AU to β Pictoris and closer than 3530 AU to Vega (estimation for porous silicate and graphite grains). Only the larger grains (above ~few μm for β Pictoris and ~10 μm for Vega) have $\beta < 1$ and are not repulsed by radiation.

For the solar type stars, the values of β are smaller and the main force acting on small grains approaching the astropause is the Lorentz force. The strength of the grain coupling to the magnetic field can be expressed by its Larmor rotation time τ_L, the inverse of the Larmor frequency $\Omega_\mathrm{L} = Q|\mathbf{B}|/mc$, where Q and m are the charge and the mass of the grain and $\mathbf{B}$ the magnetic field. If τ_L is much smaller than the characteristic time L/V (where L is the size of the astrosphere and V the speed of the grain, or of the interstellar flow relative to the astrosphere) the grains are coupled to the interstellar plasma flow and do not enter the astrosphere. This is the case of very small grains (~ 0.001 μm for the case of the heliosphere) with large charge-to-mass ratio. Large grains (> few 0.1 μm for the heliosphere) with τ_L large compared to L/V, enter the astrospheres freely (Linde and Gombosi 2000). The larger of the middle sized grains (~ few 0.01 μm for the heliosphere) can enter the astrosphere but are deflected from closer approaching the star by the magnetic field of the star (Linde and Gombosi 2000; Landgraf 2000) although the structure of the astrospheric magnetic field may sometime allow particles to approach close to the star (Czechowski and Mann 2003a). The smaller of those (up to ~0.01 μm for the case of the heliosphere) with $\tau_\mathrm{L}/(L/V) \sim 0.1$ stay outside the heliosphere but their velocity distribution is modified by the encounter (Czechowski and Mann 2003b). The stellar bow shock, which will form in the ISM if the star velocity is supersonic with respect to ISM, has an interesting effect on the grain dynamics: since crossing the shock slows down the plasma but not the dust grain, the grains downstream from the shock acquire the velocity difference relative to the ISM plasma (Czechowski and Mann 2003b) equal to the drop in plasma velocity across the shock. The velocity distribution of these grains is therefore significantly modified near the astrospheres. The "draping" of the interstellar magnetic field at the astropause may cause streaming of those grains along

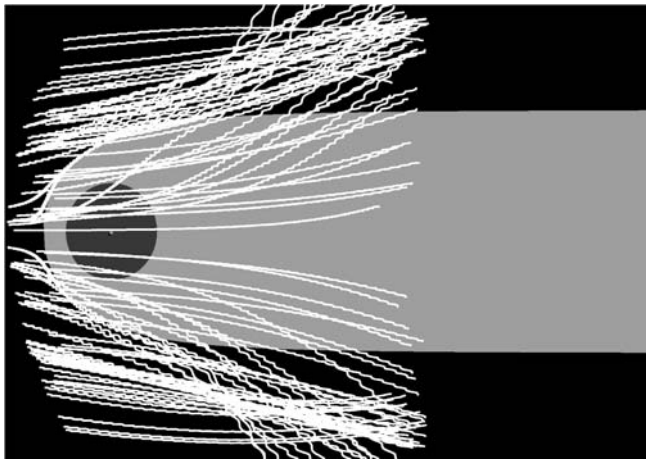

Fig. 12 Trajectories of dust grains of ∼0.01 μm size in the vicinity of the astrosphere. The interstellar magnetic field is perpendicular to the velocity of the star relative to the interstellar medium and lies in the plane of the figure. The grains with the initial trajectories passing close to the boundary of the astrosphere are caused to stream away from it along the magnetic field lines (Czechowski and Mann 2001, 2003b)

the magnetic field lines, away from the astrosphere (Czechowski and Mann 2001, 2003b). This is illustrated in Fig. 12.

In distinction to the small effect on the grains in the ISM, the astrosphere affects strongly the dust that enters it: dust particles that can enter into the outer part of the astrosphere, are deflected from the inner part by the star's magnetic field and radiation pressure. Only the bigger grains can pass into the vicinity of the star. In the case of the Sun, the dust particles of interstellar origin were detected by ULYSSES with dust at masses $<10^{-16}$ kg suppressed compared to the interstellar dust mass distribution derived from extinction measurements (Grün et al. 1994; Grün and Landgraf 2000; Krüger et al. 2001).

An interesting question is the effect of the astrosphere on the dust in large circumstellar disks. Artymowicz and Clampin (1997) have considered the possibility of 'sandblasting' of the circumstellar disk by the grains from the interstellar medium for the stars known to have large circumstellar disks. They found that the radiation pressure prevents these grains from entering the disks, except for the peripheral parts. For the stars closer to the solar type, a similar shielding could be provided by the astrosphere. If the large dust disk extends outside of the astrosphere, the interaction with the interstellar dust would be stronger.

A possible example: HD 32297 The dust around HD 32297 that was recently imaged is a system that possibly shows both, the planetary debris dust and interstellar medium dust. Kalas (2006) points out in his analysis that the blue colour indicated from the observations would agree with Raleigh scattering at interstellar medium dust. However, he points out that the inner structure shows typical characteristics of a debris disk: it is relatively symmetric and has a radial brightness decrease with distance that is comparable to other systems. The asymmetry in the disk that occurs at large distances from the star may result from overlap with interstellar dust signal at distances beyond 190 AU (Kalas 2006). It is quite possible that the

structure is not a result of the erosion of the planetary debris due to interstellar dust impacts, but rather a result of the local accumulation of interstellar dust: either as a result of the radiation pressure acting on the interstellar dust or as a result of interstellar dust deflection at the astrosphere. Unfortunately, there is no information about the astrosphere of HD 32297.

8 Optical properties and the evolution of matter

The properties of dust that are derived from observations are albedo, emissivity and polarisation. These properties can be used to compare dust in different systems. Comparison to light-scattering models allows the study of the dust properties by means of these observational data. Comparison of thermal emission measurements shows similarities of planetary debris dust to cometary dust in the solar system.

8.1 Light scattering

The typical shape of an empirical scattering function is shown in Fig. 13. It describes the average scattering cross-section as a function of the scattering angle θ. The scattering function has its maximum for small angles (forward scattering), is nearly isotropic for scattering angles between 45° and 160° and then increases again by a factor of 2. The polarization of scattered light is in a similar way given as a function of scattering angle.

8.2 Albedo

The albedo of dust particles is inferred from the comparison of thermal emission and scattered light brightness, while the geometric albedo is derived from the brightness data under assumptions of the dust geometric cross-sectional area by integration of the differential size distribution of dust. We discuss the geometric albedo of dust particles given as the generalized geometric albedo for 90° scattering angle (see Hanner et al. 1981 for definition). Based on the comparison of the visible zodiacal light to IRAS data, the albedo was determined to be 15% at maximum for particles at 1 AU, applying thermal emission data from the rocket photometry by Murdock and Price (1985) gives values less than 10%. The difference between the data sets may be explained by the uncertainty of the absolute calibration in the IRAS measurements. Laboratory experiments with irregular particles of meteoritic as well as terrestrial samples of dark opaque material yield albedo values between 5 and 9% and could also reproduce the empirical scattering function derived from Helios observations (Weiss-Wrana 1983). Values for the albedo of cometary dust are typically lower (see Kolokolova et al. 2004 for a review) which is often discussed as evidence that the cometary dust is more pristine.

Aside from the absolute value, the values derived from one data set show a trend to an increasing albedo with decreasing distance from the Sun. In a similar way the polarisation at 90° scattering angles derived for the distances from the Sun decreases with decreasing distances from the Sun. This reflects either the

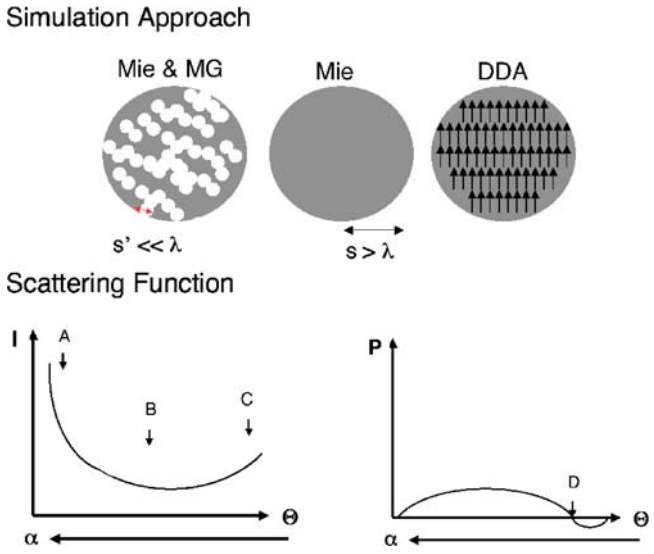

Fig. 13 Scattering properties of dust: A typical sketch of intensity, I, and linear polarization, P, of scattered light as a function of scattering angle θ. The incident solar/stellar light is unpolarized. Some observers discuss the scattering properties as function of the phase angle α, $\alpha = 180° - \theta$, that is also shown. The intensity of scattered light (marked with 'A') has a maximum at small scattering angles, a broad minimum (marked with 'B') at medium scattering angles and a slight enhancement at backscattering for scattering angles close to $\theta = 180°$ (marked with 'C'). The linear polarization is zero for $\theta = 0°$, has a maximum at medium scattering angles and turns to negative polarization ('D') at $\theta > 160°$. The scattering properties of dust depend on the material composition, described by its index of refraction, on the size, s, and shape and characteristic subshape sizes s' of the particles. Some of the theoretical approaches to describe the light scattering at dust particles that are discussed in the text are depicted in the upper part of the figure: Mie theory provides rigorous solutions of the light-scattering problem for particles of certain defined shape. Mie theory can be combined with the Maxwell–Garnett mixing rule (Mie & MG) to simulate particles consisting of different materials. Particles can be approximated as an array of dipoles (discrete dipole approximation, DDA) in order to calculate the light scattering of particles of arbitrary shape. The scattering properties are also an important parameter to determine the temperature of particles and to determine the appearance of characteristic emission features

gradual change of dust optical properties while they drift to the Sun or the change in the composition of the dust cloud. While data between 0.3 and 1 AU describe moderate changes of albedo and polarisation the change at distances <0.3 AU from the Sun cannot be explained by gradual changes of particle properties (Mann 1993).

8.3 Polarisation

8.3.1 Observations

The local polarisation of interplanetary dust and its variation with scattering angle has been derived from zodiacal light observations. The polarisation function, i.e. degree of linear polarisation of the scattered natural light, has a negative branch

at large scattering angles, a neutral point around 160° followed by an approximately linear increase. The minimum of polarisation for interplanetary dust derived from Gegenschein observations is $-2 \pm 1\%$ (Levasseur-Regourd et al. 2001). The absolute value of the maximum polarisation decreases for particles close to the Sun, while the albedo increases. Linear polarisation of comets is a smooth function of phase angle α with a maximum of typically 10–30% around $\alpha = 90°$ and a negative branch at $\alpha \leq 20°$ with a minimum of a few percent, and increases with wavelength (Dobrovolsky et al. 1986; Dollfus et al. 1988; Kolokolova et al. 2004). These dependences of linear polarisation on phase angle and wavelength are consistent with visible and near-infrared observations of a number of comets (Chernova et al. 1993; Dollfus and Suchail 1987; Ganesh et al. 1998; Hadamcik and Levasseur-Regourd 2003; Kikuchi et al. 1989, 1987; Kiselev and Velichko 1997; Manset and Bastien 2000; Sen et al. 1991b). The spatial distribution of the polarisation in the coma is highly inhomogeneous. In the jets, the polarisation is higher and positive irrespective of the phase angle (Hadamcik and Levasseur-Regourd 2003). Sun-ward side of coma of Hale–Bopp shows higher degree of linear polarisation than anti-Sun-ward side (Hadamcik and Levasseur-Regourd 2003; Kiselev and Velichko 1997). A decrease in the polarisation with distance from the nucleus was observed along the dust tail of comet Hale–Bopp at the projected distance of approximately 4×10^4 km and outward, while the polarisation closer to the nucleus was nearly independent of the distance (Manset and Bastien 2000). This tendency was observed along Sun-ward direction but the polarisation in anti-Sun-ward direction was nearly constant (Hadamcik and Levasseur-Regourd 2003). The Optical Probe Experiment onboard Giotto measured in situ the local polarisation of dust from comet Halley (Levasseur-Regourd et al. 1999). The polarisation of 10–30% gradually increases with distance from the nucleus in the 10^3–10^5 km range. Spatially resolved observations at comet Encke show variations in colour of albedo that are explained with particle properties changing on time scales of hours (Jewitt 2004). Faint circular polarisation less than 1% with both signs was detected for comets Halley and Hale–Bopp (Dollfus and Suchail 1987; Manset and Bastien 2000) and interpreted with the presences of partially aligned non-spherical dust particles or multiple scattering in the innermost coma.

It was suggested that according to the values for the maximum polarisation, comets could be classified into two groups (Dobrovolsky et al. 1986; Levasseur-Regourd et al. 1996). Comets in the high and low polarisation classes are known to be dust-rich and gas-rich, respectively. However, observations of comet Hale–Bopp revealed the polarisation higher than expected for dusty comets belonging to the high-polarisation class (Hadamcik and Levasseur-Regourd 1999; Kiselev and Velichko 1997; Manset and Bastien 2000). Hence the distinction into two groups may also arise from observational biases.

8.4 Light-scattering models and laboratory measurements

8.4.1 Particle model

While first model calculations to describe optical properties of cosmic dust were made with Mie theory describing spherical (or in some cases cylindrical) particles, it became more and more evident, that dust particles in many cases are irregularly

shaped. As a tool to describe irregular particles with reproducible properties, so-called ballistic particle cluster aggregates (BPCA) and ballistic cluster aggregates (BCCA) are used (see cf. Mukai et al. 1992), and references there). BCCAs are numerically produced by randomly shooting cluster of monomers onto each other: starting with two monomers that form a cluster, then followed by collision of two of the two-monomer clusters, then four-monomer clusters and so forth. As a result a relatively open structure is formed. For BPCA on the initially formed cluster, further single monomers are attached, so that a more closed structure evolves. For a small number of monomers these clusters look quite similar but for larger numbers of monomers the differences are significant, and it is especially questionable whether the BCCAs do resemble any of the dust components observed in our solar system. Still this is a model to describe very porous grains and also to systematically study variations of properties with the size and structure of particles. In many cases, the BPCAs and BCCAs are used as a model to reproducibly describe irregular particles, irrestistive of their path of formation.

8.4.2 Numerical simulations

Exact theoretical results are given for some particular cases such as a homogenous sphere where the Mie formalism describes the interaction of electromagnetic waves with an obstacle of given index of refraction. This formalism holds for particles of well-defined shape and size parameters $x = 2\pi s/\lambda$ (see van de Hulst 1957; Bohren and Huffman 1983), it is valid for any sizes of particles. Effective medium approximations are often applied to describe the effective refractive index of irregular dust particles as aggregates that consist of building stones of submicrometre sizes (cf. Mukai et al. 1992): this is described by a porous medium as illustrated in Fig. 13. The approach is valid as long as the size of the inclusions is small compared to the wavelength of scattered light. In this case it means the aggregates of approximate sizes of 0.01 μm.

The Discrete-Dipole Approximation (DDA) originally proposed by Purcell and Pennypacker (1973) provides the opportunity of studying light scattering by arbitrarily shaped particles (Draine 1988; Draine and Flatau 1994).

The superposition T-matrix method (TMM) rigorously provides solutions for light scattering by a cluster of spheres (Mackowski and Mishchenko 1996). Petrova et al. (2000) applied the TMM to compute light scattering by small clusters of spheres that are located on a lattice. Because linear polarisation of each cluster shows oscillations with phase angle, reasonable results could be obtained only with averaging over different sizes of clusters.

Mie theory allows to compute light scattering by a sphere of arbitrary size (Bohren and Huffman 1983; Mie 1908). Therefore, it has often been used to compute the degree of linear polarisation of cometary dust. Mukai et al. (1987) were the first to successfully reproduce the phase-angle and wavelength dependences of linear polarisation observed in the range 0–20° for dust in comet Halley by numerical calculations on the basis of Mie theory. They used the size distribution of dust in comet Halley derived from in situ measurements (Mazets et al. 1986). The complex refractive indices estimated in the visible wavelength range are consistent with a mixture of ice and silicate. Sen et al. (1991a) used the same method for the same comet to obtain almost the same values for the refractive indices.

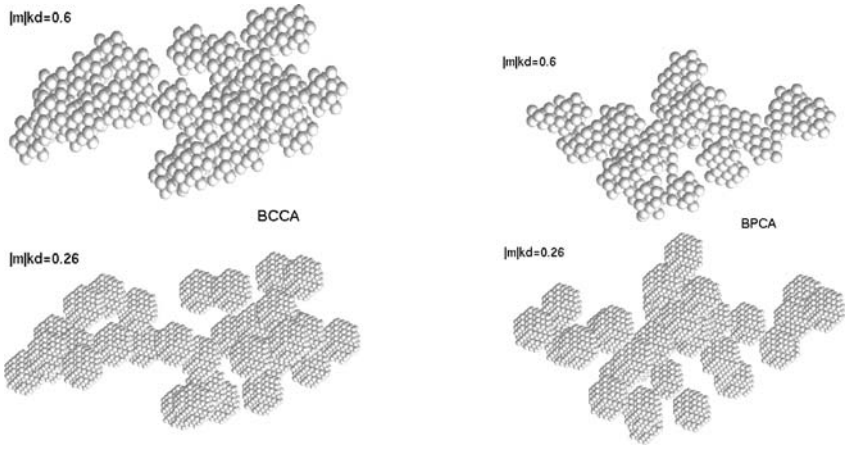

Fig. 14 Aggregates with 32 monomers consisting of two different arrays of dipoles; *left*: ballistic cluster–cluster aggregates; *right*: ballistic particle–cluster aggregates (Köhler et al. 2005). This illustrates how DDA is applied to aggregate particles: mkd denotes the distance with which the dipoles are located on the grid in order to describe the particle. Note that for small numbers of monomers, shown here, BPCA and BCCA look similar

Sen et al. (1991b) applied the same method to polarimetric observations of dust from comet Austin and obtained similar refractive indices, but a steeper size distribution.

Mukai and Mukai (1990) took into account light scattering by large particles having rough surface to explain the data observed at 0°–65° for linear polarisation of dust in comets Halley and Bradfield. The fits of the numerical results to the data were improved, in particular, at 0°–20° with the consideration of rough-surface particles consisting of a mixture of ice and silicate.

Lumme and Rahola (1994) showed from their numerical calculations with DDA that linear polarisation of highly absorbing aggregates averaged over six sizes with a power-law size distribution resembles the phase-angle dependence observed for cometary dust. DDA calculations of the light scattering by fractal aggregates (Kozasa et al. 1993) provide results that are similar to Raleigh scattering showing no negative polarisation at small phase angle and a large maximum near 90°. This apparently results from the assumption of small constituent dust particles, which are 10–30 nm in radius. Light scattering by aggregates of different shapes and compositions described by DDA (Xing and Hanner 1997) results in oscillations in the phase function of linear polarisation, which are inconsistent with observations. These oscillations arise from the use of large constituent dust particles, which are 250–500 nm in radius. Various types of non-spherical shapes for compact dust particles were used to compute their light-scattering properties, but none of the results were successful (Yanamandra-Fisher and Hanner 1999a).

Lumme et al. (1997) were able to show using DDA that the phase-angle dependence of linear polarisation observed for cometary dust can be qualitatively explained with light scattering by aggregates consisting of water ice or silicate without averaging over different sizes and compositions. Levasseur-Regourd et al.

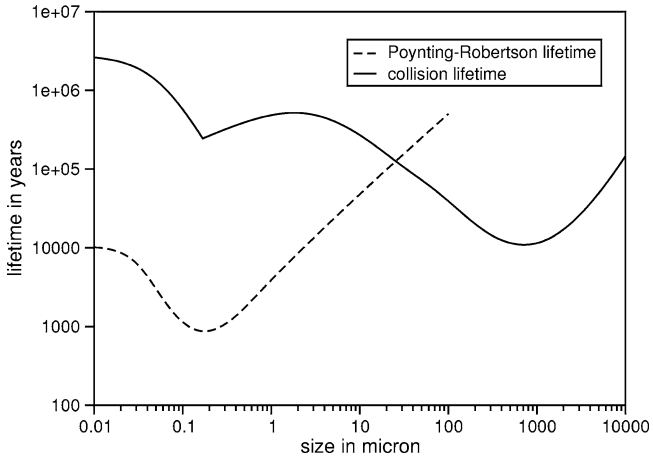

Fig. 15 Calculated lifetime of dust particles in the solar system at 1 AU due to the Poynting–Robertson effect (*dashed line*) and collisions (*solid line*)

(1997) and Haudebourg et al. (1999) showed a large difference in the light-scattering properties between highly fluffy and relatively compact fractal aggregates from their DDA calculations, but their results were not confirmed by Kimura (2001) who utilized both the TMM and DDA to study light scattering by large fractal aggregates consisting of silicate or carbon. Quantitatively best result was obtained with the aggregates consisting of silicate dust particles whose radius is 150 nm, based on the TMM computations. Recently, Kimura et al. (2003) achieved qualitatively best result for the phase-angle and wavelength dependences of not only polarisation but also brightness for cometary dust. They used the TMM with the fractal aggregates consisting of absorbing materials derived from a mixture of silicate, iron, organic refractory and amorphous carbon with the elemental abundances of Halley's dust.

8.4.3 Laboratory measurements

Microwave analogue experiments showed that large fluffy absorbing particles account for the phase-angle dependence of linear polarisation observed for the zodiacal light (Giese et al. 1978) and also the influence of an absorbing mantle material was measured (Zerull et al. 1993). Gustafson and Kolokolova (1999) used microwave analogue technique to study the wavelength and phase-angle dependences of polarisation and intensity for a variety of aggregates with different sizes, shapes, and compositions of the constituent particles. They obtained proper dependences with fluffy aggregates consisting of wavelength-size absorbing constituents. Weiss-Wrana (1983) used electrostatic levitation and a laser beam to study light scattering by single dust particles. The phase-angle dependence of linear polarisation consistent with zodiacal light observations was achieved with fluffy dark particles in the size range of 20–120 μm. Muñoz et al. (2000) studied scattering matrices for olivine and Allende meteorite particles using lasers at two wavelengths. Their results with micrometre-size olivine particles show the

phase-angle and wavelength dependences of polarisation that are similar to those observed for cometary dust particles.

8.5 Temperature and thermal emission

Dust particles in interplanetary space usually attain their equilibrium temperature of absorbed radiation integrated over the solar spectrum and the emitted radiation determined by the optical properties of the particles. The conditions for the equilibrium temperature, $T_{\rm dust}$, are given by

$$\pi \left(\frac{R_\star}{r}\right)^2 \int_0^\infty F_\star(\lambda) C_{\rm abs}(s,\lambda)\,{\rm d}\lambda = 4\pi \int_0^\infty B(\lambda, T_{\rm dust}) C_{\rm abs}(s,\lambda)\,{\rm d}\lambda, \qquad (13)$$

where $C_{\rm abs}$ is the absorption cross-section and B denotes the Planck function, $F_\star$ the brightness of the stellar photosphere, $R_\star$ the radius of the star, r, the distance of the particle from the star and λ the wavelength of absorbed and emitted radiation. Further smaller contributions to the energy budget (neglected in the previous equation) are the sublimation energy and kinetic energy from the impact of plasma particles (Mukai and Schwehm 1981).

By approximating the stellar spectrum with the blackbody emission and assuming particles with constant albedo, A, (i.e. the ratio of the in-falling and scattered radiation is constant with λ) one can estimate the temperature of particles by approximating with the Stefan–Boltzmann law both the in-falling stellar radiation at distance r from the star and the thermally emitted radiation of the dust and obtains the relation:

$$T_{\rm dust} = T_\star \left(\frac{1-A}{4}\right)^{1/4} \left(\frac{R_\star}{r}\right)^{1/2} \qquad (14)$$

where $T_\star$ is the temperature of the stellar photosphere. The dust temperature varies approximately as $r^{1/2}$ in a given system and for a given distance increases proportionally with the temperature of the stellar photosphere. Assuming $T_\star = 5800$ K for the solar photosphere and $A = 0$ for a blackbody results in the dust temperature in the solar system of 280 K at 1 AU.

Note that the real solar and stellar spectra deviate from the blackbody emission that is assumed in this equation (see also the discussion of the radiation pressure force in Sect. 4.2). Moreover, the dust properties are different from the blackbody. The absorption cross-section varies with wavelength and depends on the size and the composition of the dust particles. "Small" particles show typical emission features such as the features around 10 μm attributed to the emission from silicate. Even if these features are not observed, the low absorptivity of silicates in the visible and higher absorptivity in the near infrared lead to temperature profiles (i.e. variation of temperature with distance from the star) that are different from those of a blackbody. Large dust particles, especially when they consist of different materials, show only a weak wavelength dependence of the absorptivity over wavelength and reach approximately blackbody temperature.

8.6 Emission features

Silicate mineralogy of the cosmic dust is revealed in observational data by the characteristic vibration and rotation bands of the molecules that influences the spectral slope of the thermal emission brightness. While thermal emission features are small in the zodiacal light, they are clearly seen in some comets and in circumstellar systems. They provide information on dust composition, size and structure.

8.6.1 Zodiacal light

Early infrared photometry of the zodiacal light by rocket experiments have not shown any features at a spectral resolution of $0.1 \leq \Delta\lambda/\lambda \leq 0.4$ (Murdock and Price 1985). The first attempt of detecting spectral infrared features in the wavelength range of 5–16.5 μm using the mid-infrared camera (ISOCAM) on the Infrared Space Observatory (ISO) was also unsuccessful at a level of 15% of the continuum (Reach et al. 1996). Later ISOCAM observations have revealed a weak excess in the wavelength range of 9–11 μm at a level of 6% of the continuum (Reach et al. 2003). Description of the features with spherical particles was possible with known size distributions of the interplanetary dust cloud slightly enhanced for small particles, while size distributions of cometary or interstellar dust due to the higher amount of small grains produced too strong features (Reach et al. 2003). The features were best described with a mixture of Mg-rich olivine, dirty crystalline olivine and hydrous silicates. The authors note a slight tendency towards enhanced features above the ecliptic and toward the Sun.

We suggest this tendency possibly indicates that in those regions there is a higher amount of cometary dust. Cometary dust is assumed to be darker than asteroidal dust and moreover is likely to have a fluffy structure which enhances the appearance of features for larger particles.

8.6.2 Cometary dust

Maas et al. (1970) suggested the excess emission from comet Bennett over blackbody-like continuum at wavelengths of 10 μm, likely originated from silicate dust particles. In the infrared spectra from comet Halley, Bregman et al. (1987) identified the presence of crystalline olivines and Campins and Ryan (1989) confirmed a strong peak at 11.3 μm attributed to crystalline olivine as well as another strong peak near 9.7 μm. The peak feature of crystalline olivine and the broad maximum around 9.7 μm, which may originate from amorphous olivine, have also been detected in infrared spectra from comets C/1987 Bradfield, C/1993a Mueller, C/1990 Levy and Hale–Bopp, while no feature of crystalline olivine has been detected in comets C/1973 Kohoutek, C/1987 Wilson, C/1989 Okazaki-Levy-Rudenko, C/1989 Austin, 23P/Brorsen-Metcalf, P/Borrelly, 4P/Faye, and 19P/Schaumasse (Hanner et al. 1994a,b, 1990; Wooden et al. 1999). From spectra of comet 103P/Hartley 2 measured by ISO, Crovisier et al. (1999) detected a peak at 11.3 μm while Colangeli et al. (1999) found no feature of olivines.

The appearance of features may also vary along the orbit of the comet. For comet Hale–Bopp, Wooden et al. (1999) note that the postperihelion dropping of

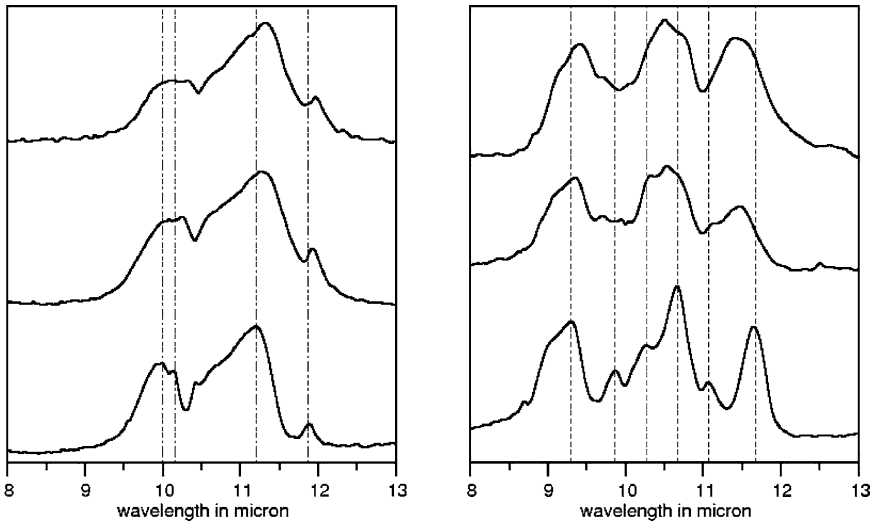

Fig. 16 Example for transmission spectra (*left*) for olivine with a magnesium content of 100 mol% (Fo_{100}) (*bottom*), of 80 mol% (Fo_{80}) (*middle*) and of 60 mol% (Fo_{60}) (*top*) and pyroxene spectra (*right*) obtained by laboratory measurements of meteoritic samples. Shown are spectra for pyroxene with a magnesium content of 100 mol% (En_{100}) (*bottom*), of 80 mol% (En_{80}) (*middle*) and of 75 mol% (En_{75}) (*top*): intensity and position of the features change with the magnesium content of the silicates (Köhler 2005; Morlok et al. 2005)

the feature happens more rapidly than expected from preperihelion spectra. They suggest that the relative abundance of submicron-sized grains decreased during the perihelion passage and also note that the temperature of the different dust components may play a role for the material that is then seen in the comet.

8.6.3 Circumstellar dust

With its large IR excess and its relative proximity to the solar system β Pictoris is one of the best studied stars. Observations with the IRTF telescope indicate a feature at 10 μm attributed to a silicate component of the dust (Telesco and Knacke 1991). Subsequent observations (Knacke et al. 1993) of the dust disk of β Pictoris again with IRTF showed that the spectrum of β Pictoris is in good agreement with the features in the spectrum of comet Halley (Fig. 17).

Low spectral resolution ISOPHOT measurements also indicate a rise in emission from 9 to 11.6 μm (Heinrichsen et al. 1999). Observations with the ISO SWS (de Graauw et al. 1996; Pantin et al. 1999; Malfait and Waelkens 1999) were made in the wavelength range from 2.4 to 45.2 μm (Reach et al. 2003) and then compared with the ISOPHOT data (Heinrichsen et al. 1999), IRAS data and IRTF data (Knacke et al. 1993). IRTF, ISOCAM and SWS data are clearly different, the differences begin around 8 μm and increase to longer wavelength. This indicates that the dust composition varies within the disk: CAM and IRTF observe the inner disk, while SWS and PHOT observe the entire disk including colder emission. The southwest part of the disk was observed with the Keck Long Wavelength Spectrograph (LWS) in a wavelength range of 8–13 μm (Weinberger et al. 2003). Features

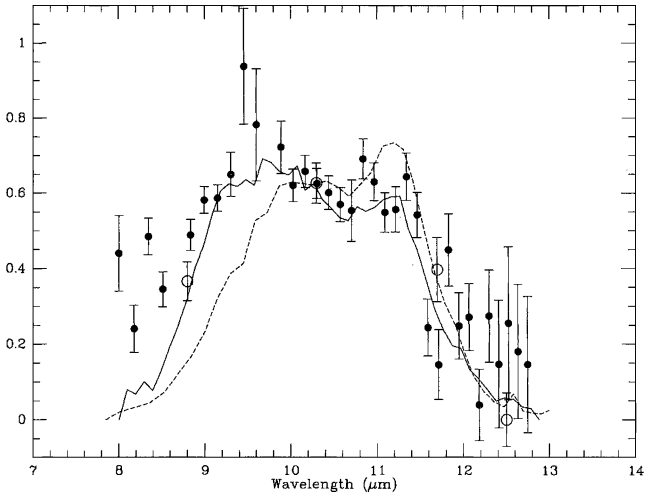

Fig. 17 Comparison of the infrared spectra from the dust disk around β Pictoris with comet Halley (*solid line*) and comet Levy 1990 XX (*dashed line*) (Knacke et al. 1993)

are observable outward to 1 arcsec. The authors conclude that within 20 AU particles must be smaller than 10 μm to produce the features.

The circumstellar dust observations were also compared to model calculations. Li and Greenberg (1998) compared observations in the wavelength range from 2.6 to 1300 μm with their model calculations. They calculated the emission brightness for two types of particles: amorphous silicate core-organic refractory mantel grains and crystalline silicates grains. The particles are assumed to have an ice mantle at distances larger than 100 AU from the star and to have porosities of 0.95 up to 0.975. Three different size distributions were applied within the disk. On the basis of the model they suggest that both components: amorphous silicate core-organic refractory mantle aggregates and crystalline silicate aggregates occur in the material composition of the dust particles.

Heinrichsen et al. (1999) compared the ISOPHOT and IRAS observations with a model of silicate grains in the 1 μm to 5 mm size range with a size distribution $n(s) \propto s^{-4.1}$, where s is the grain radius. They reproduced the spectrum with a mixture of thermal black body emission ($T = 300$–500 K) and a silicate emission feature which confirms previous work (Knacke et al. 1993).

Features are currently observed for many young circumstellar dust systems, but not so much for Vega-like systems: The photosphere of ε Eridani, for instance, dominates the spectrum out to 11.6 μm such that silicate features are not detectable. For Vega it is suggested that a dip in the spectrum around 34 μm is caused by forsterite (Mg-rich olivine) dust (Min et al. 2004).

8.7 Influence of dust size and structure on the emission features

Aside from material composition the appearance of features depends on the size, shape and structure of particles. Recent studies show that the appearance of sharp peaks in the infrared does not necessarily mean a large contribution from small

dust particles to the brightness. When Mukai and Koike (1990) computed thermal emission from compact olivine spheres having the size distribution derived from in situ measurement of comet Halley, they could not reproduce the twin peaks of olivines seen in the observations. Okamoto et al. (1994) computed the thermal emission of fractal aggregates of small (10 nm) monomers and could find the peak structure. They have shown that the prominent twin peaks of olivines observed for several comets are easily obtained with highly fluffy aggregates, irrespective of their sizes. Yanamandra-Fisher and Hanner (1999b) showed that the thermal emission peak at a wavelength of 11.2 μm can be matched with submicrometre tetrahedrons, moderately elongated bricks, aggregates of spheres and aggregates of tetrahedrons of magnesium-rich olivine, but not with spheres. Moreno et al. (2003) used DDA and a combination of Mie theory and Maxwell–Garnett effective medium approximation to calculate thermal radiation over wavelengths of 8–40 μm from aggregates of a mixture of crystalline and amorphous olivines and glassy carbon with a power-law size distribution. They obtained reasonable fits to the infrared spectra of comet Hale–Bopp measured with ISO from heliocentric distances from 2.8 to 3.9 AU.

The refractive index of a material is usually obtained from laboratory measurements. The exact position and relative intensities of emission bands change with the microscopic structure of the sample materials as well as with the temperature of the samples. The laboratory spectra in mid- and far-infrared region obtained for olivine particles that were continuously cooled down to 10 K show for instance that the peaks become stronger and narrower with decreasing temperature (Koike et al. 2005). Recent studies of silicates extracted from meteorite material show similar infrared spectra compared to previous measurements at synthetic or terrestrial minerals (Köhler 2005). The spectra of silicates vary with their Fe/Mg content (Fig. 16), which allows using the observation of the features for studies of the material evolution of silicates.

8.8 Evolution of matter

Dust particles provide the opportunity to study the evolution of matter in the solar system and in planetary debris disks as indicated in Fig. 18. During the evolution of a planetary system dust is either formed by accumulation of primordial dust, by condensation out of the gas phase, or by a combination of both. It is accumulated in large objects and subsequently released during their fragmentation caused by heating and collisions. Cometary material, as well as the material in the typically observed outer regions of planetary debris disks is assumed to be relatively pristine: it contains condensed volatiles and therefore may still contain unprocessed dust material, though the present location is not necessarily the region of formation of these objects. Understanding the composition of the dust and the planetesimals and comparing them to other dust populations helps to trace down the evolution of the planetary systems. An important issue in this context is the evolution of silicates.

First detection of crystalline silicate came from observations of features attributed to crystalline olivine in comet Halley (Bregman et al. 1987; Campins and Ryan 1989). Crystalline silicate features were also observed in other comets, in evolved stars, in some young stellar objects as well as crystalline silicates were

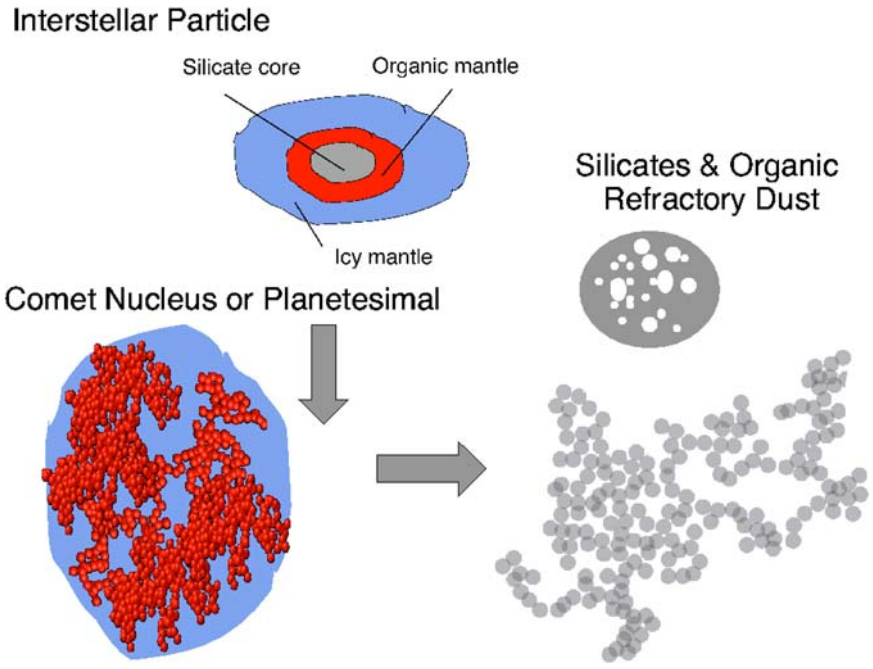

Fig. 18 The evolution path of dust in planetary systems: A sketch of the dust evolution during planetary system formation: interstellar dust is partially melted and recondensed in the proto-planetary nebula and then incorporated in larger solar system objects. From those it is released and further processed during fragmentation and by physical processes occurring in the interplanetary medium

detected in IDPs. A fraction of crystalline silicate was also found in the zodiacal light spectra (Reach et al. 2003). No crystalline silicates were observed in the ISM, in molecular clouds and in young stellar objects in their early stage (Hanner 1999, 2003 for a review). The features are observed in both hot and cold regions, and they are similar in shape. Hence a mixture model of cometary dust assumes that part of the silicates is amorphous in the solar nebula while portions of the dust are either annealed at high temperatures or are recondensed from the gas phase in the solar nebula. This model requires a process to mix crystalline and amorphous silicates. It is also plausible to assume that some amounts of crystalline silicates existed in the interstellar dust cloud out of which the solar system was formed.

Dust particles that are condensed in supernovae or AGB stars may be formed as crystalline. Interstellar dust particles, due to processing in the ISM mainly consist of amorphous silicate. Irradiation in the ISM leads to amorphisation of initial crystalline silicates. Nevertheless dust particles that were recently formed did exist in the proto-solar nebula and are in some cases still observed as presolar dust particles. Presolar dust particles exist in meteorites and IDPs. They are formed before formation of the solar system and attributed to different sources, since their measured isotope ratios differ greatly. The existence of short-lived radionuclides in presolar dust particles indicates those were formed shortly before the formation of the solar system ($<10^7$ years) and hence were not greatly processed in the ISM.

This points to the possible existence of crystalline silicate dust in the ISM at the time of the solar system formation.

The amount of amorphous versus crystalline silicates at the time of the formation of the solar system depends on the amount of typical ISM dust versus freshly produced dust in the ISM plus solar nebular condensates at the time of the solar system formation. Comparison to dust in different planetary debris disks will show to what extent the ISM conditions at the time of the formation of the host star influence the appearance of the silicates in the planetary systems.

9 Summary

The past decade has brought a wealth of information about the spatial structures of at least some of the planetary debris disks and progress was made in understanding the influence of planets on the spatial distribution of dust and planetesimals. Planetary debris disks were first discovered by the infrared excess that their host stars reveal relative to the typical spectral energy distribution of a star of that type and evolutionary stage. Studying planetary-debris disks by their infrared excess alone is difficult and spatially resolved observations or sub-mm data are extremely important.

The planetary debris disks surround main-sequence stars or late pre-main-sequence stars of ages that clearly exceed the lifetime of dust in those systems. The lifetimes of dust particles are limited by catastrophic collisions, orbital perturbations induced by planets, photon Poynting–Robertson effect due to radiation pressure force and/or plasma Poynting–Robertson effect due to momentum transfer from stellar wind particles. We compare these systems to the dust cloud in our solar system where all the listed effects occur as well. While observational methods at first glance appear to be more sophisticated for the case of our solar system, we show that detailed observational results there are limited to the region near 1 AU. However, in contrast to other systems, it is possible to study actual dust samples in the laboratory. Moreover, cometary dust observations give direct information about relatively pristine material within the dust cloud.

Major sources of our solar system dust cloud are asteroids and comets. The planetary debris disks are sustained by fragmentation of planetesimals. The occurrence of fast evaporating bodies in the β Pictoris system shows some similarity to the Sungrazing comets, but is more frequent. The fast evaporating bodies indicate the existence of cometary activity. The fast evaporating bodies, as well as the extension of the spatially resolved disks from their symmetry planes indicate the presence of perturbing objects in the disks. The spatial distribution of the dust in planetary debris disks in general is less homogenous than appears to be in the solar system and is influenced by the presence of planetesimals and possibly planets. A closer look at the solar system dust cloud, indicates, however, that it is unevenly distributed outside from several astronomical units distance from the Sun and possibly also near the Sun, i.e., at distances smaller than 0.5 AU. Recently, it was found that, rather than direct influence of orbital resonances on the dust particles, uneven distribution of parent bodies can cause spatial density variations of dust in the planetary debris disks, similar to the dust trails and bands observed in the solar system.

Aside from the gravitational forces, the major forces on the dust particles are the radiation pressure of the central star and, in some cases, stellar-wind forces which can be as important as the force resulting from radiation pressure. Radiation pressure is typically stronger than in the case of the solar system dust cloud, as well as the surface charge of grains and therefore the Lorentz force. Similar to the solar system, the dust size distribution of the planetary debris disks is determined by the interplay of collisional fragmentation of particles and ejection of particles by radiation pressure. Collisions also cause a dust depletion in the inner zones of the disks, so that the observation of inner depletion zones, does not necessarily require the presence of a planet. There is no direct observation of the stellar wind in the planetary debris disks. The parameters of stellar winds in some cases can be inferred from measurements of the enhanced density of neutral hydrogen (the so-called 'hydrogen wall') at the boundary region between stellar wind and the plasma of the interstellar medium, and give values of the mass loss between 0.1 and 20 solar mass loss rates. The entry of interstellar dust provides a further dust constituent to the planetary debris disks, and it can also stir up the dust production in these disks. Neutral and singly charged gas components observed in Keplerian orbits about β Pictoris still lack a final explanation.

The properties of dust that are derived from observations are albedo, emissivity and polarisation. These optical properties can be used to compare dust in different systems. From observations of thermal emission features, the dust in planetary debris disks appears similar to cometary dust in our solar system, rather than to zodiacal dust.

Further progress in understanding planetary debris disks will be made by combining the dynamical considerations with other findings about the material properties as well as the interactions with the gas component. While the presence of planets is certainly of high interest, the study of the observed planetary debris disks provides far more information, which – in contrast to the planet detection – cannot be given otherwise. By measuring particle size, particle properties, and composition, the material properties can be compared to solar system dust as well as to dust in the interstellar medium. For this, infrared and polarization measurements are of great interest. Their interpretation needs improved models of optical dust properties as well as supporting laboratory measurements. A further open issue is to understand the presence or absence of gas components, which may give further clues about the evolutionary stage of the systems. Advanced observational programs will allow to study the infrared spectra as well as the gas content of planetary debris disks.

Acknowledgements We thank Martin Huber for his suggestion to write this article and for his patience with the authors. A significant part of the preparations for this review was carried out during I.M.s stay at ESA Space Science Department and was funded by the European Space Agency under ESTEC/Contract 14647/00/NL/NB. We wish to thank Sabine Dude for assistance in preparing the manuscript. Parts of this research have been supported by the German Aerospace Center, DLR (project 'Rosetta: MIDAS, MIRO, MUPUS' RD-RX-50 QP 0403) and by the Japanese Ministry of Education, Culture, Sports, Science and Technology, MEXT, (Monbu Kagaku Sho) under Grant-in-Aid for Scientific Research on Priority Areas "Development of Extra-Solar Planetary Science" (16077203).

References

Altenhoff, W. J., Bertoldi, F., Menten, K. M., et al. 2002, A&A, 391, 353
Artymowicz, P. 1988, ApJ, 335, L79
Artymowicz, P. 1997, Ann. Rev. Earth Planet. Sci., 25, 175
Artymowicz, P. & Clampin, M. 1997, ApJ, 490, 863
Augereau, J. C., Lagrange, A. M., Mouillet, D., & Ménard, F. 1999a, A&A, 350, L51
Augereau, J. C., Lagrange, A. M., Mouillet, D., Papaloizou, J. C. B., & Grorod, P. A. 1999b, A&A, 348, 557
Augereau, J. C. & Papaloizou, J. C. B. 2004, A&A, 414, 1153
Aumann, H. H., Beichman, C. A., Gillett, F. C., et al. 1984, ApJ, 278, L23
Backman, D. E., Dasgupta, A., & Stencel, R. E. 1995, ApJ, 450, L35
Backman, D. E. & Paresce, F. 1993, in Protostars and Planets III ed. E. Levy, J. Lunine (Univ. of Arizona Press), 1253–1304
Bandermann, L. W. & Wolstencroft, R. D. 1977, Ap&SS, 49, 253
Baranov, V. B. & Malama, Y. G. 1993, J. Geophys. Res., 98, 15157
Barge, P., Pellat, R., & Millet, J. 1982a, A&A, 109, 228
Barge, P., Pellat, R., & Millet, J. 1982b, A&A, 115, 8
Behr, A. & Siedentopf, H. 1953, Z. Astrophys., 32, 19
Beichman, C. A., Bryden, G., Rieke, G. H., et al. 2005, ApJ, 622, 1160
Bemporad, A., Poletto, G., Raymond, J. C., et al. 2005, ApJ, 620, 523
Berriman, G. B., Boggess, N. W., Hauser, M. G., et al. 1994, ApJ, 431, L63
Bertaux, J. L. & Blamont, J. E. 1976, Nature, 262, 263
Beust, H., Lagrange-Henri, A. M., Vidal-Madjar, A., & Ferlet, R. 1989, A&A, 223, 304
Beust, H. & Morbidelli, A. 1996, Icarus, 120, 358
Biesecker, D. A., Lamy, P., Cyr, O. C. S., Llebaria, A., & Howard, R. A. 2002, Icarus, 157, 323
Blackwell, D. E. 1956, MNRAS, 116, 365
Blackwell, D. E. & Ingham, M. F. 1961a, MNRAS, 122, 113
Blackwell, D. E. & Ingham, M. F. 1961b, MNRAS, 122, 129
Blackwell, D. E. & Ingham, M. F. 1961c, MNRAS, 122, 143
Blackwell, D. E. & Petford, A. D. 1966, MNRAS, 131, 383
Boccaletti, A., Augereau, J. C., Marchis, F., & Hahn, J., 2003, ApJ, 585, 494
Bohren, C. F. & Huffman, D. R. 1983, Absorption and Scattering of Light by Small Particles (Wiley and Sons: New York – Chichester – Brisbane – Toronto – Singapore)
Bradley, J. P., Brownlee, D. E., & Fraundorf, P. 1984, Science, 226, 1432
Brandeker, A., Liseau, R., Olofsson, G., & Fridlund, M., 2004, in ASP Conf. Ser. 324: Debris Disks and the Formation of Planets, 228
Bregman, J. D., Witteborn, F. C., Allamandola, L. J., et al. 1987, A&A, 187, 616
Brownlee, D. E. 1978 (Wiley-Interscience), 295
Burns, J. A., Lamy, P. L., & Soter, S. 1979, Icarus, 40, 1
Campins, H. & Ryan, E. V. 1989, ApJ, 341, 1059
Ceplecha, Z., Borovička, J., Elford, W. G., et al. Apr. 1998, Space Sci. Rev., 84, 327
Chernova, G. P., Kiselev, N. N., & Jockers, K. 1993, Icarus, 103, 144
Chini, R., Kruegel, E., & Kreysa, E. 1990, A&A, 227, L5
Ciardi, D. R., van Belle, G. T., Akeson, R. L., et al. 2001, ApJ, 559, 1147
Colangeli, L., Bussoletti, E., Checchi Pestellini, C., et al. 1998, Icarus, 134, 35
Colangeli, L., Epifani, E., Brucato, J. R., et al. 1999, A&A, 343, L87
Consolmagno, G. 1979, Icarus, 38, 398
Consolmagno, G. 1980, Icarus, 43, 203
Crifo, F., Vidal-Madjar, A., Lallement, R., Relet, R., & Garbaldi, M. 1997, A&A, 320, L29
Crovisier, J., Encrenaz, T., Lellouch, E., et al. 1999, ESA-SP, 427, 161
Czechowski, A. & Mann, I. 2001, in The Outer Heliosphere: The Next Frontiers, 365
Czechowski, A. & Mann, I. 2003a, A&A, 410, 165
Czechowski, A. & Mann, I. 2003b, J. Geophys. Res., in print
de Graauw, T., Haser, L. N., Beintema, D. A., et al. Nov. 1996, A&A, 315, L49
de Pater, I., Forster, J. R., Wright, M., et al. 1998, AJ, 116, 987
Decin, G., Dominik, C., Waters, L. B. F. M., & Waelkens, C. 2003, ApJ, 598, 636
Dent, W. R. F., Walker, H. J., Holland, W. S., & Greaves, J. S., 2000, MNRAS, 314, 702
Dermott, S. F., Jayaraman, S., Xu, Y. L., Gustafson, B. A. S., & Liou, J. C. 1994, Nature, 369, 719

Deul, E. R. & Wolstencroft, R. D. 1988, A&A, 196, 277
Di Folco, E., Thévenin, F., Kervella, P., et al. 2004, A&A, 426, 601
Dobrovolsky, O. V., Kiselev, N. N., & Chernova, G. P. 1986, Earth, Moon, Planets, 34, 189
Dohnanyi, J. S. 1969, J. Geophys. Res., 74, 2531
Dohnanyi, J. S. 1978, in Cosmic Dust, ed J. A. M. MacDonnell (J. Wiley & Sons, Chicheseter–New–York–Brisbane–Toronto), 527–605
Dollfus, A., Bastien, P., Le Borgne, J. F., Levasseur-Regourd, A. C., & Mukai, T. 1988, A&A, 206, 348
Dollfus, A. & Suchail, J. L. 1987, A&A, 187, 669
Dominik, C. & Decin, G. 2003, ApJ, 598, 626
Dominik, C., Laureijs, R. J., Jourdain de Muizon, M., & Habing, H. J. 1998, A&A, 329, L53
Draine, B. T. 1988, ApJ, 333, 848
Draine, B. T. & Flatau, P. J. 1994, J. Opt. Soc. Am., A11, 1491
Dumont, R. 1965, Ann. d'Astrophys., 28, 265
Dumont, R. 1973, Planet Space sci., 21, 2149
Dumont, R. & Levasseur-Regourd, A. C. 1978, A&A, 64, 9
Dumont, R. & Sanchez, F. 1975a, A&A, 38, 397
Dumont, R. & Sanchez, F. 1975b, A&A, 38, 405
Dumont, R. & Sanchez, F. 1976, A&A, 51, 393
Eaton, N. & Zarnecki, J. C. 1985, MNRAS, 217, 659
Edenhofer, P., Bird, M. K., Brenkle, J. P., et al. 1987, A&A, 187, 712
Epifani, E., Colangeli, L., Fulle, M., et al. 2001, Icarus, 149, 339
Fajardo-Acosta, S. B., Telesco, C. M., Knacke, R. F. 1998, Infrared Photometry of beta Pictoris Type Systems. Astron. J. 115, 2101–2121
Fechtig, H., Leinert, C., & Berg, O. E. 2001, Historical Perspectives (Springer-Verlag), 1–55
Finson, M. L. & Probstein, R. F. 1968, ApJ, 154, 353
Flynn, G. J. 1989, Icarus, 77, 287
Flynn, G. J. 1996, Meteorit. Planet. Sci., 31, 45
Fomenkova, M., Jones, B., Pina, R., et al. 1995, AJ, 110, 1866
Frey, A., Hofmann, W., Lemke, D., & Thum, C. 1974, A&A, 36, 447
Fujiwara, A., Kamimoto, G., & Tsukamoto, A. 1977, Icarus, 31, 277
Fulle, M. 1988, A&A, 201, 161
Fulle, M. 1992, Nature, 359, 42
Fulle, M. 1996, A&A, 311, 333
Fulle, M. 2000, Icarus, 145, 239
Fulle, M., Böhm, C., Mengoli, G., et al. 1994, A&A, 292, 304
Fulle, M., Bosio, S., Cremonese, G., et al. 1993a, A&A, 272, 634
Fulle, M., Cremonese, G., & Böhm, C. 1998, AJ, 116, 1470
Fulle, M., Cremonese, G., Jockers, K., & Rauer, H. 1992, A&A, 253, 615
Fulle, M., Mennella, V., Rotundi, A., et al. 1993b, A&A, 276, 582
Fulle, M., Mikuž H., & Bosio, S. 1997, A&A, 324, 1197
Ganesh, S., Joshi, U. C., Baliyan, K. S., & Deshpande, M. R., 1998, A&AS, 129, 489
Giese, R., Kneissel, B., & Rittich, U. 1986, Icarus, 68, 395
Giese, R. H., Weiss, K., Zerull, R. H., & Ono, T. 1978, A&A, 65, 265
Gledhill, T. M., Scarrott, S. M., & Wolstencroft, R. 1991, MNRAS, 252, 50
Gloeckler, G., Fisk, L. A., Geiss, J., Schwadron, N. A., & Zurbuchen, T. H. 2000, J. Geophys. Res., 105, 7459
Golimowsky, D. A., Durrance, S. T., & Clampin, M. 1993, ApJ, 411, L41
Good, J. C., Hauser, M. G., & Gautier, T. N. 1986, Adv. Space Res., 6, 83
Grady, C. A., Sitko, M. L., Russell, R. W., et al. May 2000, Protostars and Planets IV, 613
Greaves, J. S., Holland, W. S., Jayawardhana, R., Wyatt, M. C., & Dent, W. R. F. 2004a, MNRAS, 348, 1097
Greaves, J. S., Holland, W. S., Moriarty-Schieven, G., et al. 1998, ApJ, 506, L133
Greaves, J. S., Holland, W. S., Wyatt, M. C., et al. Feb. 2005, ApJ, 619, L187
Greaves, J. S., Wyatt, M. C., Holland, W. S., & Dent, W. R. F. 2004b, MNRAS, 351, L54
Grün, E., Gustafson, B., Mann, I., et al. 1994, A&A, 286, 915
Grün, E., Hanner, M. S., Peschke, S. B., et al. 2001, A&A, 377, 1098
Grün, E. & Landgraf, M. 2000, J. Geophys. R., 105, 10291
Gurnett, D. A., Ansher, J. A., Kurth, W. S., & Granroth, L. J., 1997, Geophys. Res. Lett., 24, 3125

Gustafson, B. A. A. S. 1985, in Properties and interactions of interplanetary dust; Proceedings of the Eighty-fifth Colloquium, Marseille, France, July 9–12, 1984, ed R. Giese & P. Lamy (Dordrecht, D. Reidel Publishing Co.), 385–388
Gustafson, B. A. S. & Kolokolova, L. 1999, J. Geophys. Res., 104, 31711
Gustafson, B. A. S. & Misconi, N. Y. 1986, Icarus, 66, 280
Hadamcik, E. & Levasseur-Regourd, A. C. 2003, A&A, 403, 757
Hadamcik, E., Levasseur-Regourd, A. C., & Renard, J. B. 1999, Earth, Moon, Planets, 78, 365
Hahn, J. M. & Rettig, T. W. 2000, Icarus, 146, 501
Hamilton, D. P., Grün, E., & Baguhl, M. 1996, in: Physics, Chemistry, and Dynamics of Interplanetary Dust (ASP Conf. Series, vol. 104), ed. B. A. A. S. Gustafson, & M. S. Hanner (ASP, San Francisco), 31–34, proc. IAU Coll. No. 150
Hanner, M. S. 1999, Space Sci. Rev., 90, 99
Hanner, M. S. 2003, LNP Vol. 609: Astromineralogy, 609, 171
Hanner, M. S., Giese, R. H., Weiss, K., & Zerull, R. H. 1981, A&A, 104, 42
Hanner, M. S., Hackwell, J. A., Russell, R. W., & Lynch, D. K., 1994a, Icarus, 112, 490
Hanner, M. S. & Hayward, T. L. 2003, Icarus, 161, 164
Hanner, M. S., Lynch, D. K., & Russell, R. W., 1994b, ApJ, 425, 274
Hanner, M. S. & Newburn, R. L. 1989, AJ, 97, 254
Hanner, M. S., Newburn, R. L., Gehrz, R. D., et al. 1990, ApJ, 348, 312
Hanner, M. S., Newburn, R. L., Spinrad, H., & Veeder, G. J., 1987a, AJ, 94, 1081
Hanner, M. S., Russel, R. W., Lynch, D. K., & Brooke, T. Y., 1993, Icarus, 101, 64
Hanner, M. S., Tokunaga, A. T., Golisch, W. F., Griep, D. M., & Kaminski C. D. 1987b, A&A, 187, 653
Hanner, M. S., Veeder, G. J., & Tokunaga, A. T. 1992, AJ, 104, 386
Haudebourg, V., Cabane, M., & Levasseur-Regourd, A. C. 1999, Physics and Chemistry of the Earth, Part C: Solar, Terrestrial & Planetary Science, 24, 603
Heap, S. R., Lindler, D. J., Lanz, T. M., et al. 2000, ApJ, 539, 435
Heinrichsen, I., Walker, H. J., & Klaas, U. 1998, MNRAS, 293, L78
Heinrichsen, I., Walker, H. J., Klaas, U., Sylvester, R. J., & Lemke, D. 1999, MNRAS, 304, 589
Henry, T. J., Soderblom, D. R., Donahue, R. A., & Baliunas, S. L. 1996, AJ, 111, 439
Hirayama, K. 1918, AJ, 31, 185
Holland, W. S., Greaves, J. S., Dent, W. R. F., et al. 2003, ApJ, 582, 1141
Holland, W. S., Greaves, J. S., Zuckerman, B., et al. 1998, Nature, 392, 788
Hudson, B., Flynn, G. J., Fraundorf, P., Hohenberg, C. M., & Shirck, J. 1981, Science, 211, 383
Humes, D. H. 1980, J. Geophys. Res., 85, 5841
Ishiguro, M., Nakamura, R., Fujii, Y., & Mukai, T. 1999, Publ. Astron. Soc. Jap., 51, 363
Ishiguro, M., Watanabe, J., Usui, F., et al. 2002, ApJL, 572, L117
Ishimoto, H. 1999, Adv. Space Res., 25, (2)281
Ishimoto, H. 2000, A&A, 362, 1158
Ishimoto, H. & Mann, I. 1998, Planet. Space Sci., 47, 225
Jessberger, E. K., Stephan, T., Rost, D., et al. 2001, Properties of Interplanetary Dust: Information from Collected Samples (Springer-Verlag), 253–294
Jewitt, D. 2004, AJ, 128, 3061
Jewitt, D. & Luu, J. 1995, Ap&SS, 223, 164
Jewitt, D. & Matthews, H. E. 1997, AJ, 113, 1145
Jewitt, D. & Matthews, H. E. 1999, ApJ, 117, 1056
Jones, A. P., Tielens, A. G. G. M., & Hollenbach, D. J., 1996, ApJ, 469, 740
Kalas, P. 2006, ApJL, in print
Kalas, P., Deltron, J. M., & Larwood, J. 2001, ApJ, 553, 410
Kalas, P. & Jewitt, D. 1995, AJ, 110, 794
Kalas, P., Larwood .J., Smith, B. A., & Schultz, A. 2000, ApJ, 530, L133
Kalas, P., Liu, M. C., & Matthews, B. C. 2004, Science, 303, 1990
Kalas, P. G. 1998, Earth, Moon, Planets, 81, 27
Kelsall, T., Weiland, J. L., Franz, B. A., et al. 1999, ApJ, 508, 44
Kenyon, S. J., & Bromley, B. C. 2001, AJ, 121, 538
Kikuchi, S., Mikami, Y., Mukai, T., & Mukai, S. 1989, A&A, 214, 386
Kikuchi, S., Mikami, Y., Mukai, T., Mukai, S., & Hough, J. H., 1987, A&A, 187, 689
Kimura, H. 2001, J. Quant. Spectrosc. Radiat. Transfer, 70, 581
Kimura, H., Ishimoto, H., & Mukai, T. 1997, A&A, 326, 263
Kimura, H., Kolokolova, L., & Mann, I. 2003, A&A, 407, L5

Kimura, H. & Mann, I. 1998a, Earth Planets Space, 50, 493
Kimura, H. & Mann, I. 1998b, ApJ, 499, 454
Kimura, H., Mann, I., Biesecker, D. A., & Jessberger, E. 2002, Icarus, 159, 529
Kiselev, N. N. & Velichko, F. P. 1997, Conference Paper: 28th Annual Lunar Planet. Sci. Conference, 733
Knacke, R. F., Fajardo-Acosta, S. B., Telesco, C. M., et al. 1993, ApJ, 418, 440
Kneissel, B. & Mann, I. 1990, in Physics of the outer heliosphere; Proceedings of the 1st COSPAR Colloquium, Warsaw, Poland, Sept. 19–22, 1989 (A91-55051 24-90) (Oxford, England and Elmsford, NY, Pergamon Press), 93–95
Kneissel, B. & Mann, I. 1991, in Origin and Evolution of Interplanetary Dust, ed. A. Levasseur-Regourd, & H. Hasegawa, (Kluwer), 139–146
Koerner, D. W., Sargent, A. I., & Ostroff, N. A. 2001, ApJ, 560, L181
Köhler, M. 2005, PhD Thesis, Westfälische Wilhelms-Universität
Köhler, M., Kimura, H., & Mann, I. 2006, A&A, 448, 395
Koike, C., Suto, H., Chihara, H., et al. 2005, In: The Dusty and Molecular Universe: A Prelude to Herschel and ALMA, 375–376
Kolokolova, L., Hanner, M. S., Levasseur-Regourd, A. C., & Gustafson, B. A. S. 2004, in Comets II (M. Festou and, U. Keller and H. Weaver)
Kozasa, T., Blum, J., Okamoto, H., & Mukai, T. 1993, A&A, 276, 278
Krishna Swamy, K. S. 1991, A&A, 241, 260
Krivov, A. V., Kimura, H., & Mann, I. 1998, Icarus, 134, 311
Krivov, A. V., Mann, I., & Krivova, N. A. 2000, A&A, 362, 1127
Krivova, N. A., Krivov, A. V., & Mann, I. 2000, ApJ, 539, in press
Krüger, H., Grün, E., Landgraf, M., et al. Nov. 2001, Planet. Space Sci., 49, 1303
Kuchner, M. J., & Holman, M. J. 2003, ApJ, 588, 1110
Kuchner, M. J., Reach, W. T., & Brown, M. E. 2000, Icarus, 145, 44
Kurat, G., Koeberl, C., Presper, T., Brandstatter, F., & Maurette, M. 1994, Geochim. and Cosmochimica Acta, 58, 3879
Lagage, P. O., de Boula, O., Cesarsky, C. J., et al. Mar. 1999, In: ESA SP-427: The Universe as Seen by ISO, 207–+
Lagage, P. O., & Pantin, E. 1994, Nature, 369, 628
Lagrange, A. M., Ferlet, R., & Vidal-Madjar, A. 1989, A&A, 173, 289
Lallement, R. 2001, Ap&SS, 277, 205
Lamy, P. 1974a, A&A, 33, 191
Lamy, P. 1976, in IAU Colloq. 31: Interplanetary Dust and Zodiacal Light, 437–442
Lamy, P. L. 1974b, A&A, 35, 197
Lamy, P. L., Toth, I., A'Hearn, M. F., & Weaver, H. A. 1999, Icarus, 140, 424
Lamy, P. L., Toth, I., Grün, E., et al. 1996, Icarus, 119, 370
Lamy, P. L., Toth, I., Jorda, L., et al. 2002, Icarus, 156, 442
Lamy, P. L., Toth, I., Jorda, L., Weaver, H. A., & A'Hearn, M., 1998a, A&A, 335, L25
Lamy, P. L., Toth, I., & Weaver, H. A. 1998b, A&A, 337, 945
Landaberry, S. J. C., Singh, P. D., & de Freitas Pacheco, J. A., 1991, A&A, 246, 597
Landgraf, M., May 2000, J. Geophys. Res., 105, 10303
Landgraf, M., Liou, J. C., Zook, H. A., & Grün, E., 2002, AJ, 123, 2857
Lanz, T. 1986, A&AS, 65, 195
Lanzerotti, L. J., Brown, W. L., Augustyniak, W. M., Johnson, R. E., & Armstrong, T. P. 1982, ApJ, 259, 920
Larwood, J. D. & Kalas, P. G. 2001, MNRAS, 323, 402
Lecalvelier Des Etangs, A., Perrin, G., Ferlet, R., et al. 1993, A&A, 274, 877
Lecavelier Des Etangs, A., Nitschelm, C., Olsen, E. H., Vidal-Madjar, A., & Ferlet, R. 2005, A&A, 439, 571
Lecavelier Des Etangs, A., Scholl, H., Roques, F., Sicardy, B., & Vidal-Madjar, A. 1996, Icarus, 123, 168
Leinert, C. 1975, Space Sci. Rev., 18, 281
Leinert, C., Bowyer, S., Haikala, L. K., et al. 1998, A&AS, 127
Leinert, C. & Grün, E. 1990, Interplanetary Dust (Physics of the Inner Heliosphere I) (Springer, Berlin), 207
Leinert, C., Hanner, M., Richter, I., & Pitz, E. 1980, A&A, 82, 328
Leinert, C., Link, H., & Pitz, E. 1974, A&A, 30, 411
Leinert, C., Link, H., Pitz, E., & Giese, R. H. 1976, A&A, 47, 221

Leinert, C., Pitz, E., Hanner, M., & Link, H. 1977, J. Geophys. Res., 42, 699
Leinert, C., Richter, I., Pitz, E., & Hanner, M., 1982a, A&A, 110, 355
Leinert, C., Richter, I., Pitz, E., & Planck, B. 1981, A&A, 103, 177
Leinert, C., Richter, I., & Planck, B. 1982b, A&A, 110, 111
Leinert, C., Röser, S., & Buitrago, J. 1983, A&A, 118, 345
Lellouch, E., Crovisier, J., Lim, T., et al. 1998, A&A, 339, L9
Levasseur-Regourd, A. C. 1996, in A.S.P. Conference, Vol. 104, Physics, Chemistry, and Dynamics of Interplanetary Dust, ed. B. A. S. Gustafson, & M. S. Hanner (Astronomical Society of the Pacific Press, San Francisco), 301–308
Levasseur-Regourd, A. C., Cabane, M., Worms, J. C., & Haudebourg, V. 1997, Adv. Space Res., 20, 1585
Levasseur-Regourd, A. C., Hadamcik, E., & Renard, J. B. 1996, A&A, 313, 327
Levasseur-Regourd, A. C., Mann, I., Dumont, R., & Hanner, M. S., 2001, Optical and thermal Properties of Interplanetary Dust (Springer-Verlag), 57–94
Levasseur-Regourd, A. C., McBride, N., Hadamcik, E., & Fulle, M., 1999, A&A, 348, 636
Levison, H. F., Duncan, M. J., & Wetherill, G. W. 1994, Nature, 372, 441
Li, A. & Greenberg, J. M. 1998, A&A, 331, 291
Li, A. & Lunine, J. I. 2003a, ApJ, 594, 987
Li, A. & Lunine, J. I. 2003b, ApJ, 590, 368
Li, A., Lunine, J. I., & Bendo, G. J. 2003, ApJ, 598, L51
Linde, T. J. & Gombosi, T. I. 2000, J. Geophys. Res., 105, 10411
Linsky, J. L. & Wood, B. E. 1996, ApJ, 463, 254
Liou, J. C., Zook, H. A., & Dermott, S. F. 1996, Icarus, 124, 429
Liseau, R. 1999, A&A, 348, 133
Liseau, R., Brandeker, A., Fridlund, M., et al. 2003, A&A, 402, 183
Lisse, C. 2002, Earth, Moon, and Planets, 90, 497
Lisse, C. M., Freudenreich, H. T., Hauser, M. G., et al. 1994, ApJ, 432, L71
Lisse, C. M., A'Hearn, M. F., Hauser, M. G., et al. 1998, ApJ, 496, 971
Liu, M. C. 2004, Science, 305, 1442
Liu, M. C., Matthews, B. C., Williams, J. P., & Kalas, P. G. 2004, ApJ, 608, 526
Lumme, K. & Rahola, J. 1994, ApJ, 425, 653
Lumme, K., Rahola, J., & Hovenier, J. W. 1997, Icarus, 126, 455
Lynch, D. K., Russel, R. W., Hackwell, J. A., Hanner, M. S., & Hammel, H. B. 1992, Icarus, 100, 197
Maas, R. W., Ney, E. P., & Woolf, N. J. 1970, ApJ, 160, L101
Macintosh, B., Becklin, E., Kaisler, D., Konopacky, Q., & Zuckerman, B. 2003, ApJ, 594, 538
Mackowski, D. W. & Mishchenko, M. I. 1996, J. Opt. Soc. Am., A13, 2266
MacQueen, R. M. 1968, ApJ, 154, 1059
Malfait, K. & Waelkens, C. 1999, LPI Contributions, 969, 17
Mann, I. 1992, A&A, 261, 329
Mann, I. 1993, Planet. Space Sci., 41, 301
Mann, I. 1998a, Earth Planets Space, 50, 465
Mann, I. 1998b, Earth, Planets, and Space, 50, 465
Mann, I. & Czechowski, A. 2005, ApJ, 621, L73
Mann, I., Czechowski, A., & Grzedzielski, S., 2004a, Adv. Space Res., 34, 179
Mann, I., Czechowski, A., Kimura, H., et al. 2006, in IAU Symposium 229 - Asteroids, Comets, Meteors, ed. D. Lazzaro, S. Ferraz-Mello, & J. Fernandez (Cambridge University Press, Cambridge), 41–66
Mann, I., Grün, E., & Wilck, M. 1996, Icarus, 120, 399
Mann, I. & Hanner, M. 1998, in Proc. of the NASA Exozodiacal Dust Workshop, ed. D. Backman, L. Caroff, S. Sandford, D. Wooden, (NASA/CP-1998-10155), 85–99
Mann, I. & Kimura, H. 2000, J. Geophys. Res., 105, 10317
Mann, I., Kimura, H., Biesecker, D. A., et al. Feb. 2004b, Space Sci. Rev., 110, 269
Mann, I., Krivov, A., & Kimura, H. 2000, Icarus, 146, 568
Mann, I. & Murad, E. 2005, ApJ, 624, L125
Mann, I., Okamoto, H., Mukai, T., Kimura, H., & Kitada, Y. 1994, A&A, 291, 1011
Manset, N. & Bastien, P. 2000, Icarus, 145, 203
Marsden, B. G. 1967, AJ, 72, 1170
Marsh, K. A., Silverstone, M. D., Becklin, E. E., et al. 2002, ApJ, 573, 425
Maurette, M., Olinger, C., Michel-Levy, M. C., et al. 1991, Nature, 351, 44

Mazets, E. P., Aptekar, R. L., Golenetskii, S. V., et al. 1986, Nature, 321, 276
Mazets, E. P., Sagdeev, R. Z., Aptekar, R. L., et al. Nov. 1987, A&A, 187, 699
Messenger, S. 2000, in Astrochemistry: From Molecular Clouds to Planetary, 527
Metchev, S. A., Eisner, J. A., Hillenbrand, L. A., & Wolf, S. 2005, ApJ, 622, 451
Michels, D., Sheeley, Jr., N., Howard, R. A., & Koomen, M. J., 1982, Science, 215, 1097
Mie, G. 1908, Ann. Physik, 25, 377
Min, M., Dominik, C., & Waters, L. B. F. M. 2004, A&A, 413, L35
Minato, T., Köhler, M., Kimura, H., Mann, I., & Yamamoto T. 2004, A&A, 424, L13
Minato, T., Köhler, M., Kimura, H., Mann, I., & Yamamoto T. 2006, A&A, in print
Moreno, F., Lara, L. M., López-Moreno, J. J., et al. 2003, A&A, 399, 789
Morfill, G. E. & Grün, E. 1979, Planet. Space Sci., 27, 1269
Morlok, A., Bowey, J., Köhler, M., & Grady, M. 2005, Meteoritics and Planetary Science, in print
Mouillet, D., Lagrange, A., Beuzit, J., & Renaud, N., 1997a, A&A, 324, 1083
Mouillet, D., Lagrange, A. M., Augereau, J. C., & Ménard, F. 2001, A&A, 372, L61
Mouillet, D., Larwood, J. D., Papaloizou, J. C. B., & Lagrange, A. M. 1997b, MNRAS, 292, 896
Muñoz, O., Volten, H., de Haan, J. F., Vassen, W., & Hovenier, J. W. 2000, A&A, 360, 777
Mukai, S. & Mukai, T. 1990, Icarus, 86, 257
Mukai, T. 1981, A&A, 99, 1
Mukai, T. 1986, A&A, 164, 397
Mukai, T., Blum, J., Nakamura, A. M., Johnson, R. E., & Havnes, O. 2001, Physical Processes on Interplanetary Dust (Springer Verlag), 445–507
Mukai, T., Fujino, M., Ishiguro, M., et al. 2003, Icarus, 162, 337
Mukai, T., Ishimoto, H., Kozasa, T., Blum, J., & Greenberg, J. M. 1992, A&A, 262, 315
Mukai, T. & Koike, C. 1990, Icarus, 87, 180
Mukai, T. & Mukai, S. 1973, Publ. Astron. Soc. Jap., 25, 481
Mukai, T., Mukai, S., Fechtig, H., Grün, E., & Giese, R. H., 1985, Adv. Space Res., 5, 339
Mukai, T., Mukai, S., & Kikuchi, S. 1987, Variation of grain properties at the dust outbursts, In ESA, Proceedings of the International Symposium on the Diversity and Similarity of Comets p 427–430 (SEE N88-21884 14-91)
Mukai, T. & Schwehm, G. 1981, A&A, 95, 373
Mukai, T. & Yamamoto, T. 1979, Publ. Astron. Soc. Jap., 31, 585
Mukai, T. & Yamamoto, T. 1982, A&A, 107, 97
Mukai, T., Yamamoto, T., Hasegawa, H., Fujiwara, A., & Koike, C., 1974, Publ. Astron. Soc. Jap., 26, 445
Murdock, T. L. & Price, S. D. 1985, AJ, 90, 375
Nesvorný D., Bottke, W. F., Levison, H. F., & Dones, L. 2003, ApJ, 591, 486
Newburn Jr. R. L. & Spinrad, H. 1989, AJ, 97, 552
Ney, E. P. 1982, in Comets, Space Science Series, ed. L. L. Wilkening (The University of Arizona Press, Tucson), 323–340
Ohgaito, R., Mann, I., Kuhn, J. R., MacQueen, R. M., & Kimura H. 2002, ApJ, 578, 610
Okamoto, H., Mukai, T., & Kozasa, T. 1994, Planet. Space Sci., 42, 643
Okamoto, Y. K., Kataza, H., Honda, M., et al. 2004, Nature, 431, 660
Olofsson, G., Liseau, R., & Brandeker, A. 2001, ApJL, 563, L77
Over, J. 1958, in Proceedings, Koninklijke Nederlandse Akademie van Wetenschappen, Vol. 61 B, 74
Ozernoy, L. M., Gorkavyi, N. N., Mather, J. C., & Taidakova, T. A. 2000, ApJ, 537, L147
Pantin, E., Lagage, P. O., & Artymowicz, P. 1997, A&A, 327, 1123
Pantin, E., Waelkens, C., & Malfait, K. 1999, in ESA SP-427: The Universe as Seen by ISO, 385
Paresce, F. & Burrows, C. 1987, ApJ, 319, L23
Pellicori, S. F., Russell, E. E., & Watts, L. A. 1973, Appl. Opt., 12, 1246
Peterson, A. W. 1961, ApJ, 133, 668
Peterson, A. W. 1963, ApJ, 138, 1218
Peterson, A. W. 1967, ApJ, 148, L37
Peterson, A. W. 1969, ApJ, 155, 1009
Petrova, E. V., Jockers, K., & Kiselev, N. N. 2000, Icarus, 148, 526
Pitz, E., Leinert, C., Schulz, A., & Link, H. 1979, A&A, 74, 15
Plavchan, P., Jura, M., & Lipscy, S. J. 2005, ApJ, 631, 1161

Purcell, E. M., & Pennypacker, C. R. 1973, ApJ, 186, 705
Quillen, A. C. & Thorndike, S. 2002, AJ, 578, L149
Rauer, H., Arpigny, C., Boehnhardt, H., et al. 1997, Science, 275, 1909
Reach, W. 1988, ApJ, 335, 468
Reach, W., Abergel, A., Boulanger, F., et al. 1996, A&A, 315, L381
Reach, W. T. 1991, ApJ, 369, 529
Reach, W. T., Franz, B. A., Weiland, J. L., et al. Apr. 1995, Nature, 374, 521
Reach, W. T., Morris, P., Boulanger, F., & Okumura, K. 2003, Icarus, 164, 384
Rietmeijer, F. J. M. 1998, Interplanetary dust particles (Papike, J. J., Washington D. C), 2–1–87
Robley, R. 1975, A&A, 41, 385
Röser, S. & Staude, H. J. 1978, A&A, 67, 381
Roques, F., Scholl, H., Sicardy, B., & Smith, B. A., 1994, Icarus, 108, 37
Rowan-Robinson, M., Hughes, J., Vedi, K., & Walker, D. W. 1990, MNRAS, 246, 273
Rozenbush, V. K., Rspaev, F. K., Churyumov, K. I., Vid'machenko, A. P., & Gorodetskii, D. I. 1989, Sov. Astronom. Lett., 15, 155
Saar, S. H. & Osten, R. A. 1997, MNRAS, 284, 803
Sanzovo, G. C., de Almeida, A. A., Misra, A., et al. 2001, MNRAS, 326, 852
Sanzovo, G. C., Singh, P. D., & Huebner, W. F. 1996, A&AS, 120, 301
Sarmecanic, M., Fomenkova, M., & Jones, B. 1997, ApJ, 483, L69
Scherer, K. 1999, J. Geophys. Res., in press
Schneider, G., Silverstone, M. D., & Hines, D. C. 2005, ApJ, 629, L117
Schneider, G., Smith, B. A., Becklin, E. E., et al. 1999, ApJ, 513, L127
Sekanina, Z. & Schuster, H. E. 1978a, A&A, 65, 29
Sekanina, Z. & Schuster, H. E. 1978b, A&A, 68, 429
Sen, A. K., Deshpande, M. R., Joshi, U. C., Rao, N. K., & Raveendran, A. V. 1991a, A&A, 242, 496
Sen, A. K., Joshi, U. C., & Deshpande, M. R. 1991b, MNRAS, 253, 738
Sheret, I., Dent, W. R. F., & Wyatt, M. C. 2004, MNRAS, 348, 1282
Shestakova, L. I. & Tambovtseva, L. V. 1995, A&A, 8, 59
Singh, P. D., de Almeida, A. A., & Huebner, W. F. 1992, AJ, 104, 949
Singh, P. D., Huebner, W. F., Costa, R. D. D., Landaberry, S. J. C., & de Freitas Pacheco J. A. 1997, Planet. Space Sci., 45, 455
Smith, B. A. & Terrile, R. 1984, Science, 226, 1421
Sparrow, J. G. & Weinberg, J. L. 1975, A&A, 41, 475
Staude, J. & Schmidt, T. 1972, A&A, 20, 163
Stern, S. A. 1995, AJ, 110, 856
Stern, S. A. 1996, A&A, 310, 999
Suto, H., Maihara, T., Mizutani, K., Yamamoto, T., & Thomas, J. A. 1987, Publ. Astron. Soc. Jap., 39, 925
Sykes, M. 1990, Icarus, 85, 267
Sykes, M. V., Lebofsky, L. A., Hunten, D. M., & Low, F., 1986, Science, 232, 1115
Sykes, M. V. & Walker, R. G. 1992, in Asteroids, Comets, Meteors 1991, 587–591
Sylvester, R. J., Barlow, M. J., & Skinner, C. J. 1994, Ap&SS, 212, 261
Sylvester, R. J., Skinner, C. J., Barlow, M. J., & Mannings, V. 1996, MNRAS, 279, 915
Tamura, M., Fukagawa, M., Kimura, H., et al. 2006, ApJ, submitted
Telesco, C. M., Fisher, R. S., Wyatt, M. C., et al. Jan. 2005, Nature, 433, 133
Telesco, C. M. & Knacke, R. F. 1991, ApJ, 372, L29
Thébault, P. & Augereau, J. C. 2005, A&A, 437, 141
Thomas, N. & Keller, H. U. 1991, A&A, 249, 258
Tokunaga, A. T., Golisch, W. F., Griep, D. M., Kaminski, C. D., & Hanner M. S. 1986, AJ, 92, 1183
Trilling, D. E. & Brown, R. H. 1998, Nature, 395, 775–777
Trilling, D. E., Brown, R. H., & Rivkin, A. S. 2000, ApJ, 529, 499
van de Hulst, H. C. 1947, ApJ, 105, 471
van de Hulst, H. C. 1957, Light scattering by small particles (Wiley and Sons, New York)
Van de Noord, E. L. 1970, ApJ, 161, 309
Vrtilek, J. M. & Hauser, M. G. 1995, ApJ, 455, 677
Wahhaj, Z., Koerner, D. W., Ressler, M. E., et al. 2003, ApJ, 581, L27
Walker, H. & Heinrichsen, I. 2000, Icarus, 143, 147
Wallis, M. K. & Hassan, M. H. A. 1985, A&A, 151, 435

Weaver, H. A., Stern, S. A., & Parker, J. W. 2003, AJ, 126, 444
Wehry, A. & Mann, I. 1999, A&A, 341, 296
Weinberg, J. L. & Hahn, R. C. 1980, IAUS, 90, 19
Weinberger, A. J., Becklin, E. E., Schneide, G., et al. 1999, ApJ, 525, L53
Weinberger, A. J., Becklin, E. E., & Zuckerman, B. 2003, ApJ, 584, L33
Weiss-Wrana, K. 1983, A&A, 126, 240
Wilner, D. J., Homan, M. J., Kuchner, M. J., & Ho, P. T. P., 2002, ApJ, 569, L115
Winkler, C., Schmidt-Kaler, T., & Schlosser, W. 1985, A&A, 143, 194
Witte, M., Rosenbauer, H., Banaszkiewicz, M., & Fahr, H. 1993, Adv. Space Res., 13, 121
Wolstencroft, R. D. & Bandermann, L. W. 1973, MNRAS, 163, 229
Wolstencroft, R. D. & Bandermann, L. W. 1974, Nature, 252, 215
Wolstencroft, R. D. & Kemp, J. C. 1972, ApJ, 177, L137
Wolstencroft, R. D. & Rose, L. J. 1967, ApJ, 147, 271
Wolstencroft, R. D., Scarrott, S. M., & Gledhill, T. 1995, Ap&SS, 224, 395
Wood, B. E. 2004, Living Reviews in Solar Physics, 1, 2
Wood, B. E. & Linsky, J. L. 1998, ApJ, 492, 788
Wood, B. E., Müller, H. R., Zank, G. P., & Linsky, J. L. 2002, ApJ, 574, 412
Wood, B. E., Müller, H. R., Zank, G. P., Linsky, J. L., & Redfield, S. 2005a, ApJ, 628, L143
Wood, B. E., Redfield, S., Linsky, J. L., Müller, H. R., & Zank, G. P. 2005b, ApJS, 159, 118
Wooden, D. H., Harker, D. E., Woodhward, C. E., et al. 1999, ApJ, 517, 1034
Wyatt, M. C. 2003, ApJ, 598, 1321
Wyatt, M. C. 2005, A&A, 440, 937
Wyatt, M. C., Dent, W. R. F., & Greaves, J. S. 2003, MNRAS, 342, 876
Wyatt, M. C., Greaves, J. S., Dent, W. R. F., & Coulson, I. M. 2005, ApJ, 620, 492
Xing, Z. & Hanner, M. S. 1997, A&A, 324, 805
Yamamoto, S. & Mukai, T. 1998, A&A, 329, 785
Yanamandra-Fisher, P. A. & Hanner, M. S. 1999a, Icarus, 138, 107
Yanamandra-Fisher, P. A. & Hanner, M. S. 1999b, Icarus, 138, 107, erratum: Volume 139, Pages 388–389 (1999)
Yeghikyan, A. G. & Fahr, H. J. 2003, Annales Geophysicae, 21, 1263
Yeghikyan, A. G. & Fahr, H. J. 2004, A&A, 415, 763
Zerull, R. H., Gustafson, B., Schulz, K., & Thiele-Corbach, E., 1993, Appl. Opt., 32, 4088
Zuckerman, B., Song, I., Bessell, M. S., & Webb, R. A., 2001, ApJ, 562, L87